信州大学審査学位論文

Analysis and engineering of MEP pathway for highly efficient isoprenoid production in cyanobacteria
(シアノバクテリアにおける高効率イソプレノイド生産のための MEP 経路の解析と改変)

平成 29 年 3 月

生物・食料科学　専攻

工藤 海

TABLE OF CONTENTS

LIST OF TABLES

LIST OF FIGURES

LIST OF ABBREVIATIONS

CDP-ME	4-diphosphocytidyl-2C-methyl D-erythritol
CDP-MEP	4-diphosphocytidyl-2C-methyl D-erythritol 2-phosphate
DMAPP	dimethylallyl diphosphate
DTT	dithiothreitol
DXP	1-deoxy-Dxylulose 5-phosphate
DXR	1-deoxy-D-xylulose-5-phosphate reductoisomerase
DXS	1-deoxy-d-xylulose 5-phosphate synthase
FPP	farnesyl diphosphate
GAP	glyceraldehyde-3-phosphate
GGPP	geranylgeranyl pyrophosphate
GPP	geranyl diphosphate
HMBPP	(E)-4-hydroxy-3-methylbut-2-enyl diphosphate
IDI	isopentenyl diphosphate isomerase
IPP	isopentenyl diphosphate
IPTG	isopropyl β-D-thiogalactopyranoside
IspD	4-diphosphocytidyl-2C-methyl-Derythritol synthase
IspE	4-diphosphocytidyl-2-C-methylerythritol kinase
IspF	2-C-methyl-D-erythritol 2,4-cyclodiphosphate synthase
IspG	1-hydroxy-2-methyl-2-(E)-butenyl 4-diphosphate synthase
IspH	1-hydroxy-2-methyl-2-(E)-butenyl 4-diphosphate reductase
IspS	isoprene synthase
ME-cPP	2-Cmethyl-D-erythritol 2,4- cyclodiphosphate
MEP	methyl-erythritol-4-phosphate
MVA	mevalonic acid
OD	optical density
RT-PCR	reverse transcription pcr
SDS-PAGE	sodium dodecyl sulfate polyacrylamide gel electrophoresis
TPP	thiamine pyrophosphate
WT	wild type

CHAPTER 1

General Introduction

Background

Increasing concerns over energy and environmental problems prompted the need to develop renewable chemicals and fuels. The sunlight is the most abundant and sustainable source of energy available to humanity. Earth receives solar energy at the rate of approximately 120,000 TW in a highly reliable fashion. This vastly exceeds the current annual worldwide energy consumption rate of ~15 TW and any conceivable future needs in this century (1-3). However, because the sunlight cannot be employed as such, it must be captured and transformed into useful forms.

The photosynthesis is especially attractive as a conversion process of sunlight energy. The photosynthesis is the complex process that carbon dioxide (CO_2) and water (H_2O) are converted into carbohydrates and other organic compounds using energy from sunlight. This process is very valuable to convert sunlight energy to chemical form, which can be easily stored. The photosynthesis is categorized into the nature photosynthesis, which is performed by the photosynthetic organisms, and the artificial photosynthesis, which is catalyzed by metals and semiconductors. In the past decade, the efficiency of the artificial photosynthesis has significantly improved and is receiving a lot of attention. However, the artificial photosynthesis has some problems. For example, so far the products synthesized by the artificial photosynthesis are limited to simple compounds, e.g. formic acid and ethanol (4, 5). Furthermore, because the energy density of sunlight is low, the instruments for the artificial photosynthesis need to be set on the large area and their constant maintenance is also required. However, it is very costly and not realistic. Therefore, some innovations are needed for the industrial use of the artificial photosynthesis. In contrast, the photosynthetic organisms can synthesize more complex compounds, e.g. long chain hydrocarbons and fatty acids. Furthermore, they can grow and easily cover a large area. Additionally, the photosynthetic organisms have the

repair mechanism to remove photodamaged and keep the photosynthesis activity without artificial maintenance. Therefore, I considered that the approach using the natural photosynthesis is suitable for the early realization of the renewable chemicals and fuels production by the sunlight energy.

Objectives of this dissertation

In this study, to enhance the isoprenoid productivity in the cyanobacterium *Synechocystis* sp. strain PCC 6803, the MEP pathway was modified and analyzed. In Chapter 2, the first enzyme of MEP pathway, DXS was overexpressed in *Synechocystis* PCC 6803 and determined the differences in the carotenoids, total sugars, total fatty acids and total proteins contents between wild type strain (WT) and DXS overexpressing strain (DXS_ox). In Chapter 3, the isoprene synthase (IspS) was introduced to *Synechocystis* PCC 6803 and the isoprene productivity was estimated. The accumulation levels of IspS and DXS in IspS expressing strains were also analyzed. In Chapter 4, to explore the DXS with the high activity and high stability, 11 *dxs* genes from 9 organisms in *E. coli* were expressed and analyzed their activity and stability. Chapter 5 summarizes this work and discusses areas for future research.

Isoprenoids

Isoprenoids are a diverse group of naturally synthesized compounds found in bacteria, fungi, animals, and plants. The more than 30,000 isoprenoids identified to date have a wide range of functions. The isoprenoids include many useful compounds with extensive applications (6-8). For example, Taxol (paclitaxel), which is an isoprenoid isolated from the *Taxus brevifolia* Pacific yew tree, is a potent anticancer drug. Artemisinin from *Artemisia annua* is one of the most effective antimalarial. Astaxanthin, which is a red color carotenoid, has remarkable antioxidative activity, utilized as a dietary supplement and cosmetic. Botryococcene, which is a hydrocarbon produced by

Botryococcus Braunii, is also a mainly composed of isoprenoids, promised as a biofuel. Other than the above, many isoprenoids are used in a wide range of fields. Therefore, they are industrially valuable compounds. Although isoprenoid products are currently obtained mainly through organic synthesis and plant extract, the yield is generally much lower. Therefore, the production using genetically modified organisms is expected to be an economical and environmentally friendly option.

Biosynthesis of isoprenoid

All isoprenoids are biologically synthesized from two common building blocks, isopentenyl diphosphate (IPP) and dimethylallyl diphosphate (DMAPP) (Fig. 1-1), which are produced via the 2-*C*-methyl-D-erythritol-4-phosphate (MEP) pathway in bacteria, cyanobacteria, algae, and plant chloroplasts (Fig.1-2). The MEP pathway involves eight enzymes and utilizes pyruvate and D-glyceraldehyde-3-phosphate (D-GAP) as starting materials; the first step of this pathway is catalyzed by 1-deoxy-D-xylulose 5-phosphate synthase (DXS), which was considered a rate limiting enzyme (9-11). In eukaryotes including plant cytosol, IPP and DMAPP are synthesized via the mevalonate (MVA) pathway (12), which involves seven enzymes; this pathway utilizes three molecules of acetyl-coenzyme A (acetyl-CoA) as the primary precursor and proceed until the production of IPP and DMAPP. The isoprenoids synthesis starts by head to tail condensation of one molecule of IPP and DMAPP, generating one molecule of geranyl diphosphate (GPP; C10) (Fig.1-3). The second molecule of IPP then condenses with GPP to form farnesyl diphosphate (FPP; C15). The further addition of IPP to FPP results in geranylgeranyl pyrophosphate (GGPP; C20). The GPP, FPP, and GGPP are used as a precursor of monoterpene, sesquiterpene and diterpene. The condensation of two FPP molecules results in the tripterpene (C30). The condensation of two GGPP molecules is the first committed step for the production of carotenoids, C40 tetraterpenes.

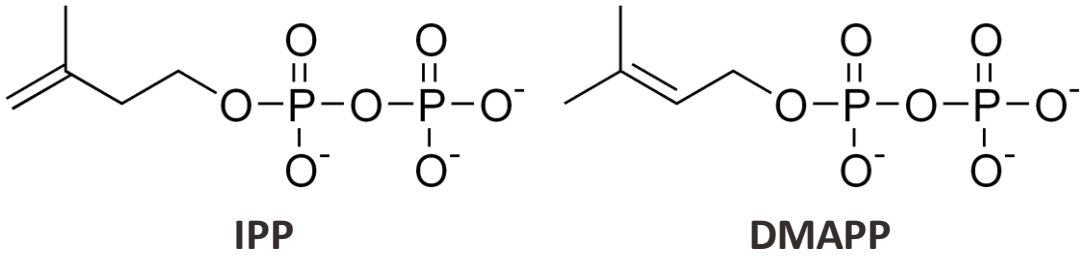

Fig. 1-1. The two common building blocks of isoprenoid, isopentenyl diphosphate (IPP) and dimethylallyl diphosphate (DMAPP).

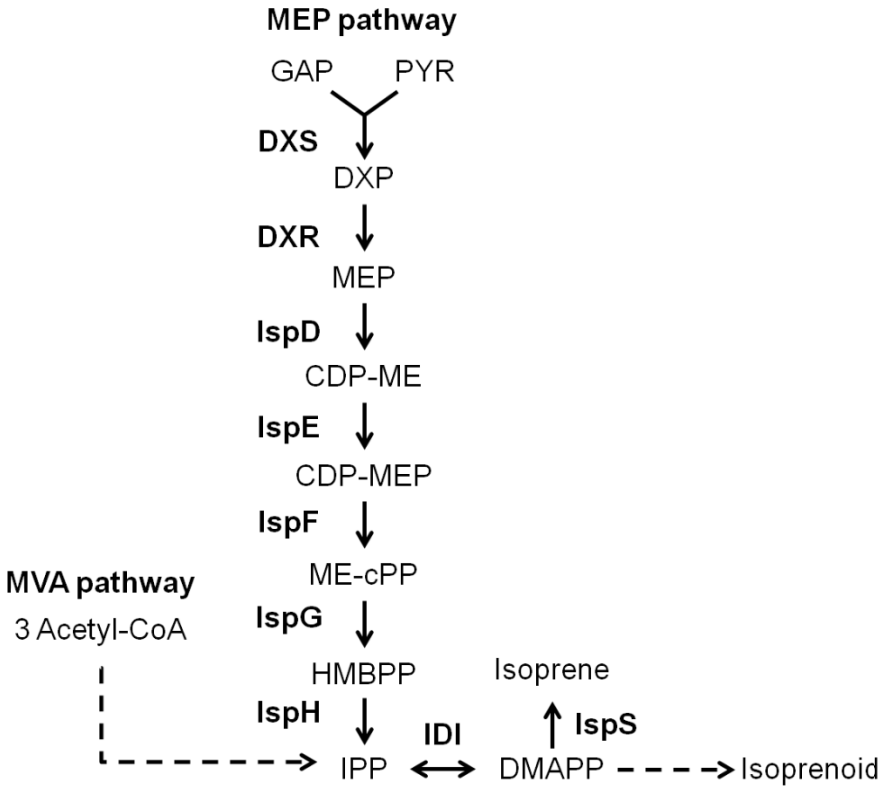

Fig. 1-2. The MEP and MVA pathway.
GAP: glyceraldehyde-3-phosphate; PYR: pyruvate; DXP: 1-deoxy-Dxylulose 5-phosphate; MEP: 2C-methyl-D-erythritol 4 phosphate; CDP-ME: 4-diphosphocytidyl-2C-methyl D-erythritol; CDP-MEP: 4-diphosphocytidyl-2C-methyl D-erythritol 2-phosphate; ME-cPP: 2Cmethyl-D-erythritol 2,4- cyclodiphosphate ; HMBPP: (E)-4-hydroxy-3-methylbut-2-enyl diphosphate ; IPP: Isopentenyl diphosphate; DMAPP: dimethylallyl diphosphate; DXS: 1-deoxy-D-xylulose 5-phosphate synthase; DXR: 1-deoxyxylulose-5-phosphate reductoisomerase; IspD: 4-diphosphocytidyl-2C-methyl-Derythritol synthase; IspE: 4-diphosphocytidyl-2-C-methylerythritol kinase; IspF: 2-C-methyl-D-erythritol 2,4-cyclodiphosphate synthase; IspG: 1-hydroxy-2-methyl-2-(E)-butenyl 4-diphosphate synthase; IspH: 1-hydroxy-2-methyl-2-(E)-butenyl 4-diphosphate reductase; IDI: isopentenyl diphosphate isomerase; IspS: isoprene synthase.

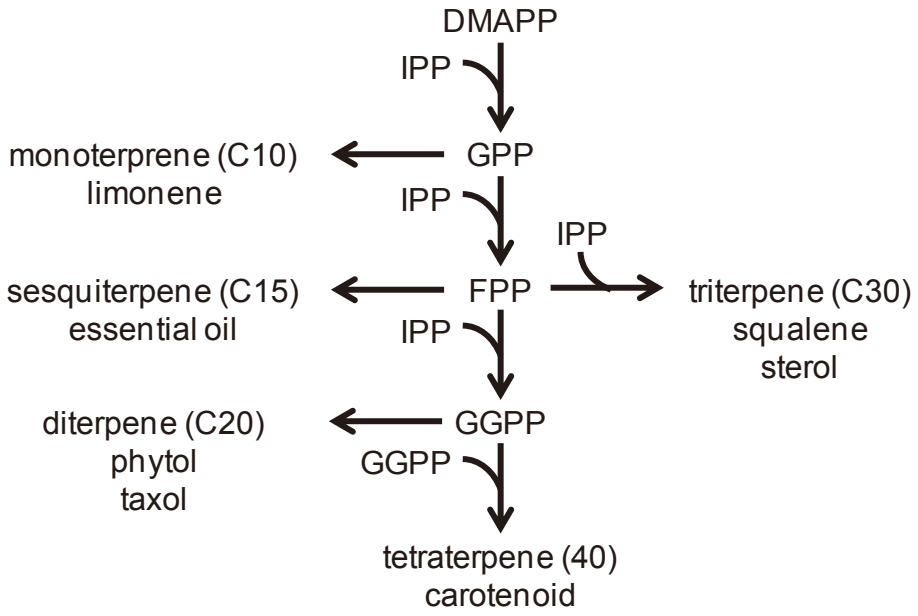

Fig. 1-3. The biosynthesis of isoprenoids.

Cyanobacteria

Cyanobacteria are not only widely used as model phototrophs for basic biological studies but are also attractive candidates for use in bioindustrial applications because of their high photosynthetic capability. Cyanobacteria can convert captured solar energy into biomass in the field at efficiencies that generally exceed those of terrestrial plant (3–9% for cyanobacteria compared with <0.25–3% for terrestrial plants) (13, 14). Many attempts have been made using cyanobacteria to produce valuable bioindustrial compounds from CO_2, for example, alcohols (15-19), aldehyde (20), fatty acids (and their derivatives) (21-25), hydrogen (26-30), formic acid (31), sugars (32-34), polyhydroxyalkanoates (and precursors) (35-44), and also isoprenoids (45-47). However, the yields of the desired products are often much lower than the theoretical yield or the total biomass. In some previous studies using *Escherichia coli* (6, 48, 49), the enhancement of isoprenoid productivity was achieved by the engineering of the MEP pathway. However, in cyanobacteria, the engineering of MEP pathway has remained untouched.

CHAPTER 2

Prerequisite for highly efficient isoprenoid production by cyanobacteria discovered through the over-expression of 1-deoxy-d-xylulose 5-phosphate synthase and carbon allocation analysis

Introduction

Cyanobacteria are not only widely used as model phototrophs for basic biological studies but are also attractive candidates for use in bioindustrial applications because of their high photosynthetic capability. Cyanobacteria can convert captured solar energy into biomass in the field at efficiencies that generally exceed those of terrestrial plant (3–9% for cyanobacteria compared with <0.25–3% for terrestrial plants) (13, 14). Many attempts have been made using cyanobacteria to produce valuable bioindustrial compounds from CO_2, for example, alcohols (15-19), aldehyde (20), fatty acids (and their derivatives) (21-25), hydrogen (26-30), formic acid (31), sugars (32-34), polyhydroxyalkanoates (and precursors) (35-44), and isoprenoids (45-47). However, the yields of the desired products are often much lower than the theoretical yield or the total biomass.

The strategies used in previous attempts can be largely divided into three categories: (i) optimization of cultivation conditions (17, 33-39, 41, 42, 44), (ii) reengineering of the light reaction (photosystems and light harvesting systems) (30, 50) and dark reaction (Calvin cycle, especially ribulose 1,5-bisphosphate carboxylase/oxygenase) (20, 51, 52), and (iii) rerouting of carbon flux (metabolic engineering). In many cases, metabolic engineering efforts have been directed towards basic studies for (iii), because naturally-occurring cyanobacteria are not optimized for the production of the desired product. Previous metabolic engineering studies have examined several aspects, including the design of artificial pathways for desired product (15-25, 31, 32, 34, 44-46), the optimization of expression levels of the enzymes required for synthesis (25, 33, 44-46), the

enhancement of cofactor or reductants supplies (30, 32, 53), circumvention of feedback inhibition (22), the destruction of competing processes (18, 22, 25, 26, 30, 34, 44), genome-wide searches of genetic targets affecting productivity or cell growth (40, 43), and protein engineering (17, 28, 31). However, little is known about how the overall carbon flux in cyanobacteria is influenced by such gene manipulations. Based on previous reports, Ducat et al. (54) estimated that even in the remarkable studies, only 5-6% of the carbon fixed through photosynthesis is used for the synthesis of the desired products, suggesting that there is plenty of room for improvement.

Why is the synthesis of the desired products so restricted in cyanobacteria? In comparison, the efficiency of the conversion of glucose into lactic acid by engineered yeast is often 80%, and other metabolically engineered organisms operate at 25-50% of the theoretical maximum efficiency (54). There are many possible causes, for example, rapid degradation of the products, rapid inactivation of the enzymes responsible for synthesis, strong competing pathways, not enough space to store the products in the cell, not surplus carbons to accumulate the products due to exhaustion the construction of cell architecture and photosynthesis apparatus, and so on. These possibilities should be examined before attempting to optimize a particular pathway. In this study, we focused on the cyanobacterial production of isoprenoids, and aimed to find strategies to design a robust production system by considering above possibilities.

Isoprenoids are derived from two common building blocks, isopentenyl pyrophosphate (IPP) and dimethylallyl pyrophosphate (DMAPP), which are synthesized via the 2-C-methyl-D-erythritol-4-phosphate (MEP) pathway in bacteria and cyanobacteria (55-59) (Fig. 2-1). Isoprenoids are a diverse group of compounds that have extensive applications as biofuels, chemical precursors, pharmaceutical and in aromatherapy (6, 8, 60). Although isoprenoids are industrially produced mainly through organic synthesis and extraction from plants, biosynthesis using genetically modified organisms is expected to be a more economical and environmentally

friendly way to produce isoprenoids.

Pioneering studies have been conducted to improve the production of isoprenoids in *Escherichia coli* (*E. coli*) (6, 48, 49, 60, 61). In the latest report, Zhao et al (62) successfully produced 2.1 g/L of β-carotene with a yield of 60 mg/g DCW after 50-60 hours of cultivation. They first introduced an exogenous β-carotene synthetic gene operon and increased the supply of IPP and DMAPP by optimizing the expression levels of two key genes in the MEP pathway, 1-deoxy-D-xylulose-5-phosphate synthase (*dxs*) and isopentenyl diphosphate isomerase (*idi*). Then the best yield (2.1 g/L of culture, 60 mg/g DCW) was achieved by modulating genes involved in ATP synthesis, the pentose phosphate pathway and the TCA cycle.

In cyanobacteria, carotenoids are vigorously produced and mainly accumulate in the thylakoid membranes where the light reactions of photosynthesis occur (59). Therefore, it has been suggested that these compounds perform important functions in photosynthesis. β-Carotene and several xanthophylls are the constituents of functional multiprotein complexes, such as photosystems I and II (PSI and PSII), cytochrome b_6/f complexes, and the light-harvesting complexes involved in photosynthetic electron transport. In addition, carotenoids are thought to play important roles in quenching reactive oxygen species, dissipating excess light energy, and maintaining proper cellular architecture, among others (63-65). Therefore, cyanobacteria are excellent isoprenoid producers and powerful and practical isoprenoid production may be realized by applying the findings from metabolic engineering studies. We prepared a recombinant *Synechocystis sp.* PCC6803 (*S.* 6803) strain, in which a rate-limiting enzyme in the MEP pathway, 1-deoxy-D-xylulose 5-phosphate synthase (DXS), is over-expressed, and determined the differences in the carotenoids, total sugars, total fatty acids and total proteins contents. Based on the results, we discussed a strategy for the design of cyanobacterial isoprenoid production systems.

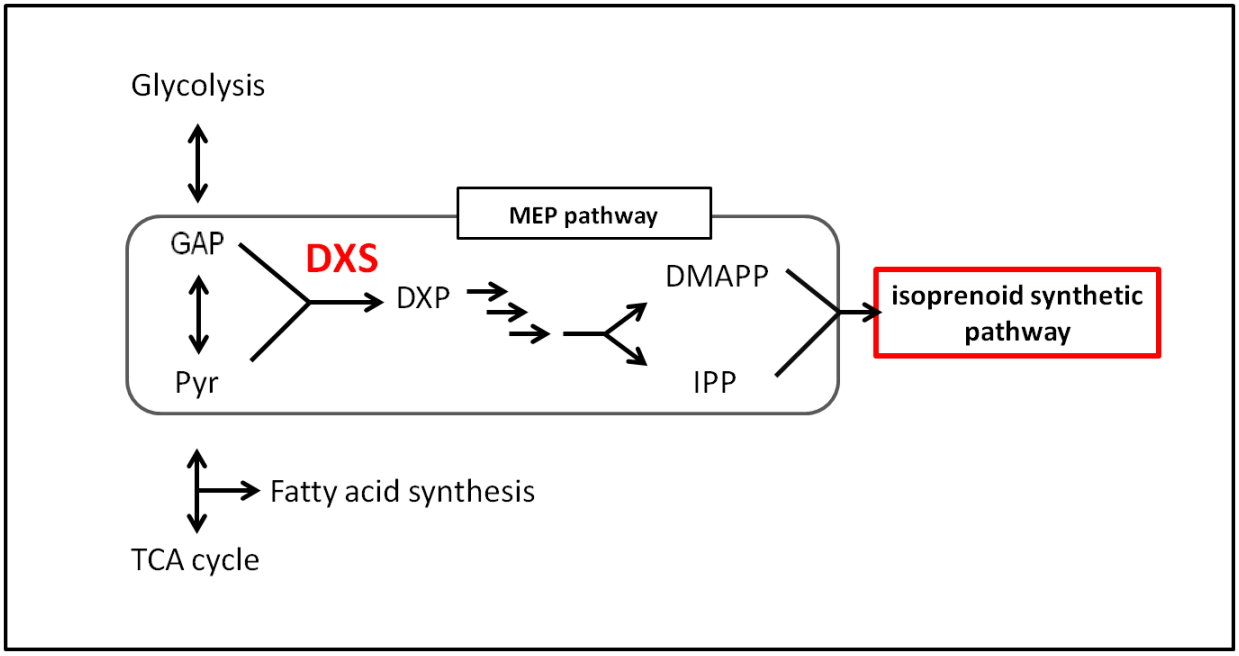

Fig. 2-1. The MEP pathway.
G3P, Glyceraldehyde 3-phosphate; Pyr, pyruvic acid; DMAPP, dimethylallyl pyrophosphate; IPP, isopentenyl pyrophosphate.

Materials and methods

Strain and growth conditions

S. 6803 was cultivated at 25°C in BG-11 medium (66) buffered with 5 mM TES-NaOH (pH 8.0), at a photon flux density of 20 or 200 μmol of photons·m^{-2}·s^{-1}, and bubbled with air. BG-11 medium was supplemented with 20 μg/mL of kanamycin for kanamycin-resistant strains. The optical density at 730 nm (OD_{730}) and UV-visible absorption spectra were measured using a UV-VIS spectrophotometer (model UV-1800; Shimadzu, Kyoto, Japan).

Plasmids

To generate a plasmid to replace *psbA2*, which encodes one of three photosystem II D1 homologs (PsbA1, PsbA2 and PsbA3) and can be safely used for an integration site, with *dxs*, three fragments were amplified from the *S.* 6803 genomic DNA; a 500-bp fragment upstream of *psbA2*, a 500-bp fragment downstream of *psbA2*, and *dxs* using the primers shown in Table 2-1. These three DNA fragments, together with a kanamycin resistance cassette, were inserted into pUC19 (TaKaRa BIO, Otsu, Japan) linearized with *Hind*III and *Eco*RI in the following order: *psbA2* upstream fragment → *dxs* → kanamycin resistance cassette → *psbA2* downstream fragment using the In-fusion cloning kit (TaKaRa BIO). The resulting plasmid, pPSBA2_dxs, was used to replace the *psbA2* gene in the *S.* 6803 genome with the *dxs* gene via double homologous recombination. (Fig. 2-2). To over-express a C-terminal His-tagged DXS protein, the *dxs* gene was cloned into pET22b (Merk, Whitehouse Station, NJ) as an *Nde*I and *Not*I fragment, to construct pET_dxs-his.

Table 2-1. Primers used in CHAPTER 2

Primers	seaequence
psbA2_up_f	5’ TTCGCTGATGTGCATATGGTTATAATTCCTTATGTATTTGTCGATG 3’
psbA2_up_rv	5’ TTCGCTGATGTGCATATGGTTATAATTCCTTATGT 3’
Dxs_f	5’ ATGCACATCAGCGAACTGAC 3’
Dxs_rv	5’ TTGATCAGATCTTGACTAACTAACTCCAGGAGCG 3’
ntp_f	5’ TCAAGATCTGATCAAGAG 3’
ntp_rv	5’ GCATTGCGTTCGTGCTCAGAAGAACTCGTCAAG 3’
psbA2_down_f	5’ GCACGAACGCAATGCCCAC 3’
psbA2_down_rv	5’ ACCATGATTACGCCACCGAGCTTTCTTTGCCGCAG 3’
Dxs_f_pET22b	5’ AAAACATATGCACATCAGCGAACTGACCCA 3’
Dxs_rv_pET22b	5’ TTTTGCGGCCGCACTAACTCCAGGAGCGACAA 3’
6803_dxs_RT_PCR_F	5’ CTCCCAAGGATGAAGCAGAG 3’
6803_dxs_RT_PCR_R	5’ TTACCAATTTCCAGCGGTTC 3’
6803_rnn16S_RT_PCR_F	5’ CAGCTCGTGTCGTGAGATGT 3’
6803_rnn16S_RT_PCR_R	5’ CGTAAGGGGCATGATGACTT 3’

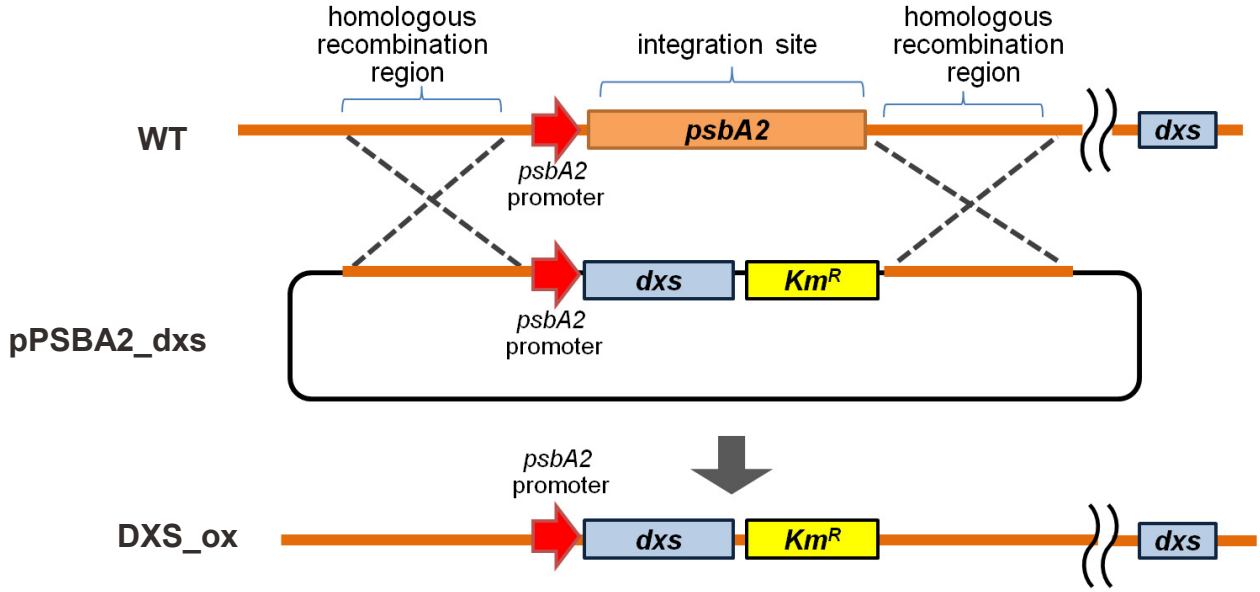

Fig. 2-2. Generation of a DXS over-expressing strain by integrating the *dxs* gene in the *S. 6803* genome. The DXS over-expressing strain of *S.* 6803 was constructed by using the *psbA2* gene as the integration site for the introduction of the *dxs* gene and a kanamycin resistance gene. This integrated construct allows the *dxs* gene to be controlled under the *psbA2* promoter.

Transformation of *S.* 6803

S. 6803 was grown in liquid BG-11 medium until the cell density reached an OD_{730} of approximately 1.0. The cells were concentrated 10-fold by centrifugation. The concentrated cell suspension (500 μL) was spread on cellulose mixed ester filters (0.45μm; Merk), which were placed on BG-11 agar plates. Then, 100 ng of plasmid DNA was spotted on the filter, and incubated at 25°C under low light (10 μmol of photons·m^{-2}·s^{-1}) for 24 h. The filter was transferred to a selective BG-11 plate containing 20 μg/mL kanamycin and incubated at 25°C in the light (20 μmol of photons·m^{-2}·s^{-1}). Single colonies were isolated after about 2 weeks, and these were inoculated into BG-11 liquid medium for analysis.

Dxs-His protein purification

E. coli BL21(DE3) cells (TaKaRa BIO) were transformed with pET_dxs-his to overproduce His-tagged DXS (DXS-His). Cells were grown in 700 mL of Luria-Bertani medium (Nacalai Tesque, Kyoto, Japan) at 37°C. Expression was induced with 0.5 mM isopropyl β-D-thiogalactopyranoside (Nacalai Tesque), and incubation was continued overnight at 30°C. The cells were then harvested by centrifugation at 5.000 g for 7 min at 4°C, resuspended in 25 mL of A buffer (50 mM Tris-HCl, pH 7.6, and 500 mM NaCl), and lysed by sonication. To remove the cell debris, the cell lysate was centrifuged at 12,000 g for 5 min at 4°C. The supernatant was mixed with 2 mL of COSMOGEL His-Accept (Nacalai Tesque), equilibrated with A buffer, and incubated for 10 min at 4°C. The slurry was poured into a column (1 × ϕ3 cm), and the flowthrough was discarded. After washing with A buffer, DXS-His was eluted with B buffer (50 mM Tris-HCl, pH 7.6, 500 mM NaCl, and 500 mM imidazole). Fractions containing DXS-His were pooled, and analyzed by SDS-PAGE (Fig. 2-3). The buffer in the purified protein was exchanged for phosphate buffered saline by using an Amicon Ultra 15 (Merk). The DXS-His protein solution was then send to antibody production services company (ITM, Matsumoto, Japan) to generate anti-DXS polyclonal rabbit antibody.

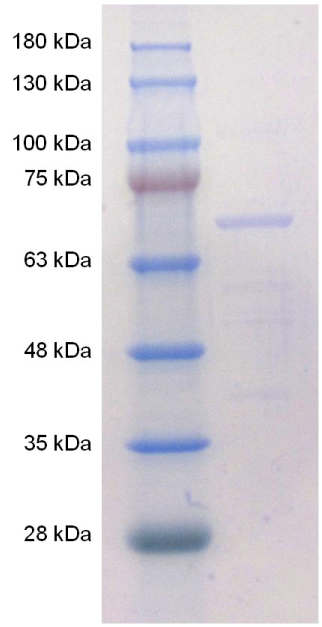

Fig. 2-3. The SDS-PAGE analysis of the purified DXS-His**.** The DXS-His protein was purified from *E. coli* BL21(DE3) cells by using affinity carrier. Purified product was loaded on an SDS gel containing 10% acrylamide. Proteins were visualized by staining with Coomassie brilliant blue. The excepted molecular weight of the DXS protein is 69.3 *k*Da.

Real-time quantitative PCR

Transcriptional levels of the *dxs* gene were determined by real-time quantitative PCR (qPCR). Total RNA was isolated by using TRIzol reagent (Invitrogen, Carlsbad, CA), according to the manufacturer's instructions. The cDNA was prepared by using the ReverTra Ace qPCR RT Master Mix (TOYOBO, Otsu, Japan). The qPCR experiment was performed on a StepOne cycler (Applied Biosystems, Foster City, CA) using the KAPA SYBR FAST qPCR Kit Master Mix (2×) Universal (Kapa Biosystems, Woburn, MA). The transcriptional level of the *rrn16S* gene was used as an internal standard to normalize the qPCR values. Table 2-1 shows the primers used for qPCR.

SDS-PAGE and western blot analysis

For the western blot analysis, *S.* 6803 crude extracts were prepared by bead beating the cells in Tris-NaCl buffer (50 mM Tris-HCl, pH 7.6, and 500 mM NaCl) with a Protease Inhibitor Cocktail (Nacalai Tesque). After bead-beating, the insoluble material was removed by centrifugation. Then, the soluble fractions were separated by 10% SDS-PAGE, blotted onto PVDF membranes (Merk), and probed sequentially with a primary specific polyclonal antibody and a goat anti-rabbit IgG-Horse radish Peroxidase conjugate (Santa Cruz Biotechnology, Santa Cruz, CA) as a secondary antibody. The protein bands were visualized by using Pierce Western Blotting Substrate (Thermo Scientific, Waltham, MA) following the manufacturer's instructions.

Carotenoid analysis

Carotenoids were extracted from the cells with an acetone:methanol solution (7:2, v/v). After centrifugation, the pellet was discarded and the supernatant was evaporated under nitrogen gas. The dried carotenoids were dissolved in ethanol and filtered using a MS PTFE syringe filter (0.22 μm, Merk). Carotenoids were separated on a Xbridge C18 column (150 mm × ϕ4.6 mm, 3.5 μm,

Waters, Milford, MA) by high-performance liquid chromatography (HPLC) (Prominence; Shimadzu), using a 15-min gradient of ethyl acetate (0%–100%) in acetonitrile:water:triethylamine (9:1:0.01, v/v/v) at a flow rate of 1.5 mL/min. The absorption data 440 nm of the eluate were recorded. Carotenoid species were identified by comparing to the chromatograms from a previous study (67). The content of each carotenoid was calculated by using a β-carotene standard curve and the molar extinction coefficients (68).

Total fatty acids analysis

Lipids were extracted from a lyophilized *S.* 6803 pellet with chloroform:methanol (2:1), according to the Folch method (69). We added 3 mL of chloroform:methanol to the lyophilized sample and vortexed the mixture for 24 h at room temperature. Then, 100 μg of nonadecanoic acid (19:0) (Nacalai Tesque) was added to each sample as internal standard to normalize the yield in the subsequent procedures. After removing the insoluble matter by centrifugation, the solvent was removed with an evaporator, while maintaining the evaporation temperature below 40°C. The residue in the evaporator, containing lipids, was dissolved in 0.40 mL of toluene, and then 3.0 mL of methanol and 0.60 mL of an 8.0% HCl solution in methanol were added in this order. One third of the mixture was transferred to a screw top glass bottle and incubated at 45°C for at least 40 h. After incubation, 1 mL of hexane and 0.2 mL of water were added to extract the fatty acid methyl esters (FAMEs) into hexane. The hexane layer was analyzed by a gas chromatograph (Shimadzu GC 2014) equipped with an Rxi-5ms capillary column (15 m × ϕ0.25 mm, 0.20 μm) and a flame ionization detector (FID). The operating conditions were as follows: split ratio 1:5; inject volume 2 μL; helium carrier gas with a constant linear velocity of 49.6 cm/s; H_2 55 mL/min, air 40 mL/min, make up gas (helium) 80 mL/min; injector temperature 250°C; detector temperature 330°C; and initial oven temperature 140°C (for 1 min) increased at a rate of 4°C/min to 220°C. The peak assignments were

determined by comparing to the retention times of each standard. The concentration of each fatty acid was determined based on the calibration curve prepared by using various concentrations of C16:0 standards.

Total sugar analysis

The total sugar content was measured by the phenol-sulfuric acid method using a glucose standard (70). S.6803 pellets (from 10-mL culture) were suspended in 200 μL of water and 200 μL of a 5% phenol aqueous solution (w/v) in a glass test tube, and then 1 mL of concentrated sulfuric acid was added. The suspension was vortexed and incubated at room temperature for 30 min. The absorbance at 490 nm was measured with a spectrophotometer (Nanophotometer, Implen GmbH, München, Germany).

Soluble sugar composition

The TLC was used to analyze the composition of the soluble sugars. For the TLC analysis, the soluble fraction was extracted from the cell lysate obtained by bead beating, which was then divided into two; one half was treated with glucoamylase (1 unit/mL) at 60°C and for 60 min, and the other half was incubated in the same way without glucoamylase. To remove the proteins, the samples were heated at 95°C and for 5 min and then centrifuged. The supernatant was concentrated with an evaporator and then applied to a TLC plate (TLC aluminum sheets, 20 cm × 20 cm, Silica gel 60 F254; Merk). Sugars were separated by using a solvent system consisting of 1-butanol:2-propanol:ethanol:water (3:2:3:2). The sugar spots were visualized by spraying with sulfuric acid solution [4% (w/v) H_2SO_4 in methanol] and heating the plates at 100°C for 5 min.

Glycogen assay

Intracellular glycogen accumulation was measured by using a glucose assay with enzymatic coloration. *S.* 6803 pellets (from a 10-mL culture) were suspended in methanol, homogenized by sonication, and centrifuged. The pellet was resuspended in water and sonicated again. The suspension was incubated at 100°C for 40 min. After a second centrifugation, the supernatant was used as an intracellular sugar extract. The extract was divided into two 50-μL aliquots. To one aliquot, 49 μL of 50 mM acetate buffer (pH 4.5) and 1 μL of glucoamylase (200 units/mL) were added and the mixture was incubated at 60°C for 60 min to promote the glycolytic reaction, which converts glycogen to glucose. Another aliquot was incubated in the same way except that glucoamylase was not added. Both aliquots were then incubated at 95°C for 2 min to inactivate the enzyme. Next, 50 μL of glucose assay solution (5 μL of glucose oxidase, 1 μL of peroxidase, and 44 μL of substrate solution [10 mM sodium citrate, 1.6 mM 3,3',5,5'-tetramethylbenzidine·2 HCl, 20% N,N-dimethylformamide, and 1.25% polyethylene glycol 4,000)] was mixed with 50 μL of the aliquot. The mixtures were incubated at 37°C for 60 min. The reaction was stopped by adding 50 μL of 1.5 M phosphate solution. The absorbance at 450 nm of the reaction solution was measured by using a microplate reader (Model 680; Bio-Rad). The amount of glucose was determined using a glucose standard curve. The amount of glycogen was estimated by subtracting the amount of glucose in the control aliquot from that in the treated aliquot.

Protein assay

S.6803 pellets (from a 5-mL culture) were suspended in 2.5 mL water and sonicated on ice for 4 min, and then centrifuged at 15,000 rpm for 5 min. The soluble fraction was used for the subsequent protein assay directly, whereas the insoluble fraction was subjected to the assay after solubilization using B-PER Reagent (Thermo Scientific). The protein concentration was determined by using the Pierce BCA Protein Assay Kit Reagent (Thermo Scientific), according to the

manufacturer's Enhanced Protocol. Extracted proteins were also separated on SuperSep™ Ace gradient SDS-polyacrylamide gels (WAKO). The protein bands were visualized with the Rapid Stain CBB kit (Nacalai Tesque) and the Sil-Best Stain-Neo for Protein and Nucleic Acid/PAGE (Nacalai Tesque). The band quantification was performed using ImageJ software (http://rsbweb.nih.gov/ij/index.html).

Transmission electron microscopy

The samples were immersed in 2% paraformaldehyde and 2.5% glutaraldehyde in 0.1 M phosphate buffer (pH 7.4) for 15 min, postfixed in 1% osmium tetroxide (OsO_4) for 15 min, dehydrated through a graded series of ethanol and embedded in Plain Resin (Nisshin EM, Tokyo, Japan). After polymerization of the resin, ultra-thin sections (60 nm) were obtained using an ultramicrotome (Super Nova; Reichert-Jung, Vienna, Austria), mounted on 200-mesh cupper grids (Nisshin EM), stained with 10% (v/v) TI Blue (Nisshin EM) and 2% (w/v) lead citrate and observed under a transmission electron microscope (JEM-1400; JEOL, Tokyo, Japan). The areas of the cell sections and granules were measured with Image J.

Results

The DXS over-expressing strain

A DXS over-expressing strain of *S*. 6803 was generated after homologous recombination between the *psbA2* gene in the genome and the *psbA2* gene fragments flanking the *dxs* gene on the integrated suicide plasmid (Fig. 2-2). This DXS overexpressing strain of *S*. 6803 (DXS_ox) was isolated on selective solid medium. The DXS_ox strain possesses two *dxs* genes, one is its normal location in the genome and a second, newly introduced *dxs* gene downstream of the *psbA2* promoter, a strong, light-dependent promoter. No band corresponding to the original *psbA2* gene was observed in the DXS_ox strain by PCR using primers upstream and downstream of *psbA2*, confirming the complete segregation in the DXS_ox strain. The *dxs* gene fragment amplified from the genome of the DXS_ox strain was confirmed by DNA sequencing.

The photo-autotrophic growth rates of the WT and the DXS_ox strains were evaluated by measuring the optical density at 730 nm (OD_{730}). The strains were grown at two light intensities, 20 and 200 μmol of photons·m^{-2}·s^{-1} (referred to as LL and HL, respectively). The growth curves for the WT and DXS_ox strains in both light conditions were nearly identical (Fig. 2-4), indicating that the additional *dxs* gene had no significant influence on growth.

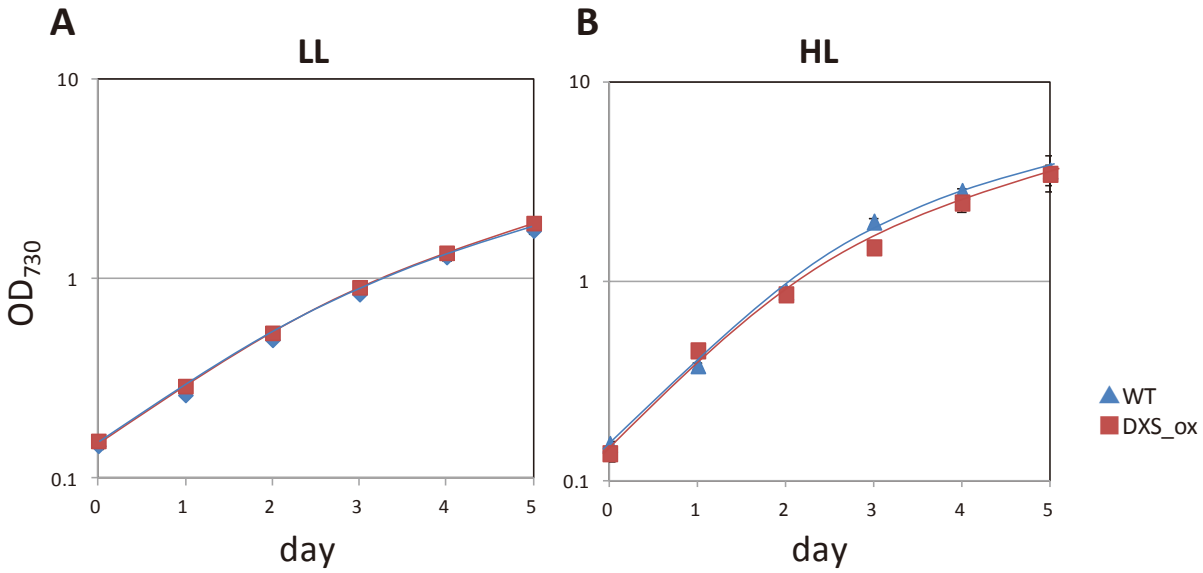

Fig. 2-4. Photo-autotrophic growth curves of the WT and the DXS_ox strain under LL (A) and HL (B). Data are mean ± SD for two replicates. (n=2)

Over-expression of the *dxs* gene

Real-time quantitative PCR (qPCR) was used to assess the mRNA expression of the *dxs* gene in the WT and DXS_ox strains. The relative mRNA levels normalized to that the level in the WT strain at OD_{730} = 0.4 under LL conditions are shown in Fig. 2-5. In all conditions, the mRNA levels in the DXS_ox strain were higher than those in the WT strain. However, we also observed that the mRNA levels in the DXS_ox strain reached a peak at OD_{730} = 0.4, and then declined sharply as the OD_{730} increased from 0.4 to 0.8, and remained at a low level thereafter.

Western blotting was performed to assess DXS protein expression. The ratios of the protein levels in the DXS_ox strain to those in WT strain under the same conditions are shown in Fig. 2-6. At an OD_{730} of 0.4 and 0.8, the DXS levels in the DXS_ox strain were 1.3–1.6-fold higher than those in the WT strain, whereas at an OD_{730} of 2.5, no significant differences were observed between the strains under either light conditions.

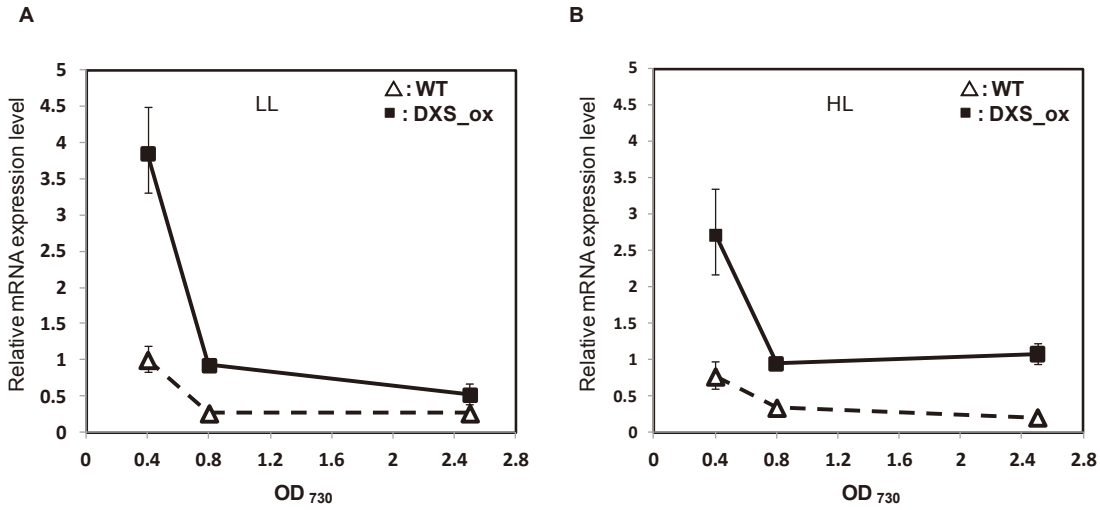

Fig. 2-5. The mRNA levels of the *dxs* gene. The mRNA levels of the *dxs* gene in the WT and DXS_ox strains under the low light (LL) (A) and high light (HL) (B) conditions were analyzed by qPCR. The relative mRNA levels were normalized to that in the WT strain at OD_{730} = 0.4 and under LL conditions. The data are the mean ± SD of three replicates (n = 3).

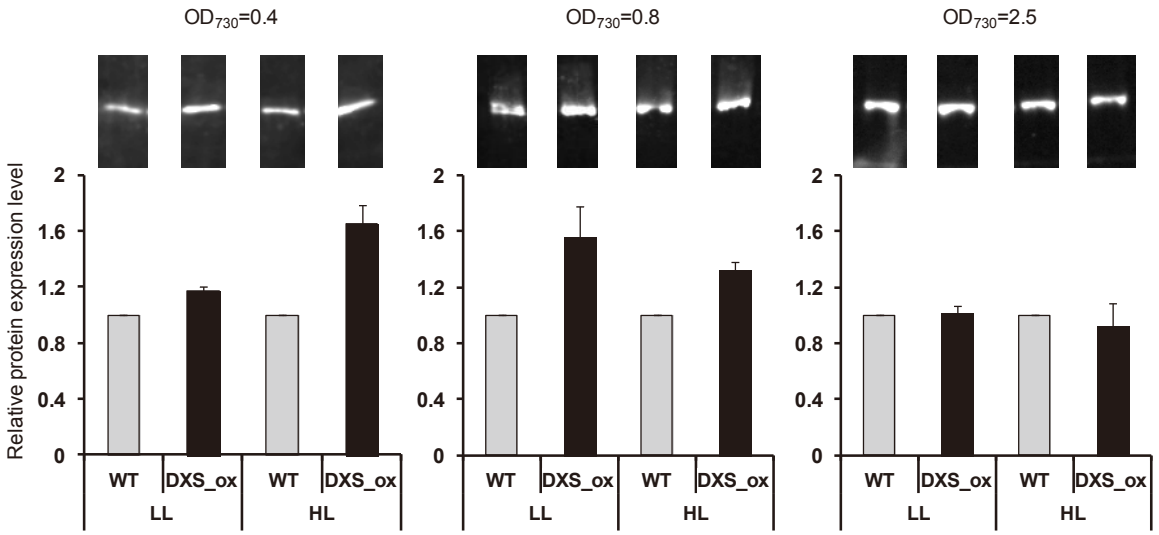

Fig. 2-6. **DXS protein expression.** The DXS protein expression levels in the WT and DXS_ox strains were confirmed by western blotting with an anti-DXS antibody. The ratios of the protein levels in the DXS_ox strain to that in the WT strain at the same condition are shown. The data are the mean ± SD of three replicates.

Carotenoid accumulation

Interestingly, we found an apparent difference between the WT and DXS_ox strains in the color of the cultures (Fig. 2-7). Indeed, as shown in Fig. 2-8, the absorbance at 450–500 nm of the DXS_ox strain grown to a density (OD_{730}) of 0.4 or 0.8 under HL conditions also was significantly higher than the corresponding absorbance of the WT strain. The 450–500 nm range overlaps with the absorbance band for carotenoids, strongly suggesting that the carotenoid content in the DXS_ox strain is significantly increased. We extracted the carotenoids from cells harvested at an OD_{730} of 0.4 and 0.8 under HL, and analyzed the carotenoid content by HPLC (Fig. 2-9). The concentration of each carotenoid was determined by using the following equation:

$$C_{car} = \left(\frac{E_{\beta ca}}{E_{car}} \times A_{car}\right) \times 0.000311 - 0.758$$

where C_{car} is the concentration (μg/mL) of a particular carotenoid in a particular extraction; $E_{\beta ca}$ and E_{car} are the extinction coefficients at 440 nm of β-carotene and a particular carotenoid, respectively; A_{car} is the peak area of a particular carotenoid in the chromatogram, which was recorded at 440 nm. Their relationship was estimated from a standard curve prepared using a β-carotene standard. The content of each carotenoid per dry cell weight (DCW) are shown in Fig. 2-10. All carotenoids we examined, except for myxoxanthophyll at OD_{730} = 0.4, were significantly higher in the DXS_ox strain than in the WT strain. Therefore, the total carotenoid content in the DXS_ox strain at OD_{730} = 0.8 (8.4 mg/g DCW) was 1.6-fold higher than that in the WT strain (5.6 mg/g DCW). It is worthwhile to note that the shift in the carotenoid content in cells growth to OD_{730} = 0.4 and 0.8 differ between the two strains. In the WT strain, increases in echinenone and β-carotene were observed instead of the decrease in myxoxanthophyll, whereas, in the DXS_ox strain, a increase in myxoxanthophyll and a decline in zeaxanthin were observed, resulting in a predominance of myxoxanthophylls in the DXS_ox strain at OD_{730} = 0.8, the largest difference (2.6-fold) between the two strains.

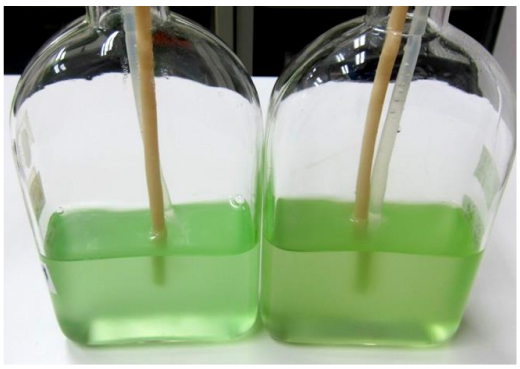

Fig. 2-7. The picture of the cultures. The left is the WT strain and the right is the DXS_ox strain. Their OD_{730} is 0.4.

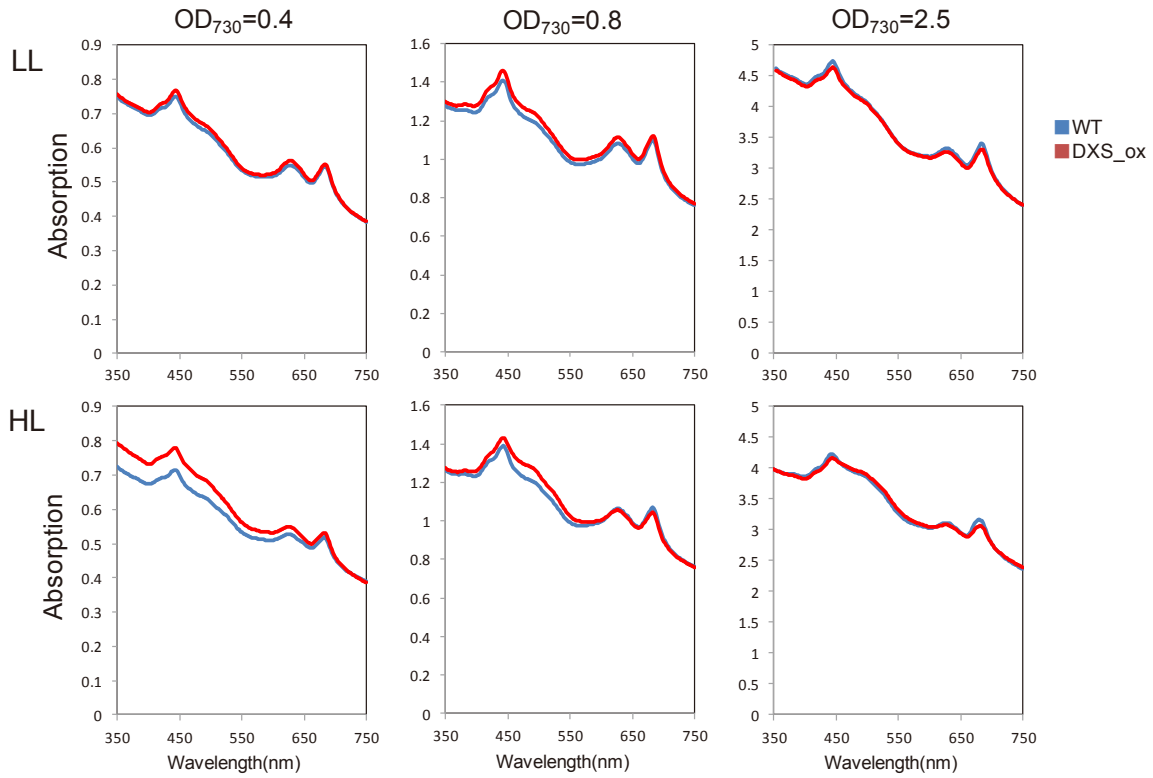

Fig. 2-8. The absorption spectra of the cultures of the WT (blue line) and DXS_ox (red line) strains.

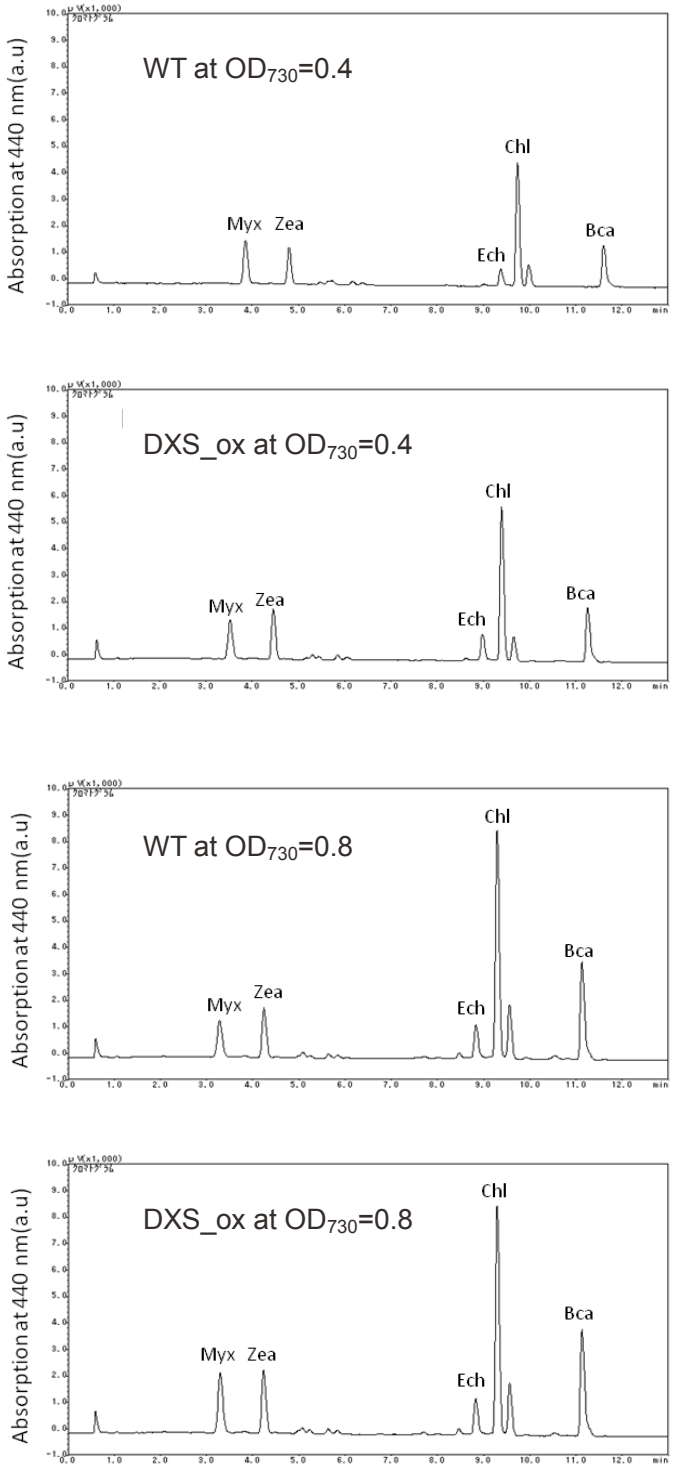

Fig. 2-9. HPLC analysis of pigments extracted from the WT and DXS_ox strains. Chromatograms were recorded as a function of the absorbance at 440 nm. Myx, Myxoxanthophyll; Zea, Zeaxanthin; Ech, Echienone; Chl, Chlorophyll; Bcar, B-carotene.

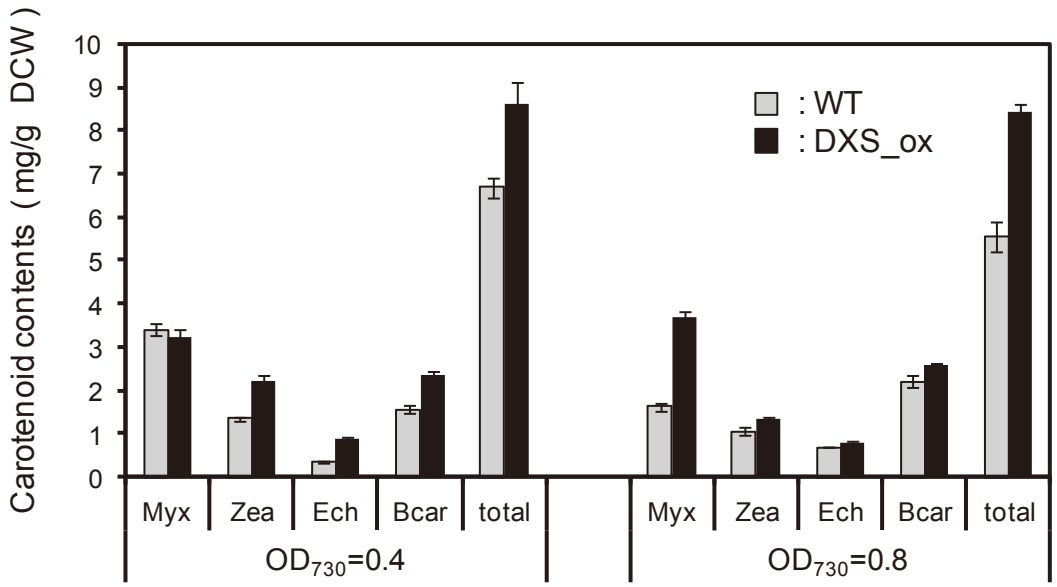

Fig. 2-10. Carotenoid contents. Carotenoids extracted from cells harvested at OD_{730} = 0.4 and 0.8 under HL conditions. The extracts were analyzed by HPLC. The data are the mean ± SD of three replicates (n = 3). Myx, Myxoxanthophyll; Zea, Zeaxanthin; Ech, Echinenone; and Bcar, β-carotene. DCWs at OD_{730} = 0.4 and 0.8 are shown in Fig. 2-11.

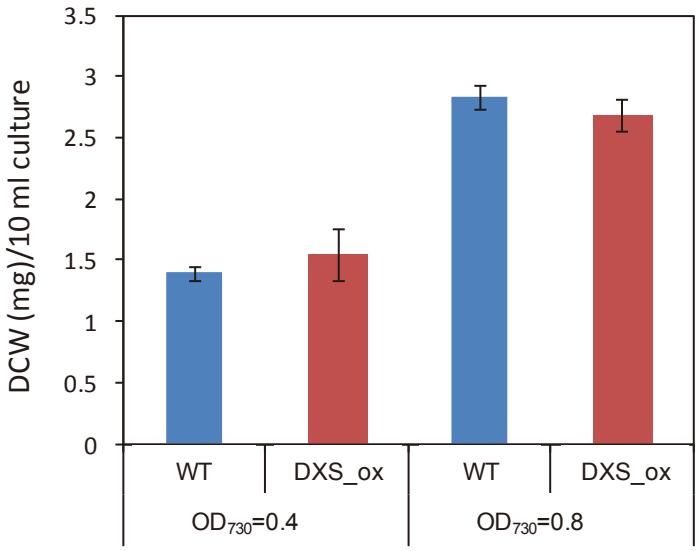

Fig. 2-11. Dry cell weights (DCW) at the different OD. The Pellets of the WT and DXS_ox strains from 50 mL of cultures were lyophilized and the weight were measured. Data are mean ± SD for four replicates. (n=4)

Lipid and sugar analyses

To examine the carbon localizations, the total sugars and total fatty acids were analyzed in the WT and DXS_ox strains at OD_{730} = 0.4 and 0.8 under HL. As described in the Material and Methods, total fatty acids were quantified by a GC assay using FAMEs forms of the extracted lipids. Peaks corresponding to six fatty acids, C16:0, C16:1, C18:0, C18:1, C18:2 and C18:3, which were considered to be main composition of fatty acids in S. 6803 (71), were identified by the retention time of each standard. The concentration of each fatty acid was determined based on a calibration curve prepared with various concentrations of C16:0 standards. The major fatty acids were C16:0 (~55% of the total fatty acids) in both strains (15 mg/g DCW) (Fig. 2-12). Other fatty acids present were C16:1 (7.7%), C18:0 (1.8%), C18:1 (6.0%), C18:2 (10%) and C18:3 (17.7%). The proportions of each fatty acid were similar in both strains under both light conditions. The total fatty acids content in the WT and DXS_ox strains at OD_{730} = 0.8 were 31 and 24 mg/g DCW, respectively (Fig. 2-13 and 12). The concentration of all fatty acids decreased by 10% ~21% in both strains as the OD_{730} increased from 0.4 to 0.8.

The total sugar content was quantified as glucose equivalents by the phenol sulfuric acid method using a glucose standard curve. The total sugar of the DXS_ox strain at OD_{730} = 0.4 (104 mg/g DCW) was approximately 30% lower than that of the WT strain (146 mg/g DCW) (Fig. 2-13). Next, the composition of soluble sugars was analyzed by TLC. In both strains, the supernatant of the lysate that was not treated with glucoamylase did not move from the starting point, except for a very weak, unidentified band (Fig. 2-14). This observation is essentially the same as that with the glycogen standard. In contrast, the glucoamylase-treated samples spots of both strains did migrate, leaving only a trace spot at the starting point, similar to glycogen standard, strongly suggesting that a large portion of the soluble sugars in S. 6803 is glycogen.

Then, the intracellular glycogen content was quantified by performing a glucose assay using

the glucoamylase-treated lysates. The glucose content in the treated and untreated lysates of the DXS_ox strain grown to an OD_{730} = 0.4 and 0.8 was below the limit of detection (>0.05 mg/g DCW) (Fig. 2-15). In contrast, the glucose content in the WT strain, treated with glucoamylase was estimated to be 0.21 and 0.37 mg/g DCW at OD_{730} = 0.4 and 0.8, respectively (Fig. 2-15). However, the content of the untreated lysates of the WT strain was also below the limit of detection. These observations indicate the following: (1) the concentration of free glucose was very low (>0.05 mg/g DCW) in our experimental conditions; (2) the WT strain accumulates glycogen in the cell and the content significantly increased when the OD_{730} increased from 0.4 to 0.8; (3) the DXS_ox strain does not accumulate glycogen.

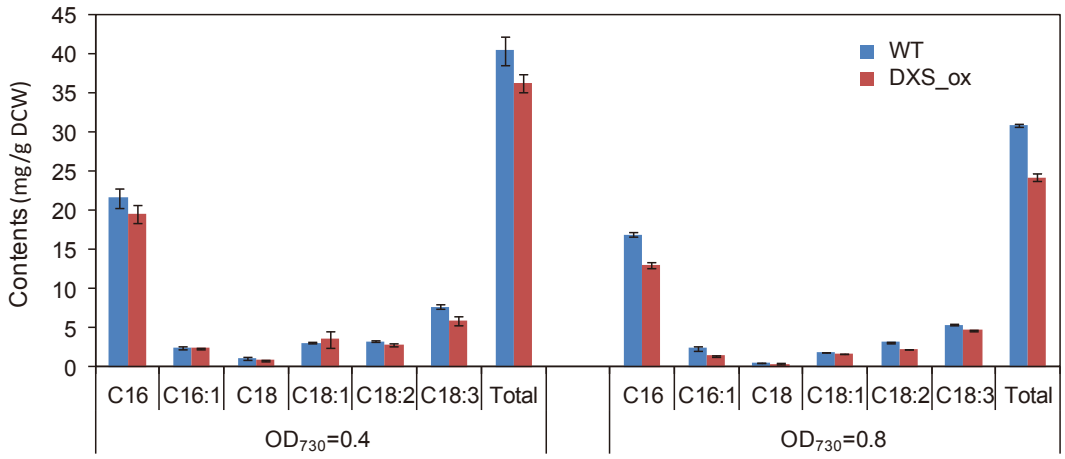

Fig. 2-12. The contents of various fatty acid analysis. Lipid extracted from the cells harvested at OD_{730}=0.4 and 0.8 and under the HL condition. The lipids were converted into FAME and analyzed by GC. Data are mean ± SD for three replicates. (n=3)

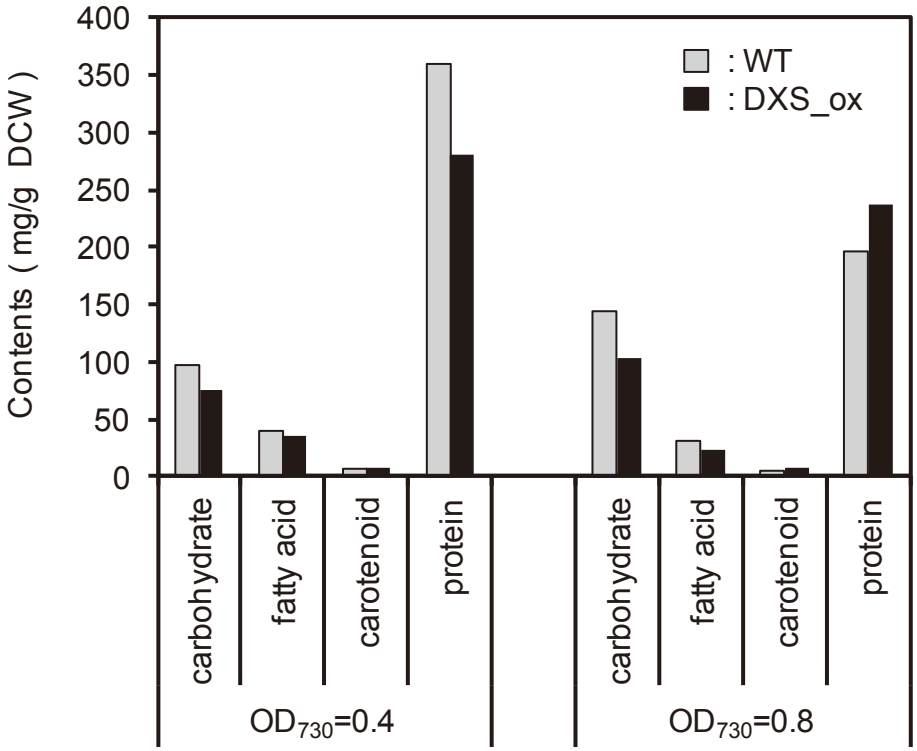

Fig. 2-13. Biomass components. The accumulation of total sugars, total fatty acids, total carotenoids, and total proteins in the WT and DXS_ox strains at OD_{730} = 0.4 and 0.8 under HL conditions was compared.

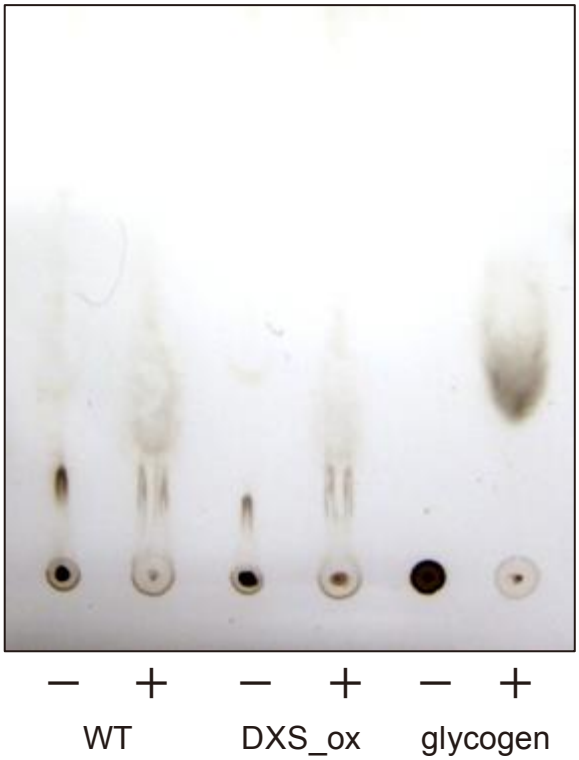

Fig. 2-14. The soluble sugar analysis. TLC was performed to analyze the composition of the soluble sugars in the WT and DXS_ox strains. Samples without (-) and with (+) glucoamylase treatment were spotted and separated.

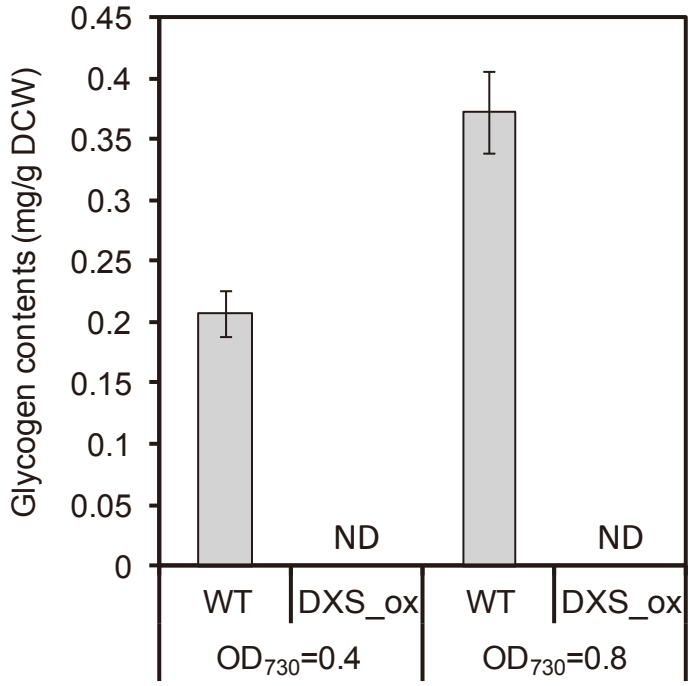

Fig. 2-15. Glycogen contents. The intracellular glycogen was measured by a glucose assay for the sonicated and glucoamylase-treated cell samples. The data are the mean ± SD of two replicates (n = 2). No significant signals were observed in the WT strain (are displayed as "ND").

Protein analysis

Total proteins were extracted from the soluble and insoluble fractions and analyzed by BCA Protein Assay and SDS-PAGE. As shown in Fig. 2-13, the total protein contents (soluble and insoluble fractions) at OD_{730}=0.4 and 0.8 were 360 and 200 mg/g DCW, respectively, in the WT strain, and 280 and 240 mg/g DCW in the DXS_ox strain. The ratios of the contents in the soluble and insoluble fractions were similar among all samples, at approximately 4:1~5:1. The CBB-stained bands in the SDS-PAGE analysis were quantified, and the phycobiliproteins with molecular weights of 10–20 kDa, i.e. allophycocyanin and phycocyanin, are major proteins (50-55%) in both strains (Fig. 2-16A). A detailed image of the proteins in the lower molecular weight range was obtained by higher density SDS-PAGE and sliver staining, which suggested that the intensity of the band at approximately 11 kDa, which corresponded to the phycocyanin α-subunit, in the DXS_ox strain grown to an OD_{730} of 0.4 seemed to be slightly weaker (by 25%) than that in the WT strain (Fig. 2-16B and 15C).

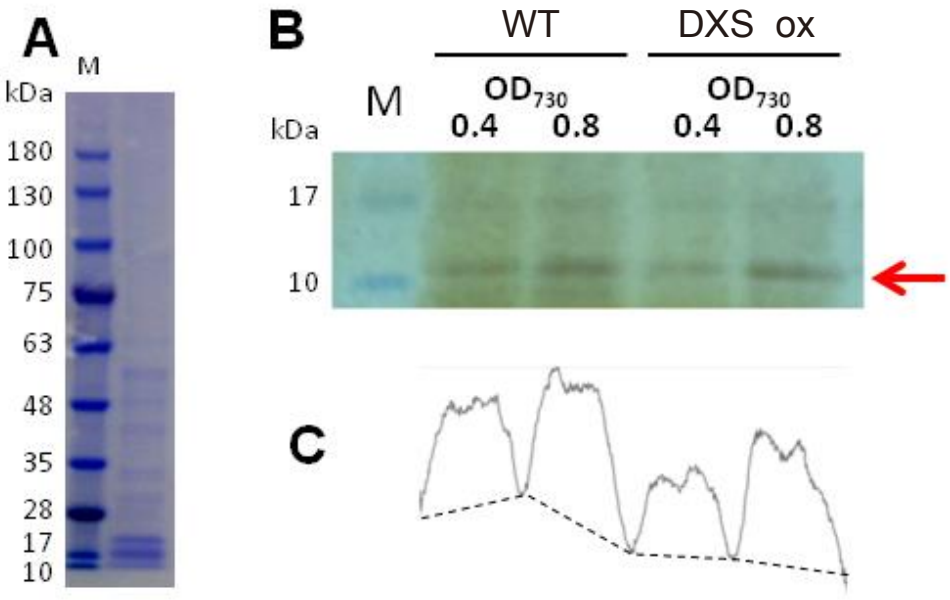

Fig. 2-16. Protein analysis. The protein samples extracted from 5 ml culture pellets were analyzed by SDS-PAGE. Protein bands were visualized with CBB (A) or silver staining (B). The intensities of the bands of ~11 kDa corresponding to phycocyanin (indicated by arrow in Fig. 2-16B) were quantified with ImageJ, and the ratio of WT at OD_{730} = 0.4 : WT at OD_{730} = 0.8 : DXS_ox at OD_{730} = 0.4 : DXS_ox at OD_{730} = 0.8 was 1 : 1.5 : 0.75 : 1.4 (C).

Morphological comparison between the WT and DXS_ox strains

To observe the changes in the cell structure directly, we took transmission electron microscopy images of ultra-thin sections of the cells (Fig. 2-17). As shown in Fig. 2-17A and 17B, the S-layers were successfully observed, and their thicknesses were measured (an example is shown using two arrows in Fig. 2-17A and 17B). Consequently, the means of the thickness were 24 ± 0.4 and 20 ± 0.1 nm in the WT and DXS_ox strains, respectively, indicating the significant phenotypic difference. The obvious difference was also observed in the section areas between the WT and DXS_ox strains (Fig. 2-17C and 17D). The three micrographs (28 x 28 μm) were randomly selected, and the areas of the cells with a section area of more than 1 μm^2 (100-136 cells) were determined (Fig. 2-18). The resulting mass average areas were 2.2 ± 0.4 and 1.6 ± 0.1 μm^2 in the WT and DXS_ox strains, respectively, indicating the DXS_ox strain has a significantly smaller cell size (~73%) compared with the WT strain. The low-electron density granules (arrowheads in Fig. 2-17C and 17D), which are assumed to be polyphosphate or cyanophycin, were evaluated by using the ratio of the total granules area to the total cells area in a micrograph. The average of the randomly selected three micrographs was ~1.5 ± 0.1 and ~1.9 ± 0.4 % in the WT and DXS_ox strains, respectively, suggesting the significant higher accumulation of the low-electron density components in the DXS_ox strain. Interestingly, many unidentified high-electron density granules with a diameter of ~ 50 nm (arrowheads in Fig. 2-17B) were observed in the vicinity of the outer membrane in the DXS_ox strain, but rarely in the WT strain.

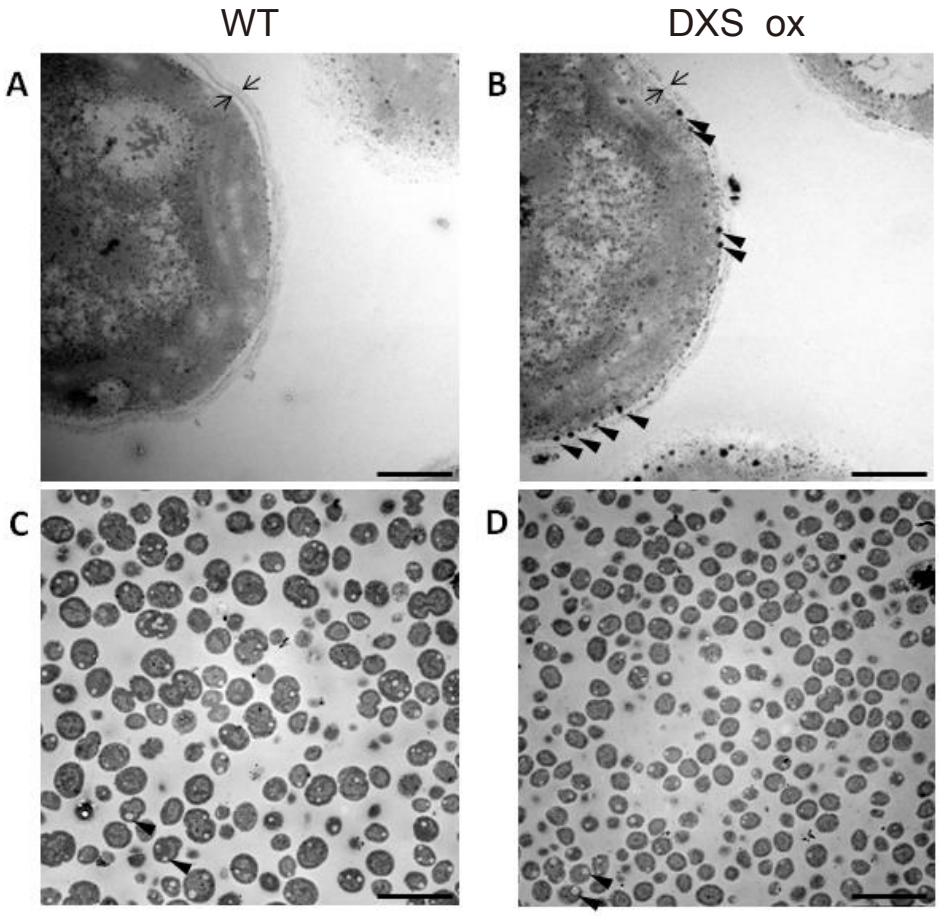

Fig. 2-17. Transmission electron microscope images. (A and B) High-magnification views of the WT and DXS_ox strains. According to the previous reports (72, 73), the most outer layer of cell (between two arrows pointing in the same direction) was likely to be S-layer. In the DXS_ox strain, many high-electron density granules (arrowheads) were appeared in the vicinity of the outer membrane. Bar = 500 nm. (C and D) Low-magnification views of the WT and DXS_ox strains. A few low-electron density granules (arrowheads) were observed in the both cell. Bar = 5 μm.

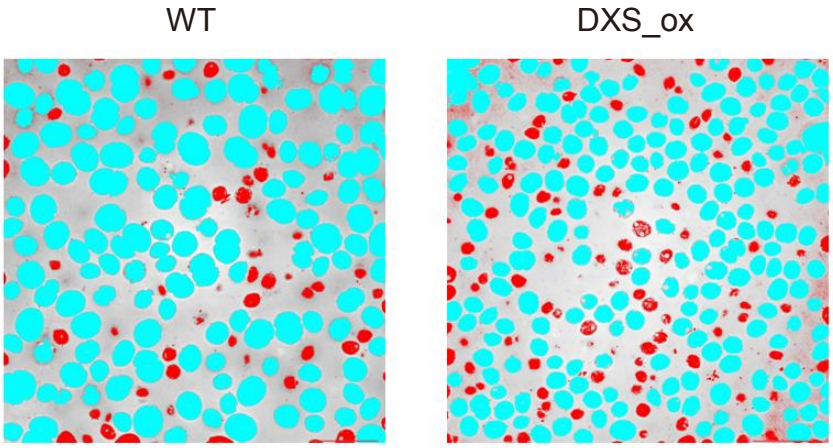

Fig. 2-18. The cell sections analysis of transmission electron microscope images. The red-colocred spots and cyan-colored the cell sections with an area of less than and more than 1 μm^2, respectively. Using the cyan-colored spots, the cell sizes of two cell sizes of two strains were discussed.

Discussion

To examine the over-expression of the DXS protein in *S.* 6803, we introduced an additional *dxs* gene downstream of the *psbA2* promoter, resulting in a strain (DXS_ox) with two copies of the *dxs* gene, the original gene regulated by the *dxs* promoter and a newly introduced one regulated by the *psbA2* promoter. As shown in Fig. 2-5, the mRNA levels in the DXS_ox strain (transcribed from the two promoters) was higher in the early growth stage (OD_{730} = 0.4), but decreased rapidly as the optical density of the culture increased. The mRNA levels in the WT strain (transcribed from the original *dxs* promoter) were ~1/4 that of the DXS_ox strain throughout the cultivation period, indicating that transcription from the original *dxs* promoter in the DXS_ox strain was negligible due to the much lower transcription activity of the *dxs* promoter. Because induction of transcription from the *psbA2* promoter is light-dependent (74, 75), it is most likely that the rapid decrease in the mRNA level in the DXS_ox strain is caused by deactivation of transcription in response to the decrease in the average amount of light received by a cell at higher cell densities (the self-shielding effect). Therefore, the influence of the new *dxs* gene on metabolic phenomena would appear more clearly in samples taken from an early stage culture (OD_{730} = 0.4 and 0.8).

Interestingly, although the profile of the DXS protein expression was similar to that of the *dxs* mRNA transcription, the differences in the DXS protein levels between the WT and DXS_ox strains were more modest (a maximum difference of 1.6 fold) (Fig. 2-6). The amount of a particular protein in the cell is determined not only by the mRNA level, but also by the stability of the protein itself in the cell (which is affected by the frequency of misfolding or aggregation, and its tendency to be a target of quality-control mechanisms) (76-79). We found that the *S.* 6803 DXS protein purified from *E. coli* was significantly likely to aggregate *in vitro* (more than 90% of the protein was insoluble after an overnight incubation at 4°C). It is known that *in vitro* protein aggregation rates are strongly inversely correlated with the half-life of the protein *in vivo* (80). Therefore, we assumed that

the DXS protein is easy to be aggregated or disposed of by quality-control mechanisms *in vivo*. Indeed, a significant DXS signal was observed in the insoluble fraction by western blotting (data not shown), supporting our assumption. If further enhancement of DXS protein levels is required, the *S.* 6803 DXS protein would need to be improved by directed evolution methods or a heterologous DXS would need to be introduced into *S. 6803*.

Although this modest increase in the DXS protein levels may be problematic for the over-production of isoprenoids, it did not inhibit the growth of the DXS_ox strain at all (Fig. 2-4), which makes it easy to assess the carbon flux changes. The carotenoid analysis showed that the total carotenoid content in the DXS_ox strain was approximately 1.5-fold that of the WT strain (Fig. 2-10). This successfully demonstrated that the carotenoid content can be enhanced by increasing the expression level of the *dxs* gene, and that DXS is the enzyme that catalyzes the rate-determining step of carotenoid synthesis in *S.* 6803. However, because the ratio of the increase in the carotenoid content was nearly identical to that of the increase in DXS protein content, we cannot conclude whether or not DXS is still the rate-determining enzyme in the DXS_ox strain.

Interestingly, the shift of the carotenoid composition in the DXS_ox strain significantly differed from that in the WT stain (Fig. 2-10). Among four carotenoids, myxoxanthophyll in the DXS_ox strain at OD_{730}=0.8 was prominent, in comparison with the corresponding carotenoid in the WT strain. Myxoxanthophyll, which is a unique in its glycoside moiety, is known to be a strongest photoprotectant and synthesized at high light conditions (81). In fact, in the WT strain, the myxoxanthophyll content at OD_{730}=0.4 was higher than that at OD_{730}=0.8 (Fig. 2-10), suggesting that the synthesis of myxoxanthophyll was stopped at OD_{730}=0.8 due to the reduced light transparency by the self-shielding effect. On the other hand, in the DXS_ox strain, the content increased slightly as the OD_{730} increased from 0.4 to 0.8. The increase in myxoxanthophyll was also observed in the S.6803 strain deficient in echinenone synthesis gene and the strain over-expressing

enzymes involving in the carotenoid biosynthesis (47). Because echinenone and myxoxanthophyll are synthesized *via* the same precursor γ-caroten, the deletion of echinenone synthesis gene would lead to the increase in carbon flow toward the myxoxanthophyll synthesis. Taken together, we assumed that under the low light intensity (or at high optical density), the myxoxanthophyll synthesis is inhibited, but is resumed preferentially in the presence of the enhanced carotenoid precursors.

How the metabolic balance was influenced by the DXS over-expression is of interest. Because the growth rate of the DXS_ox strain was nearly identical to that of the WT strain, its influence on cell viability would be limited. Most intriguingly, the glycogen content of the DXS_ox strain decreased dramatically (Fig. 2-15). Because glycogen is known to be a carbon storage compound and can be considered as an indicator of the excess carbon flux, the remarkably low level of glycogen suggests that there are almost no excess carbons in the DXS_ox strain. In addition, the content of another major storage compound, phycocyanin, also decreased by ~25% in the DXS_ox strain at OD_{730} = 0.4 (Fig. 2-16B and 16C). It is assumed that the DXS_ox strain enhances carotenoid productivity at the expense of almost all of the glycerol and a portion of the phycocyanin.

The total carotenoid content was estimated to be only 8.4~8.6 mg/g DCW (less than 1% of the biomass) in the DXS_ox strain, which raises the question, where have the remaining carbons gone? Therefore, we analyzed the total sugars (104 mg/g DCW), total fatty acids (24 mg/g DCW), and total proteins (240 mg/g DCW) (Fig. 2-13), and showed that they were much higher (12-, 2.9- and 28-fold) than that of the total carotenoids. The total sugars include both soluble and insoluble forms. Based on the TLC analysis, the soluble sugars were found to be almost all glycogen (Fig. 2-14); however this was negligible compared to the total sugars content, indicating that almost all sugars exist in insoluble forms, perhaps as cell wall components, such as the S-layer (72, 73). The fatty acids are also mainly derived from membrane components (82). Taken together, these observations suggest that 15% or more of the cell biomass is part of the cell membrane structure. The

main component, the protein, was further analyzed by SDS-PAGE, and the results indicate that the major proteins (50~55%) in both strains were phycobiliproteins, i.e. allophycocyanin and phycocyanin (Fig. 2-16A) and the percentage of phycobiliproteins is calculated to be ~13% of the biomass. Phycobiliproteins are known to be not only a critical component of the light-harvesting complex, but also a storage compound in cyanobacteria. PHB is also known to be a storage compound in cyanobacteria; however, in our culture conditions (BG11), it did not accumulate significantly. Based on all these results, we can conclude that under our experimental conditions, the major destinations of carbon are cell structures and phycobiliproteins.

As shown in Fig. 2-13, the contents of total carbohydrate and total fatty acid in the DXS_ox strain were lower than those in the WT strain (30~40% and 10~20%, respectively), suggesting the differences in the cell wall (S-layer) or membranes. In fact, transmission electron microscopy images demonstrated that the thickness of the S-layer was reduced by approximately 17% in the DXS_ox strain, explaining the reduced total carbohydrate content. Interestingly, the cell size was also was reduced by approximately 27%, and more black granules were observed in the DXS_ox strain. At present, although the relationship among the DXS protein over-expression and these phenotype changes is unclear, it is likely that the changes in phenotype on the DXS_ox strain reflect the changes in the contents of total carbohydrate and total fatty acid.

Based on the above, we can answer some of the questions we raised in the Introduction: “Does the enzymes responsible for synthesis inactivate rapidly?” “yes”; “Is there a strong competing pathway?” “yes (cell membrane and phycobiliproteins)”; “Is there not enough carbons to accumulate the products because of exhaustion for the construction of cell architecture or photosynthesis?” “partially, yes (*S*.6803 has excess carbons to store as phycobiliproteins)”. In conclusion, we proposed a strategy to remarkably increase the yield of isoprenoids. First, the stability of the DXS protein needs to be addressed. To this end, a gene encoding a stable exogenous DXS protein would need to

be introduced or the *S.*6803 DXS protein needs to be engineered for greater stability. Second, the production should be carried out in a cell state, in which the construction of cell structures is stopped. For example, under nitrogen starvation conditions, the various cell activities, including cell division, protein synthesis and photosynthesis, are weakened. If in such a state, the genes responsible for the production of the desired products and involved in photosystems and calvin cycles are placed under the control of promoters that work under nitrogen starvation conditions, a much higher yield could be achieved. Finally, downsizing the light-harvesting complex, including phycobiliproteins would be essential. These improvements would be prerequisites for maximum utilization of the most attractive quality of cyanobacteria, the high ability of the photo-biomass conversion.

CHAPTER 3

Overexpression of endogenous 1-deoxy-D-xylulose 5-phosphate synthase (DXS) in cyanobacterium *Synechocystis* sp. PCC6803 accelerates protein aggregation

Introduction

Isoprene, the simplest member of the isoprenoids (83-85), is an important feedstock in the synthetic chemistry industry and is widely used in the production of synthetic rubber, medicines, pesticides, and synthetic oil additives, and as a vulcanizing agent for rubber. Isoprene also can be converted into biofuel, e.g., aviation fuel (45, 86). Currently, isoprene used in industry is mainly produced from C5 petroleum distillate, as a byproduct of the oil refining process, via the fractionation of petroleum. However, in light of high oil prices and environmental concerns, isoprene from renewable materials is a potential substitute for a petroleum-based product (87).

In biology, isoprene is a member of the isoprenoid family and is synthesized *via* the mevalonic acid (MVA) pathway or the methyl-erythritol-4-phosphate (MEP) pathway (reviewed by Rodriguez-Concepcion and Boronat (88)). Through these biosynthetic pathways, two common isoprenoid precursors, dimethylallyl diphosphate (DMAPP) and isopentenyl diphosphate (IPP), are produced and converted into various isoprenoids. Isoprene is synthesized from DMAPP directly by isoprene synthase (IspS). The MVA pathway operates in eukaryotes (including all mammals), archaea, a few eubacteria, and in the cytosol and mitochondria of plants and fungi (12, 89), whereas the MEP pathway is present in eubacteria including cyanobacteria, plant chloroplasts, algae, and apicomplexan parasites (56, 90, 91). Some eubacteria possess both of these pathways for the synthesis of isoprenoid feedstocks (92, 93). The two pathways are quite different regarding stoichiometry, energy consumption, and the oxidation/reduction balance during the conversion of glucose to IPP (94). The MEP pathway has a higher theoretical yield, while the MVA pathway has a

lower energy consumption.

Cyanobacteria are not only widely used model phototrophs for basic biological studies, but are also attractive candidates for use in bio-industrial applications because of their high photosynthetic capability. Cyanobacteria can convert captured solar energy into biomass at efficiencies exceeding those of terrestrial plants (cyanobacteria, 3%–9%; terrestrial plants, 0.25%–3%) (14). As cyanobacteria possess the MEP pathway but lack the *isps* gene, Lindberg *et al*. (45) introduced an *isps* gene from *Pueraria montana* (*skisps*) into cyanobacteria, and successfully detected isoprene in the headspace of a closed-cultivation system. However, the isoprene yield was low, constituting only a few percent of the total cyanobacterial biomass. Following this pioneering work, Bentley *et al*. (95) successfully improved the isoprene productivity of the SKIspS-expressing cells by heterologous introduction of the MVA pathway genes. Pade *et al.* (96) also tried to enhance the carbon flux into SKIspS by overexpression of the endogenous *dxs* gene, which encodes 1-deoxy-D-xylulose 5-phosphate synthase (DXS), the initial enzyme in the MEP pathway. However, the isoprene productivity was, unexpectedly, decreased. Interestingly, they also reported in the same article that the highest isoprene production rate (336 μg isoprene/g dry cell weight per day) was observed in the strain expressing only SKIspS when cultured in the open-cultivation system, in which the medium is continuously aerated and isoprene is detected at the outlet. They had assumed that in the open-cultivation system, the isoprene concentration would be lower than in the closed system, which would lower the inhibitory effects of the isoprene molecule. Very recently, seminal studies were published by Gao *et al.* (97) and Chaves *et al.* (98). They clearly demonstrated that the ratio of IPP to DMAPP is the most critical factor affecting isoprene production. Gao *et al.* showed that IPP works as an inhibitor of IspS. They then dramatically enhanced isoprene production in *Synechococcus elongatus* by inducing heterologous expression of isopentenyl diphosphate isomerase (IDI) from *Eucalyptus globulus*. They finally succeeded in redirecting up to 65% of the carbon flow

towards isoprene production by genetically modifying the latter half of the MEP pathway (downstream of 1-hydroxy-2-methyl-2-(E)-butenyl 4-diphosphate synthase (IspG)).

The key enzyme in the first half of the MEP pathway is DXS. However, many attempts to enhance isoprenoid productivities in cyanobacteria by overexpressing DXS have encountered difficulties (96, 99). Kiyota *et al.* (99) successfully observed limonene production from the limonene-synthase expressing *Synechocystis* sp. PCC6803 (*S. 6803*) strain in an open-cultivation system, but the co-expression of DXS had only a small effect. We also previously attempted the overexpression of endogenous DXS in *S. 6803*, and found that the mRNA level increased 4-fold compared with the wild-type strain, but the increase in the soluble protein levels of DXS was only 1.5-fold (100). This result suggests that the amount of soluble DXS was regulated by the events downstream of transcription, for example, mRNA degradation, protein degradation, protein aggregation, and feedback inhibition of the enzymatic activities.

A study of post-transcriptional regulation of DXS in the chloroplasts of *Arabidopsis thaliana* identified a role for the heat shock proteins (Hsps) J-protein J20 and Hsp70 in the activation of DXS (101). However, we have no information about the post-transcriptional regulation of DXS in cyanobacteria. To resolve this situation, we quantified mRNA levels, soluble and insoluble protein levels, and isoprene production of the DXS-SKIspS co-expressing strains from induction phase to late-logarithmic phase. To minimize the potential inhibitory feedback effect of isoprene, we used the newly developed open-cultivation system equipped with an activated carbon tube at the outlet for stoichiometric isoprene harvest (Fig. 3-1).

Materials and methods

Strains and growth conditions

S. 6803 strains were cultivated at 25°C in BG-11 medium buffered with 5 mM N-Tris(hydroxymethyl)methyl-2-aminoethanesulfonic acid (TES)-NaOH (pH 8.0), at a photon flux density of 100 μmol photons·m^{-2}·s^{-1}, and aerated using air bubbles at a rate of 200 mL·min^{-1} under these conditions. Antibiotics were added into each culture according to the resistance of the strains at the following concentrations: kanamycin (20 μg·L^{-1}) (Tokyo Chemical Industry Co., Ltd., Tokyo, Japan), spectinomycin (5 μg·L^{-1}) (LKT Laboratories, St. Paul, Minnesota, USA), streptomycin (10 μg·L^{-1}) (Nacalai Tesque, Kyoto, Japan). The optical density at 730 nm (OD_{730}) was measured using a UV–VIS spectrophotometer (model V630; JASCO, Tokyo, Japan).

Plasmid construction and transformation

All primer sequences are shown in Table 3-1. The sequences of the *trc* promoter and the *ispS* gene were amplified from the laboratory plasmids pT31CTH_TePixJ (102) and pUC19-trc-SkIspS, which harbors *skisps* from pBA2SkIKmA2 (addgene: Cambridge, MA, USA) (45), respectively, using the primers trc_2831a_F and skisps_2831a_R. They were then inserted into *NotI* site of pRL2831a, generating pRL2831a-Ptrc-SkIspS. The plasmid was introduced to the wild type (WT) strain of *S.6803* and a DXS overexpressing strain (DXS_ox) (100) using the conjugation method. The conjugation between *E. coli* and the WT or DXS_ox strains was performed as described by Wolk and Elhai (103). The WT and DXS_ox strains harboring pRL2831a-Ptrc-SkIspS were named WT-isP and DXSox-isP, respectively.

Table 3-1. Primers used in CHAPTER 3.

Primers	Primer sequence(5′→3′)
trc_2831a_F	ATATTCGATGCGGCCCGCTTCGTTAATACAGACG
skisps_2831a_R	CTCTTACGAGCGGCCTTACACGTACATTAATTGATTAATTGG
dxs_qPCR_F	ATGCACATCAGCGAACTGAC
dxs_qPCR_R	CTCCTTGACCCTTTCCATCT
isps_qPCR_F	GCTGGTTTTTGGATAAATATGAACCG
isps_qPCR_R	ATGCGGGGATAATTTTGTTG
16sRNA_qPCR_F	ACCGCAGTATTCTGACCTGC
16sRNA_qPCR_R	ACAAGCGGTGGAGTATGTGG

Isoprene absorption test by activated carbon tube

Isoprene collection from air and the analysis was performed as follows. To capture isoprene, a five-connected activated carbon tube (No.258; GASTEC, Kanagawa, Japan) was attached without or with a condenser and a tube packed with calcium chloride to the exhaust port of a 500-ml flask containing 500 mL water (Fig. 3-1A). A 10-L bin filled with gaseous isoprene (corresponding 5 μL liquid isoprene) was connected to the inflow port of the flask. The air including gaseous isoprene was flowed to the carbon tube through the flask at 200 ml/min for 12 min. After the flow, the normal air was flowed at 200 mL/min for 6 h. To analyze volatiles from the tube, the activated carbon were eluted with 500 μL of dichloromethane and the eluate was subjected to gas chromatography (GC14B; Shimadzu, Kyoto, Japan) equipped with a PEG20M 10% shinwasorb-S-60-80 column (Shinwa Chemical Industries Ltd, Kyoto, Japan) and a flame ionization detector (FID). The operating conditions were as follows: split ratio 1:10; inject volume 2 μL; injector temperature 100°C; detector temperature 230°C; and oven temperature 72°C. The amounts of isoprene production were calculated using a calibration curve prepared by using pure isoprene.

Isoprene collection from culture and analysis

The IspS-expressing strains were grown to OD_{730} of 2.0-3.0 as the seed culture and then inoculated to an OD_{730} of 0.2 to 500-mL flasks containing 500 mL BG11. An activated carbon tube was attached with a condenser to the exhaust port of each flask to capture isoprene from the culture. The collection was performed for 6 h from specific culture time. The elution and analysis of volatiles from the tube were performed in the same way as isoprene absorption test.

Semi-quantitative PCR

The transcriptional levels of the *dxs* and *isps* genes were determined by semi-quantitative

PCR. Total RNA from pellets was isolated by acid guanidinium thiocyanate-phenol-chloroform extraction methods (104) and subjected to the reverse transcription reaction with M-MLV Reverse Transcriptase (Nippon Gene, Tokyo, Japan). The resultant cDNA was used as a template for semi-quantitative RT-PCR. The *dxs* and *isps* gene were amplified from the cDNAs by using primers dxs_qPCR_F and dxs_qPCR_R, isps_qPCR_F and isps_qPCR_R, respectively. 16S rRNA gene was chosen as an internal control which was amplified by using primers 16sRNA_qPCR_F and 16sRNA_qPCR_R. PCR products obtained from different cycles were taken for comparison of the amounts of these products by electrophoresis on 1.5% agarose gels and visualized by GelRed (Biotium, Hayward, CA, USA).

RNA-seq analysis

RNA for RNA-seq analysis was extracted by RNeasy Mini Kit (Qiagen, Hilden, Germany). The 23S rRNA and 16S rRNA were removed from the extracted RNA using MICROBExpres kit (Ambion, Austin, TX). The cDNA library was constructed following the manufacturer's instructions using a NEBNext mRNA Library Prep Master Mix Set for Illumina (New England Biolabs, Ipswich, MA, USA) and NEBNext Multiplex Oligos for Illumina (New England Biolabs). Short fragments were detected using 1.8% agarose gel electrophoresis and then were quantified by qPCR through a Library Quantification Kit-Illumina GA Universal system (Kapa, KK4824). Finally, the sequencing library was constructed by PCR amplification (15 cycles) and sequenced using the Illumina Genome Analyzer IIx sequencing platform. The Illumina cBOT (Illumina Inc., San Diego, CA) was then used for cluster generation which was sequenced on the Illumina HiSeqTM 2500 platform. Data analyses and base calling were performed using the Illumina instrument software.

SDS-PAGE and western blot analysis

For the western blot analysis, crude extracts of IspS-expressing strains were prepared by bead beating the cells in Tris buffer (500 mM Tris–HCl, pH 7.4). After bead-beating, the insoluble fractions were removed by centrifugation at 12,000 g for 10 min. Then, the soluble fractions were separated by 7.5% SDS-PAGE, blotted onto PVDF membranes (Merck), and probed sequentially with a primary specific polyclonal antibody to DXS or IspS and a goat anti-rabbit IgG-Horse radish Peroxidase conjugate (Santa Cruz Biotechnology, Santa Cruz, CA, USA) as a secondary antibody. Protein bands were visualized using the Pierce Western Blotting Substrate (Thermo SCIENTIFIC) following the manufacturer's instruction. The western blotting images were acquired using ImageQuant LAS 4000 mini (GE Healthcare). For the solubility analysis of DXS and IspS, the insoluble fractions were resuspended to 2% w/v SDS aqueous solution. The same protein contents of the soluble fractions and suspended insoluble fractions were subjected to 12% w/v SDS-PAGE and blotted onto PVDF membranes. The detection and quantification was performed using the same antibodies, apparatus, and software as descried above.

Results

Isoprene collection by an activated carbon tube

To estimate the recovery yield of gaseous isoprene by activated carbon tubes, 2400 mL of air containing 0.82 mg of isoprene was introduced into 600 mL flat flasks (“Roux” flasks) equipped with a water-cooled condenser, a drying tube packed with calcium chloride, and five activated carbon tubes connected in series (Fig. 3-1.). The flask was then aerated with bubbles at a rate of 200 $mL \cdot min^{-1}$ for 6 h. The isoprene recovered by an individual tube was extracted into dichloromethane and analyzed by GC. For validation of the effect of the condenser and the drying tube, we also examined a system equipped with only activated carbon tubes. Although isoprene leaked significantly into downstream tubes in the system lacking the condenser and the drying tube, it was found exclusively in the first tube in the full system, which was quantified as 0.58 mg (70% of recovery yield) (Fig. 3-1B and C).

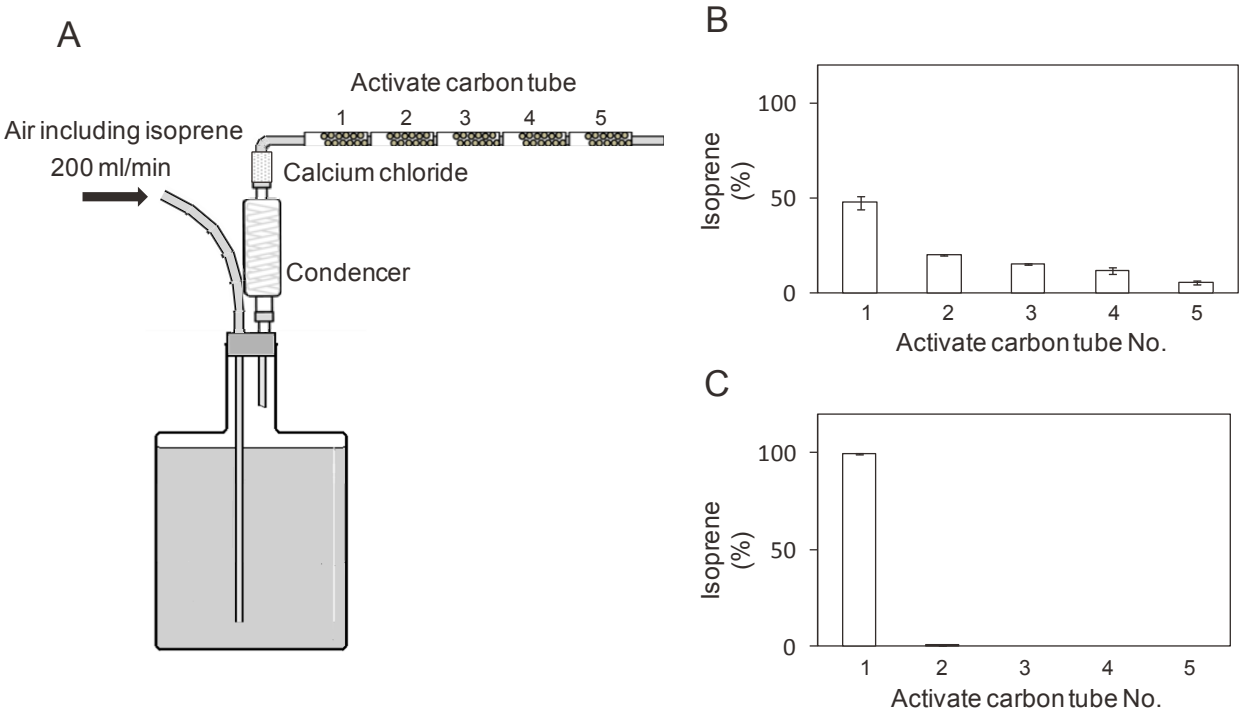

Fig. 3-1. Isoprene collection test.
Diagram of the apparatus for capturing volatile isoprene (A). The activated carbon tube was attached to the exhaust port of the sealed flask to capture isoprene. Air containing gaseous isoprene was injected into the carbon tube through the flask at 200 mL/min for 12 min. Subsequently normal air was injected at 200 mL/min for 6 h, either with or without cooling and drying by a condenser and a tube packed with calcium chloride. The dichloromethane extract from each tube was analyzed by gas chromatography (GC). The differences between the conditions are shown in B (without cooling and drying) and C (with cooling and drying).

Isoprene production the IspS expressing strains

The IspS expressing strains (WT-isP and DXSox-isP) were generated by transformation of a plasmid harboring *isps,* controlled by the *trc* promoter, into the WT or DXS_ox strain, respectively (Table 3-1). The WT-isP and DXSox-isP strains were cultivated under continuous air-flow conditions in Roux flasks equipped with a water-cooled condenser, a drying tube, and an activated carbon tube connected to the outlet in series. Isoprene production was successfully observed in the IspS expressing strains (Fig. 3-2A), but not in the WT and DXS_ox strains (data not shown). The isoprene productivities ($\mu g \cdot h^{-1} \cdot OD_{730}^{-1}$) of the WT-isP and DXSox-isP strains were 0.9–1.2 and 1.5–1.7 during the induction phase, respectively, but during the late-logarithmic phase decreased to 0.2–0.3 and 0.2–0.5, respectively (Fig. 3-2B). In the early-logarithmic phase, the DXSox-isP strain showed a slightly but significantly (1.4- to 1.8-fold) high productivity than that of the WT-isP strain.

Table. 3-2. Strains in CHAPTER 3.

Strain	Promoter for additional *dxs* expression*	Promoter for *ispS* expression**	Reference
WT	—	—	—
WT-isP	—	trc promoter	this study
DXS_ox	psbA2 promoter	—	100
DXSox-isP	psbA2 promoter	trc promoter	this study

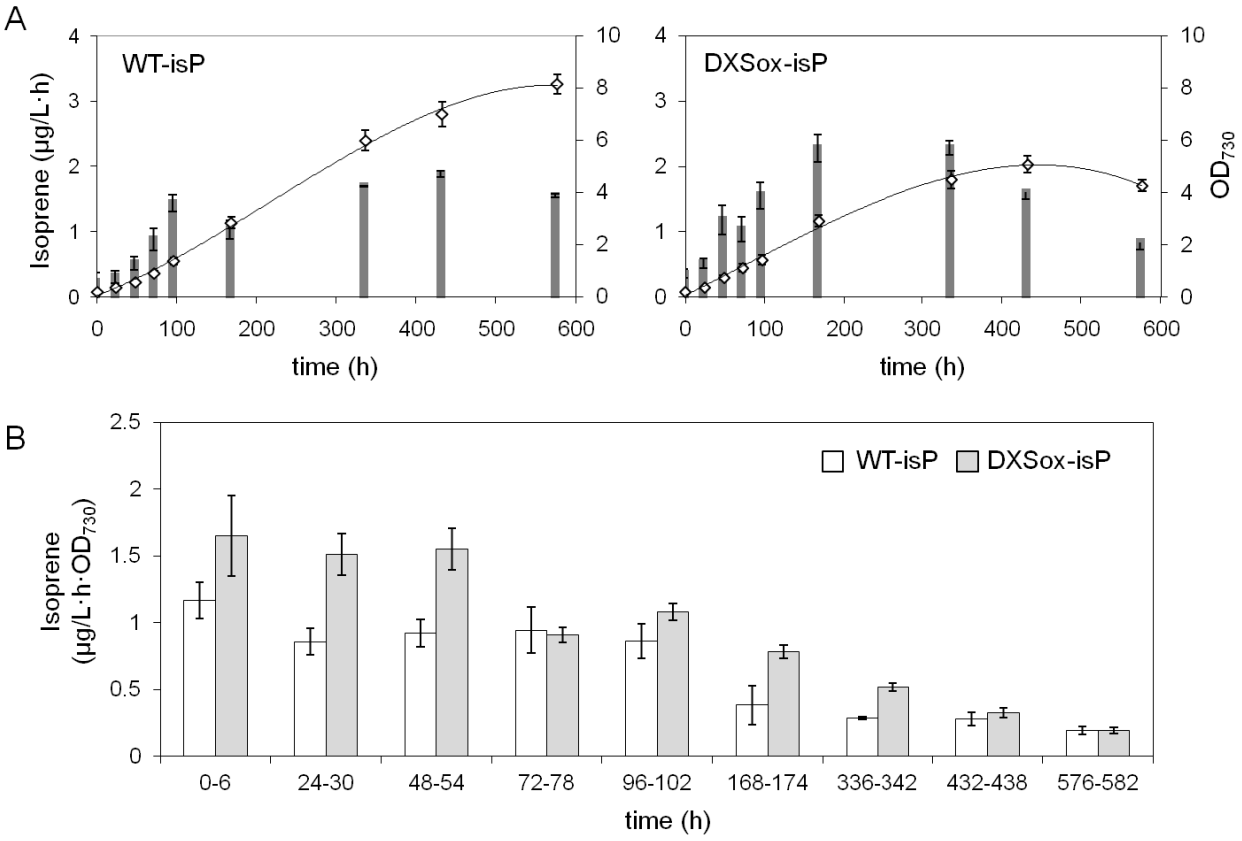

Fig.3-2. Time courses of isoprene titer and productivities.
Total isoprene captured in the activated carbon tube for 6 h from the specified time in IspS expressing strains was analyzed. The isoprene titers (μg·L·h) and growth curves in the WT-isP and DXSox-isP strains are shown in A. The isoprene productivities (μg·h·OD_{730}) in the WT-isP and DXSox-isP strains are shown in B. All experiments were performed under 100 μmol photons·m^{-2}·s^{-1} and aerated with air bubbles at a rate of 200 mL·min^{-1} under these conditions. The data are presented as mean ± standard error (SE) of three replicates.

Transcriptional analysis

The mRNA levels of the genes responsible for the MEP pathway in the WT and DXS_ox strains were analyzed by RNA-seq (Fig. 3-3). The mRNA levels of the *dxs* and *isps* genes in the IspS-expressing strains were analyzed by semi-quantitative PCR (Fig. 3-4). During all cultivation periods of the WT and DXS_ox strains, the *dxs* and 4-diphosphocytidyl-2C-methyl-derythritol synthase (*ispD*) mRNA levels were remarkably higher and notably lower, respectively, compared with those of other genes in the MEP pathway (Fig. 3-3A). Furthermore, the *idi* mRNA level significantly decreased in the late-logarithmic phase. These observations support previous reports indicating that the step involving IspD and IDI is one of the rate-limiting steps in the MEP pathway (97). Comparing the WT and DXS_ox strains, the *dxs* mRNA levels in the DXS_ox strain were 2- to 4-fold higher than in the WT strain (Fig. 3-3A) during all cultivation periods, indicating that the *psbA*II promoter works constantly even in the late-logarithmic phase in which the self-shade effect becomes more pronounced. In the cases of the DXS-IspS co-expressing strains, the DXSox-isP strain exhibited a higher *dxs* mRNA level, but a comparable *isps* mRNA level compared with the WT-isP strain (Fig. 3-4). In the semi-quantitative PCR using the samples from the WT-isP strain at 336 h, we encountered the unusually weak band for 16s rRNA and a deviation from the exponential trend, and finally could not obtain any reproducible and significant results. It might be due to a low stability of mRNA in the late-logarithmic phase.

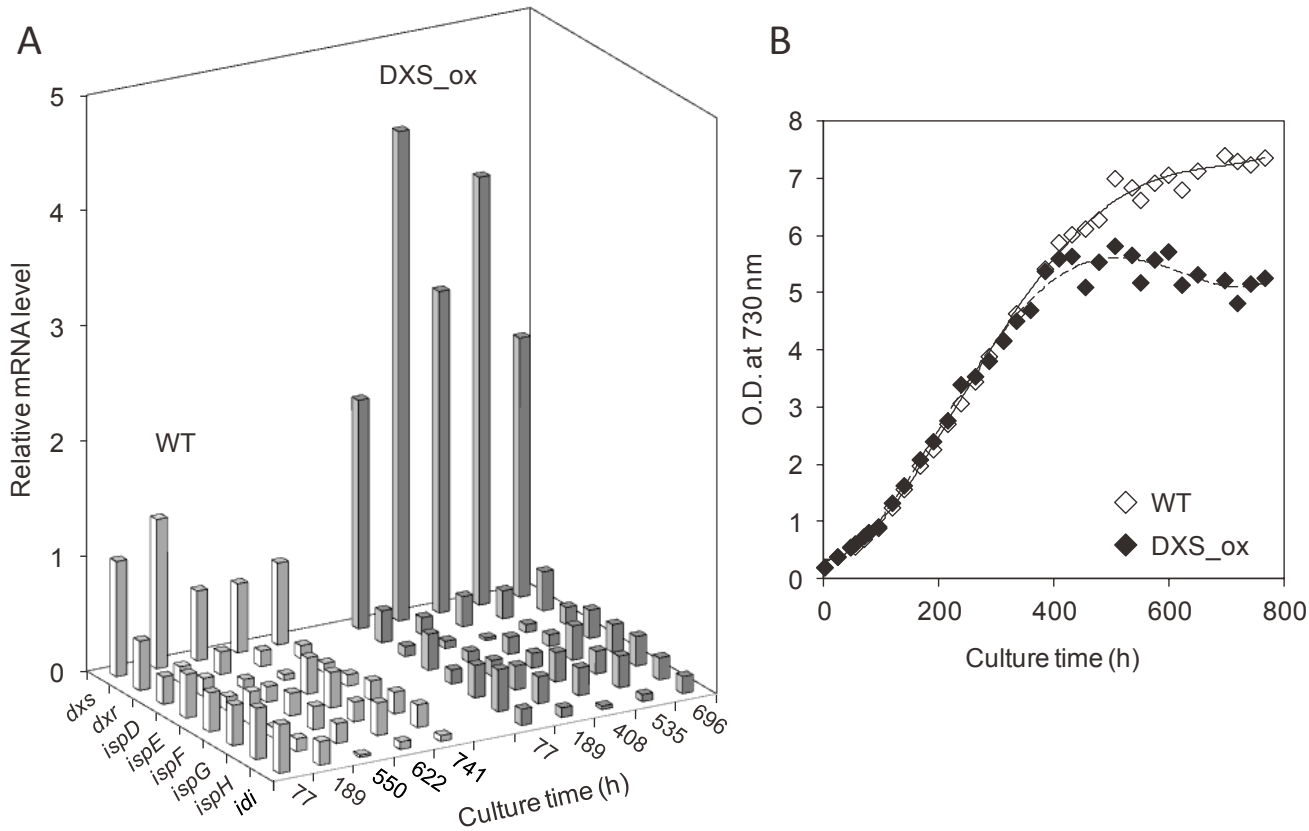

Fig. 3-3. RNA-seq analyses of the MEP pathway in the WT and DXS_ox strains.
The mRNA levels of the genes responsible for the methyl-erythritol-4-phosphate (MEP) pathway were analyzed by RNA-seq. In Fig. 3-3A, the mRNA levels for the MEP pathway in the WT and DXS_ox strains are shown relative to the *dxs* mRNA in the WT strain at 77 h. In Fig. 3-3B, the growth curves of the WT and DXS_ox strains are shown.

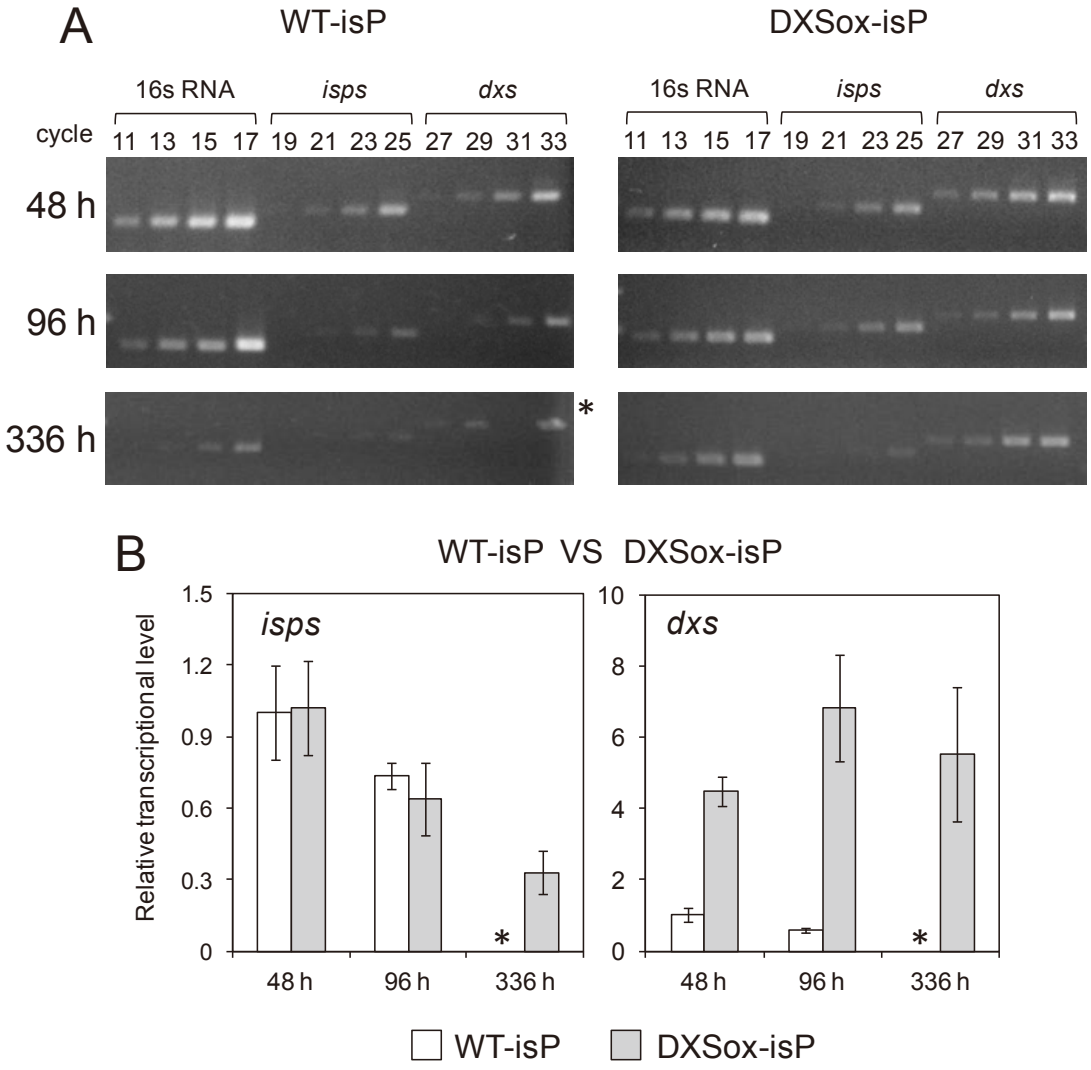

Fig. 3-4. Semi-quantitative RT-PCR of *isps* and *dxs* genes in WT-isP and DXSox-isP.
Total RNA from the WT-isP and DXSox-isP strains at 48 h, 96 h, and 336 h were analyzed by RT-PCR for the *isps* and *dxs* genes. The 16S rRNA gene was used as an internal standard to normalize the semi-quantitative RT-PCR value. The amplified products were separated on a 1.5% agarose gel and visualized by GelRed (Biotium) (A). The expression levels of the *isps* and *dxs* genes are shown relative to levels in the WT-isP strain at 48 h (B). The data are presented as mean ± standard error (SE) of three replicates. The asterisk indicates that no reproducible and significant data was obtained.

Accumulation levels of DXS and IspS proteins

The cell lysates of the IspS-expressing strains were fractionated into soluble and insoluble fractions by centrifugation, and the DXS and IspS accumulation in the soluble fractions was analyzed by western blotting, and plotted relative to the amounts in the WT-isP strain at 48 hour (h). As shown in Fig. 3-5A, the soluble DXS level in the WT-isP strain sharply increased until 96 h, and then rapidly decreased during the logarithmic phase. On the other hand, in the DXSox-isP strain, the level was decreased until 96 h, and reverted to the initial level by 100-300 h. During the late-logarithmic phase, the levels in both strains gradually decreased with increasing cultivation time.

The soluble IspS levels showed similar trends in both strains, increasing up until 96 h, and subsequently maintained at the same level, as shown in Fig. 3-5B. The soluble IspS level in the WT-isP strain was slightly higher than in the DXSox-isP strain during the entire cultivation period.

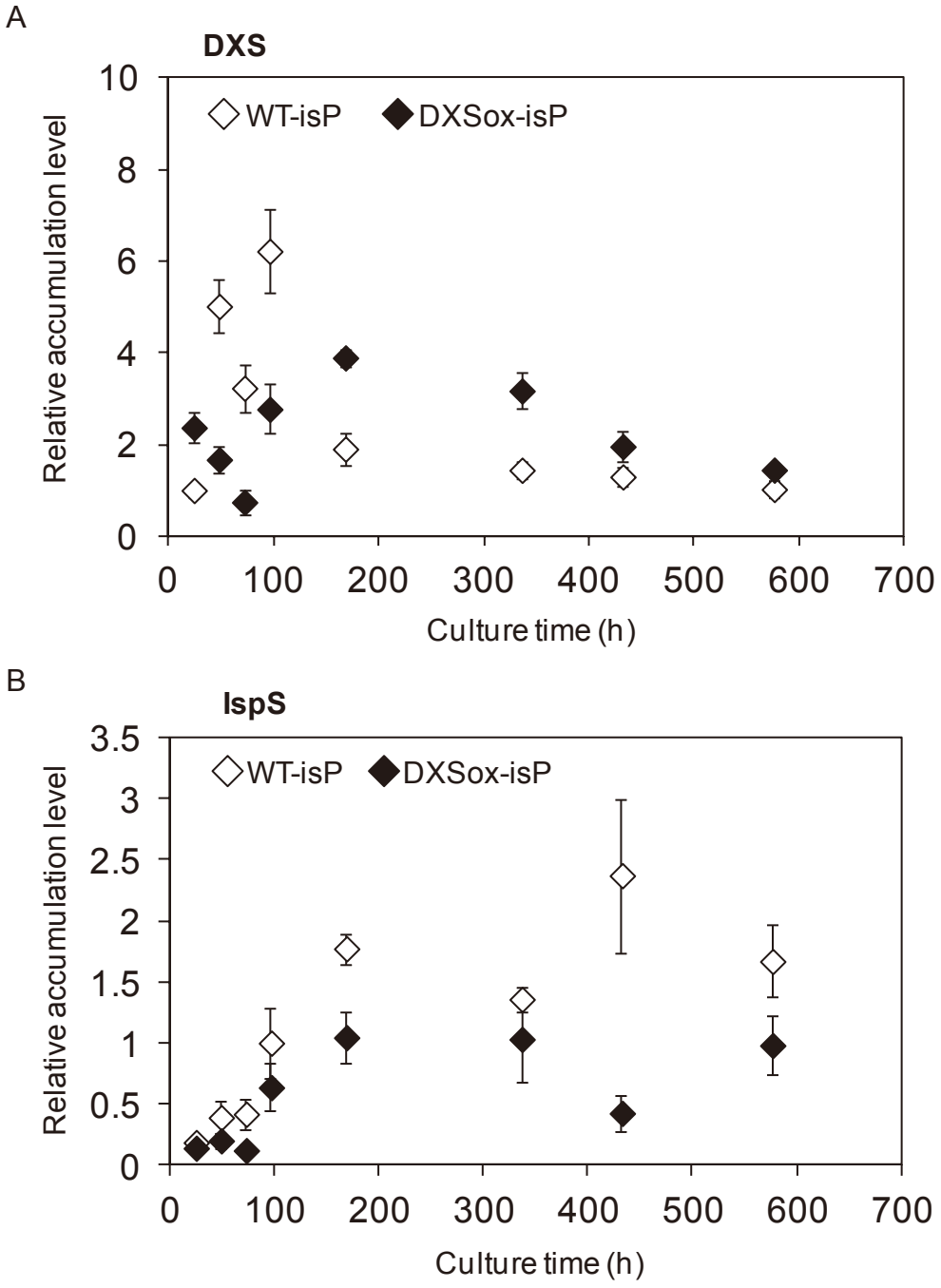

Fig. 3-5. Relative DXS and IspS protein levels.
The levels of soluble 1-deoxy-D-xylulose 5-phosphate synthase (DXS) and isoprene synthase (IspS) accumulation in the soluble fraction were confirmed using western blotting with an anti-DXS antibody and an anti-IspS antibody, respectively. In part A, DXS accumulation is shown relative to levels in the soluble fraction from the WT-isP strain at 24 h. In part B, IspS accumulation is shown relative to levels in the soluble fraction from the WT-isP strain at 96 h. The data are presented as mean ± standard error (SE) of three replicates.

Solubility of DXS and IspS

To estimate the *in vivo* solubility of the DXS and IspS, the soluble and insoluble fractions of cell lysates taken at 48, 96, and 336 h of cultivation were analyzed by western blotting (Fig. 3-6). The ratio of soluble:insoluble DXS in the DXSox-isP strain was dramatically lower (7%) at 48 h compared with any other time point, but then gradually increased with the cultivation time. In the WT-isP strain, the ratios of soluble:insoluble DXS were significantly higher than in the DXSox-isP strain and maintained at 68-84% between 48-336 h of culture. In contrast to DXS, the ratios of soluble:insoluble IspS were not significantly different between the both strains, and constantly lower than those of DXS, except for that of the DXSox-isP strain at 48 h.

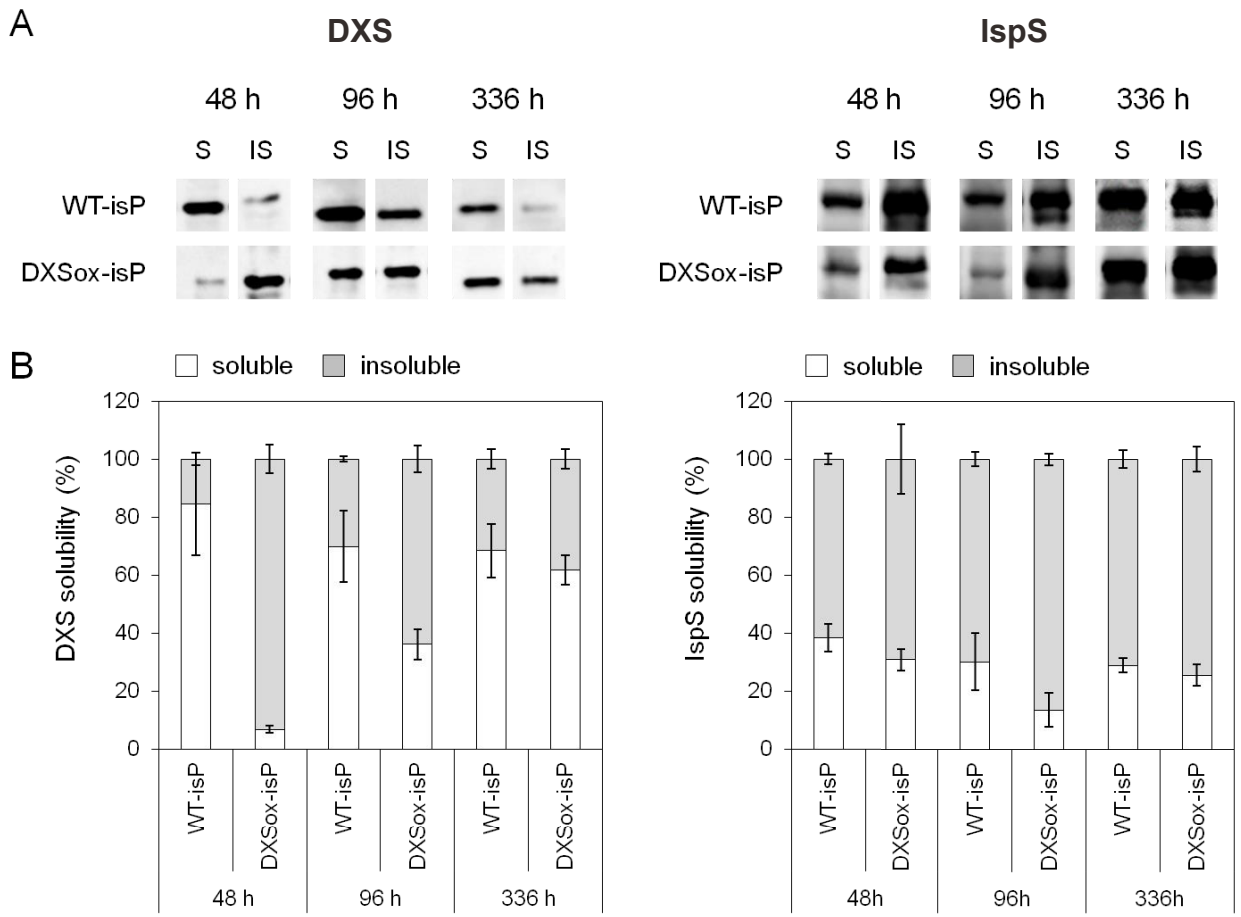

Fig.3-6. Solubilities of DXS and IspS.
The western blotting band images of 1-deoxy-D-xylulose 5-phosphate synthase (DXS) and isoprene synthase (IspS) in the soluble (S) and insoluble (IS) fractions extracted from the WT-isP and DXSox-isP strains at 48 h, 96 h, and 336 h (A). The solubilities of DXS and IspS were estimated from the western blotting bands (B). The data are presented as mean ± standard error (SE) of three replicates.

Discussion

We found that the ratio of soluble:insoluble DXS in the DXSox-isP strain was strikingly low at the induction and early-logarithmic phases (48 and 96 h) (Fig.3-6). This would lead to a comparable or lower level of soluble DXS in the DXSox-isP strain relative to that in the WT-isP strain (Fig. 3-5A), despite the overexpression of the *dxs* gene (Fig. 3-4). Although in cyanobacteria, the regulatory mechanism for DXS aggregation has not been reported, detailed studies of plastids of *A. thaliana* have demonstrated that the heat shock protein J20 is involved in the regulation of DXS aggregation (101, 105). J20 acts as an adaptor that recognizes inactive DXS proteins, including the aggregated form, and delivers them to the Hsp70 molecular chaperone. Hsp70 facilitates the activation or degradation of the inactive DXS. The DnaJ-DnaK system in cyanobacteria, corresponding to the J20-Hsp70 system in plastids of *A. thaliana*, is also known to regulate protein aggregation (106), but nothing is known about the involvement of the DnaJ-DnaK system in DXS aggregation.

Based on our results in this study, we speculated that the ratio of soluble:insoluble DXS would increase when the translation of the *dxs* gene exceeded the capacity of chaperones, such as those in the DnaJ-DnaK system. In the induction phase and the early-logarithmic phase, the transcriptional level of *dxs* in the DXSox-isP strain was significantly higher than that in the WT-isP strain (Fig. 3-4), and it therefore might have been difficult for the refolding process to catch up with the DXS transcription rate, resulting in the low ratio of soluble DXS (Fig. 3-6). In the late-logarithmic phase (336 h), although the transcriptional level of *dxs* mRNA in the DXSox-isP strain was similar to that in the early-logarithmic phase (Fig. 3-4), both the soluble:insoluble DXS ratio and the soluble DXS level were increased (Fig. 3-6). Cell activity in the late-logarithmic phase should be low, resulting in a lower translation rate. As a result, the percentage of soluble DXS proteins that is successfully processed by chaperones might be increased.

The ratios of soluble:insoluble IspS were essentially constant throughout the culture (Fig. 3-6), in spite of the changes in the *isps* mRNA level (Fig. 3-4). The results suggest that this exogenous protein will not be affected by the cyanobacterial protein quality control system, and the ratio of soluble:insoluble protein will depend on the folding ability of IspS itself.

With regard to the isoprene productivity, the DXSox-isP strain exhibited a significantly higher productivity level (1.4- to 1.8-fold) during the induction phase to the early-logarithmic phase than the WT-isP strain (Fig. 3-2). A possible explanation is that the lower level of soluble DXS in those phases (Fig. 3-5A) would lead to a lower accumulation of IPP, which is an inhibitor of IspS (97).

In this study, we found that the solubility of DXS is strictly regulated in cyanobacteria, presenting an obstacle to the enhancement of their MEP pathway flux. It is likely that this is not the case for DXS only. A way to avoid this regulation is the use of an exogenous protein with a high folding ability. Indeed, Gao *et al.* demonstrated that the heterologous expression of the IspS from six species in *S. elongates* resulted in dramatically different soluble protein levels and activities (the activity of IspS from *E. globulus* was 10–50-fold higher than that of KSIspS). We recently reported the stability and specific activity of 11 DXS proteins from nine species (30), and found that the DXS from *Paracoccus aminophilus*, *Rhodobacter capsulatus*, and *Bacillus subtilis* showed significantly higher stability than that from *S.6803*. We are now examining the solubility of these DXS proteins in the corresponding cyanobacteria recombinants.

CHAPTER 4

Exploration of the 1-deoxy-D-xylulose 5-phosphate synthases suitable for the creation of a robust isoprenoid biosynthesis system

Introduction

Isoprenoids are a diverse group of compounds with extensive applications as biofuels, chemical precursors, and pharmaceuticals and in aromatherapy (6-8). Although isoprenoid products are currently obtained mainly through organic synthesis and plant extract, production using genetically modified organisms is expected to be an economical and environmentally friendly option. All isoprenoids are biologically synthesized from two common building blocks, isopentenyl diphosphate (IPP) and dimethylallyl diphosphate (DMAPP), which are produced via the 2-*C*-methyl-D-erythritol-4-phosphate (MEP) pathway in bacteria, cyanobacteria, algae, and plant chloroplasts. The MEP pathway involves eight enzymes and utilizes pyruvate and D-glyceraldehyde-3-phosphate (D-GAP) as starting materials; the first step of this pathway is catalyzed by 1-deoxy-D-xylulose 5-phosphate synthase (DXS), which was considered a rate limiting enzyme (9-11). In eukaryotes including plant cytosol, IPP and DMAPP are synthesized via the mevalonate (MVA) pathway (12), which involves seven enzymes; this pathway begins by generating acetoacetyl-CoA from two molecules of acetyl-CoA and proceed until the production of IPP and DMAPP.

Cyanobacteria not only are widely used model phototrophs for basic biological studies but also are attractive candidates for use in bio-industrial applications because of their high photosynthetic capability. Cyanobacteria can convert captured solar energy into biomass at efficiencies exceeding those of terrestrial plants (cyanobacteria, 3–9% versus terrestrial plants, 0.25–3%) (14). I previously attempted to improve the isoprenoid productivity of cyanobacteria,

Synechocystis sp. PCC6803 (*S. 6803*), by overexpressing endogenous DXS (S.6803DXS) (100). This DXS over-expressing strain of *S. 6803* was generated by inserting an additional *dxs* gene under a strong promoter, *psbA2* promoter, and successfully produced 1.5-fold carotenoid, also an isoprenoid, compared with the original strain. However, although the mRNA level in the DXS-overexpression *S. 6803* strain showed a 4-fold increase compared with that in the original strain, the soluble protein levels of DXS showed an only 1.5-fold increase and a large fraction of DXS protein was found in an insoluble fraction as an inactivated form (107).

As shown in our previous study, S.6803DXS is likely to be inactivated after translation quickly. In contrast, when green fluorescence protein (GFP) which has relatively high solubility and high stability is exogenously over-expressed under the control of the *psbA2* promoter in *S.6803*, the significant protein expression was observed and the protein level was also consistent with the corresponding mRNA level (108). Therefore, it can be assumed that the solubility of individual enzyme is an important factor to determine the total activities *in vivo*. In addition, in the case of *Populus trichocarpa* DXS (PtDXS), the activity of DXS was also regulated in a feedback-inhibited manner with IPP and DMAPP (109). However, it has not been considered the importance of such protein-level regulation with regard to isoprenoid production properly.

In this study, to exploit “robust DXSes”, 11 *dxs* genes from nine organisms were subcloned into a pET28a plasmid and expressed in *E. coli*. The accumulation level and solubility of DXS proteins and mRNA abundance of *dxs* genes in *E. coli* were analyzed, and the activity, stability, and inhibitory effect with DMAPP were evaluated using purified DXSes. Finally, three promising DXSes were co-expressed with isoprene synthase (IspS) in *E. coli*, and isoprene production in these co-expression strains was measured.

Materials and methods

Plasmids, strains, and materials

Rhodobacter sphaeroides NBRC12203, *R. capsulatus* NBRC16435, *Micrococcus luteus* NBRC3333, *Paracoccus aminophilus* NBRC16710, and *Thermus thermophilus* NBRC101085 were obtained from Biological Resource Center, National Institute of Technology and Evaluation (Tokyo, Japan). *Bacillus subtilis* JCM11003 was purchased from the Japan Collection of Microoganisms, RIKEN BioResource Center (Tsukuba, Ibaraki, Japan).

The synthesized *Haematococcus pluvialis* DXS gene (GenBank: HQ450862.1) was obtained from GenScript Inc. (Piscataway, NJ) as full-length containing the target sequence without N-terminal truncation. The plasmid pBA2SkIKmA2, carrying the *ispS* gene from *Pueraria montana* (kudzu) in which codons were optimized for *S.6803*, was obtained from addgene (Cambridge, MA, USA) (45). *E. coli* DH5α (RBC BioScience, Taipei, Taiwan) was used for gene manipulations. *E. coli* BL21 (DE3) (TaKaRa Bio, Otsu, Japan) was used for recombinant DXSes preparations and isoprene production. The extraction of genomic and plasmid DNA was performed using a Genomic DNA Extraction Kit Mini and a HiYield Plasmid Mini Kit (RBC BioScience) according to manufacturer's instructions. Luria-Bertani (LB) medium (Nacalai Tesque, Kyoto, Japan) was used for cultivation during plasmid construction, gene expression, and isoprene production experiments. Antibiotics were added into each culture according to the resistance marker of plasmids at following concentrations: ampicillin (100 μg/L) and kanamycin (20 μg/L). Optical density at 600 nm (OD_{600}) was measured using an Implen NanoPhotometer (Implen GmbH, München, Germany).

N-terminal histidine-tagged DXS proteins and the corresponding genes are designated PaDXS and Pa*dxs* (for *Paracoccus aminophilus*, Gene ID: 16539831), BsDXS and Bs*dxs* (for *Bacillus subtilis*, Gene ID: 938609), EcDXS and Ec*dxs* (for *E. coli*, Gene ID: 945060), S.6803DXS and S.6803*dxs* (for *S.6803*, Gene ID: 12256157), RsDXSA and Rs*dxs*A (for *Rhodobacter*

sphaeroides, Gene ID: 3719396), RsDXSB and Rs*dxs*B (for *Rhodobacter sphaeroides*, Gene ID: 3720832), MlDXS and Ml*dxs* (for *Micrococcus luteus*, Gene ID: 7985882), TtDXS and Tt*dxs* (for *Thermus thermophilus*, Gene ID: 2774851), and HpDXS and Hp*dxs* (for *Haematococcus pluvialis*), respectively (Table 4-1). Two newly cloned DXSes and the corresponding genes from *R. capsulatus* NBRC16435 are named RcDXSA and Rc*dxs*A, and RcDXSB and Rc*dxs*B, respsctively. The amino acid sequences of RcDXSA and RcDXSB exhibit high homologies with those of DXSes from *R. capsulatus* determined by Hahn et al. (110) (RcDXSA: Identity 630 / 641 (98%), RcDXSB: Identity 622 / 636 (97%). The C-terminal histidine-tagged proteins corresponding to S.6803DXS, MlDXS, RcDXSB, RsDXSA, and TtDXS are abbreviated as S.6803DXS-H_6, MlDXS-H_6, RcDXSB-H_6, RsDXSA-H_6, and TtDXS-H_6, respectively (Table 4-1).

Table 4-1. Plasmids for over-expression of DXSes.

Plasmids	Parental plasmid	Insert site	Insert gene	Abbreviations of the DXS	Reference
pET28a-H_6-BsDXS	pET28a	BamHI & SalI	*B. subtilis dxs*	BsDXS	this work
pET28a-H_6-EcDXS	pET28a	NdeI & NotI	*E.coli dxs*	EcDXS	this work
pET28a-H_6-HpDXS	pET28a	NdeI & NotI	*H. pluvialis dxs*	HpDXS	this work
pET28a-H_6-MlDXS	pET28a	NdeI & NotI	*M. luteus dxs*	MlDXS	this work
pET28a-H_6-PaDXS	pET28a	NdeI & NotI	*P. aminophilus dxs*	PaDXS	this work
pET28a-H_6-RcDXSA	pET28a	NdeI & NotI	*R. capsulatus dxs*A	RcDXSA	this work
pET28a-H_6-RcDXSB	pET28a	NdeI & NotI	*R. capsulatus dxs*B	RcDXSB	this work
pET28a-H_6-RsDXSA	pET28a	NdeI & NotI	*R. sphaeroides dxs*A	RsDXSA	this work
pET28a-H_6-RsDXSB	pET28a	NdeI & NotI	*R. sphaeroides dxs*B	RsDXSB	this work
pET28a-H_6-S6803DXS	pET28a	NdeI & NotI	*S.*6803 *dxs*	S6803DXS	this work
pET28a-H_6-TtDXS	pET28a	NdeI & NotI	*T. thermophilus dxs*	TtDXS	this work
pET22b_MlDXS-H_6	pET22b	NdeI & NotI	*M. luteus dxs*	MlDXS-H_6	this work
pET22b_RcDXSB-H_6	pET22b	NdeI & NotI	*R. capsulatus dxs*B	RcDXSB-H_6	this work
pET22b_RsDXSA-H_6	pET22b	NdeI & NotI	*R. Sphaeroides dxs*A	RsDXSA-H_6	this work
pET_dxs-his	pET22b	NdeI & NotI	*S.*6803 *dxs*	S6803DXS-H_6	100
pET22b_TtDXS-H_6	pET22b	NdeI & NotI	*T. thermophilus dxs*	TtDXS-H_6	this work

Plasmid constructions

All primer sequences are shown in Table 4-2. Primers and templates used for the amplifications of individual *dxs* genes are listed in Table 4-3. The S. 6803*dxs* fragment was obtained by digesting pET_dxs-his (100) with *Nde*I and *Not*I. Overexpression plasmids are shown in Table 4-1, together with the inserted *dxs* gene fragments, pET plasmids, and their insertion sites. *ispS* and the *trc* promoter sequences were amplified from the laboratory plasmid pUC19-trc-SkIspS, which harbors *ispS* from pBA2SkIKmA2 and the *trc* promoter from pT31CTH_TePixJ, (102) by using primers trc_2831a_F and skisps_2831a_R and were inserted into *Not*I site of pRL2831a, (111) generating pRL2831a-Ptrc-SkIspS. The gene coding for 1-deoxy-D-xylulose-5-phosphate reductoisomerase (DXR) was amplified from *E. coli* genomic DNA by using primers E.coli_dxr_pET28a-F and E.coli_dxr_pET28a-R and was inserted into *Bam*HI and *Sal*I sites of pET28a, generating pET28a-H_6-EcDXR.

Table 4-2. Primer sequences used in CHAPTER 4.

Primers	Primer sequence(5′→3′)
B. subtilis_dxs_pET28a-F	CGCGGATCCGATCTTTTATCAATACAGGACCCG
B. subtilis_dxs_pET28a-R	GCGTCGACTTATGATCCAATTCCTTTGTGTG
E.coli_dxr_pET28a-F	CGCGGATCCAAGCAACTCACCATTCTGGG
E.coli_dxr_pET28a-R	CCCGTCGACTCAGCTTGCGAGACGCATCA
E.coli_dxs_pET28_F	CGCGCGGCAGCCATATGAGTTTTGATATTGCCAAATACCC
E.coli_dxs_pET28_R	TGCTCGAGTGCGGCCTTATGCCAGCCAGGCCTTG
M.luteus_dxs_pET28_F	CGCGCGGCAGCCATATGGAACATCTGCCCCC
M.luteus_dxs_pET28_R	TGCTCGAGTGCGGCCTCATGCCTGCTCCTGGTG
P.aminophilus_dxs_pET28_F	CGCGCGGCAGCCATATGACCGACGACAGCCAGC
P.aminophilus_dxs_pET28_R	TGCTCGAGTGCGGCCTCACGCCCGTCGCTCTC
R.capsulatus_dxsA_pET28_F	CGCGCGGCAGCCATATGAGCGCCACGCCATC
R.capsulatus_dxsA_pET28_R	TGCTCGAGTGCGGCCTTACGCGCTGTGCACGATC
R.capsulatus_dxsB_pET28_F	CGCGCGGCAGCCATATGAGCCAGCCCCCAGTG
R.capsulatus_dxsB_pET28_R	TGCTCGAGTGCGGCCTCAGGCGCGTTTCGCC
R.sphaeroides_dxsA_pet28_F	CGCGCGGCAGCCATATGACCAATCCCACCCCGCG
R.sphaeroides_dxsA_pet28_R	TGCTCGAGTGCGGCCTCAGACCGCCCGCGGCTTTG
R.sphaeroides_dxsB_pet28_F	CGCGCGGCAGCCATATGACCGACAGACCCTGCACGC
R.sphaeroides_dxsB_pet28_R	TGCTCGAGTGCGGCCTCAGGCGCGGCGGGC
T. thermophilus_dxs_pet28_F	CGCGCGGCAGCCATATGATCTTGGACAAGGTGAACAG
T. thermophilus_dxs_pet28_R	TGCTCGAGTGCGGCCTCAGGCCCGTTCATGC
M.luteus_dxs_pET22b_F	GAAGGAGATATACATATGGAACATCTGCCCCC
M.luteus_dxs_pET22b_R	CTCGAGTGCGGCCGCTGCCTGCTCCTGGTGG
R.capsulatus_dxsB_pET22b_F	GAAGAAGATATACATATGAGCCAGCCCCCAGT
R.capsulatus_dxsB_pET22b_R	CTCGAGTGCGGCCGCGGCGCGTTTCGCCACC
R.sphaeroides_dxsA_pET22b_F	GAAGGAGATATACATATGACCAATCCCACCCC
R.sphaeroides_dxsA_pET22b_R	CTCGAGTGCGGCCGCGACCGCCCGCGGCTTTG
T. thermophilus_dxs_pET22b_F	GAAGGAGATATACATATGATCTTGGACAAGGTG

Table 4-2. Primer sequences used in CHAPTER 4. (continued)

Primers	Primer sequence(5′→3′)
T. thermophilus_dxs_pET22b_R	CTCGAGTGCGGCCGCGGCCCGTTCATGCACC
trc_2831a_F	ATATTCGATGCGGCCCGCTTCGTTAATACAGACG
skisps_2831a_R	CTCTTACGAGCGGCCTTACACGTACATTAATTGATTAATTGG
B. subtilis_RTPCR_F	CGTAGGAATCGCAGAACAGC
B. subtilis_RTPCR_R	CTTGGTCATATGCCCTTTGC
P.aminophilus_RTPCR_F	CAGCTTTTGCTGGAAGAAGG
P.aminophilus_RTPCR_R	CATGGTCGATGAAAGTGTCG
R.capsulatus_dxsA_RTPCR_F	AGATCGTCGAAGTGGTCAGC
R.capsulatus_dxsA_RTPCR_R	GTCCCAGATCAGCTTGTCG
R.sphaeroides_dxsB_RT-PCR_F	TGAACGACAACGAGATGAGC
R.sphaeroides_dxsB_RT-PCR_R	GCCTTGAAGTCCTGGAACG
S.6803_dxs_RTPCR_F	CTCCCAAGGATGAAGCAGAG
S.6803_dxs_RTPCR_R	TTACCAATTTCCAGCGGTTC
rpoB_RTPCR_F	GTATGTCCAATCGAAACCCCT
rpoB_RTPCR_R	GGTAGTGAATTTCGTCAGTTACA
rrn16s_RTPCR_F	CATGCCGCGTGTATGAAGAA
rrn16s_RTPCR_R	CGGGTAACGTCAATGAGCAAA

Table 4-3. The primers and genomic DNA resources used for the amplifications of individual *dxs* genes.

Primer	Genome DNA
B. subtilis_dxs_pET28a-F B. subtilis_dxs_pET28a-R	*Bacillus subtilis*
E.coli_dxs_pET28_F E.coli_dxs_pET28_R	*Escherichia coli*
M.luteus_dxs_pET28_F M.luteus_dxs_pET28_R	*Micrococcus luteus*
P.aminophilus_dxs_pET28_F P.aminophilus_dxs_pET28_R	*Paracoccus aminophilus*
R.capsulatus_dxsA_pET28_F R.capsulatus_dxsA_pET28_R	*Rhodobacter capsulatus*
R.capsulatus_dxsB_pET28_F R.capsulatus_dxsB_pET28_R	*Rhodobacter capsulatus*
R.sphaeroides_dxsA_pet28_F R.sphaeroides_dxsA_pet28_R	*Rhodobacter sphaeroides*
R.sphaeroides_dxsB_pet28_F R.sphaeroides_dxsB_pet28_R	*Rhodobacter sphaeroides*
T. thermophilus_dxs_pet28_F T. thermophilus_dxs_pet28_R	*Thermus thermophilus*
M.luteus_dxs_pET22b_F M.luteus_dxs_pET22b_R	*Micrococcus luteus*
R.capsulatus_dxsB_pET22b_F R.capsulatus_dxsB_pET22b_R	*Rhodobacter capsulatus*
R.sphaeroides_dxsA_pET22b_F R.sphaeroides_dxsA_pET22b_R	*Rhodobacter sphaeroides*
T. thermophilus_dxs_pET22b_F T. thermophilus_dxs_pET22b_R	*Thermus thermophilus*

Analyses of accumulation levels of recombinant proteins

E.coli BL21 (DE3) cells were transformed with overexpression plasmids for *dxs* genes by the electroporation procedure. The transformants were incubated in LB medium overnight at 37°C as seed cultures. Ten milliliters of seed cultures were inoculated in 100 mL LB medium and were cultivated under two conditions, mild and intense induction conditions. In the mild induction condition, the culture was incubated at 26°C until OD_{600} reach 0.8, and then the protein expression was induced with 0.2 mM isopropyl β-D-thiogalactopyranoside (IPTG; Nacalai Tesque) for 5 h at 26°C. In the intense induction condition, the incubation temperature, the concentration of IPTG and induction time were 37°C, 1 mM, and 24 h, respectively. The cultures were harvested by centrifugation at 12,000 g for 5 min. The pellet (0.1 g) was resuspended into 0.4 mL of B-PER II reagent (Thermo SCIENTIFIC, Waltham, MA). The mixture was incubated for 15 min at room temperature, and the supernatant was separated from the precipitates by centrifugation at 12,000 g for 5 min. The precipitates were resuspended to the same volume of 2% w/v SDS aqueous solution as the corresponding supernatant. The same volume (2 μl) of supernatant and the suspended precipitates were subjected to 10% SDS-polyacrylamide gel electrophoresis. The separated proteins were blotted onto PVDF membranes (Merck KGaA, Darmstadt, Germany) and probed sequentially with Penta-His Biotin Conjugate (Roche, Basel, Switzerland) and Streptavidin-Horseradish Peroxidase Conjugate (Prozyme, San Leandro, CA). Protein bands were visualized using the Pierce Western Blotting Substrate (Thermo SCIENTIFIC) following the manufacturer's instruction. The western blotting images were acquired using ImageQuant LAS 4000 mini (GE Healthcare). In all western blotting analyses, the EcDXS supernatant aliquots from the intense or mild induction condition sample were applied as a reference. The intensities of the western blotting bands for DXSes on a PVDF membrane were quantified by ImageQuant TL software (GE Healthcare) and normalized to that of the reference EcDXS band in the corresponding condition. For the comparison

of the data in the two conditions, those were corrected with the ratio between the two reference intensities. The data were shown as relative levels to the soluble EcDXS under intense induction condition (Fig. 4-1B).

To analysis the accumulation level of IspS, the cultures were harvested by centrifugation at 12,000 g for 5 min. Cells were resuspended in Tris-HCl buffer (50 mM Tris-HCl (pH 7.6), 500 mM NaCl) and lysed by sonication. To remove cell debris, the cell lysate was centrifuged at 12,000 g for 5 min at 4°C. Then, the supernatant was separated by 10% SDS-PAGE, blotted onto PVDF membranes (Merck), probed sequentially with a custom synthesized polyclonal antibody (MEDICAL & BIOLOGICAL LABORATORIES CO., Nagano, Japan, antigen peptide sequence: SRRSANYQPNLWNFEFLC) and a goat anti-rabbit IgG-Horse radish Peroxidase conjugate (Santa Cruz Biotechnology, Santa Cruz, CA, USA) as a secondary antibody. The detection and quantification was performed using the same apparatus and software as descried above.

Real-time quantitative PCR

The mRNA abundance of the *dxs* genes were determined by real-time quantitative PCR (qPCR). DXS-overexpressing strains were incubated in LB medium overnight at 37°C as seed cultures. Seed cultures (10 mL) were inoculated into 100 mL LB medium and incubated at 26°C or 37°C. Overexpression was induced by adding IPTG to final concentration of 0.2 mM or 1 mM at an OD_{600} of 0.8; the cultures were incubated further for 5 h and harvested by centrifugation. The pellets were stored in RNA Save (Biological Industries, Beit-Haemek, Israel) until the RNA extraction experiments. Total RNA from pellets was isolated by acid guanidinium thiocyanate-phenol-chloroform extraction methods (104) and subjected to the reverse transcription reaction with ReverTra Ace (TOYOBO, Osaka, Japan). The resultant cDNA was used as a template for qPCR with THUNDERBIRD SYBR qPCR mix (TOYOBO) and a StepOne cycler (Applied

Biosystems, Foster City, CA, USA). The transcriptional level of the16S rRNA gene was used as an internal standard to normalize the qPCR value. Primers used for qPCR and target genes are listed in Table 4-4.

Table 4-4. The primers used for qPCR and the target genes.

Primer name	Target gene
B. subtilis_dxs_RTPCR_F B. subtilis_dxs_RTPCR_R	Bs*dxs*
P.aminophilus_dxs_RTPCR_F P.aminophilus_dxs_RTPCR_R	Pa*dxs*
R.capsulatus_dxsA_RTPCR_F R.capsulatus_dxsA_RTPCR_R	Rc*dxs*A
R.sphaeroides_dxsB_RT-PCR_F R.sphaeroides_dxsB_RT-PCR_R	Rs*dxs*B
S.6803_dxs_RTPCR_F S.6803_dxs_RTPCR_R	S6803*dxs*
rpoB_RTPCR_F rpoB_RTPCR_R	*rpoB*
rrn16s_RTPCR_F rrn16s_RTPCR_R	16S rRNA

Protein purifications

E. coli BL21 (DE3) transformants for DXSes or DXR were incubated in LB medium overnight at 37°C as seed cultures. Seed culture (20 mL) was inoculated into 1000 mL LB medium and incubated at 26°C. Overexpression was induced by adding IPTG to final concentration of 0.2 mM at an OD_{600} of 0.8, except for the case of DXR. For the overexpression of DXR, 1 mM of IPTG was used. After induction, the culture was incubated for 5 h at 26°C and harvested. Cells were resuspended in 25 mL of buffer A (50 mM Tris-HCl (pH 7.6), 500 mM NaCl and 10% glycerol) and lysed by sonication. To remove cell debris, the cell lysate was centrifuged at 12,000 g for 5 min at 4°C. The supernatant was mixed with 2 mL COSMOGEL His-Accept (Nacalai Tesque) equilibrated with buffer A and incubated for 15 min at 4°C. The slurry was poured into a column (ϕ 2 cm x 3 cm), and the flow-through fraction was discarded. After washing with buffer A, histidine-tagged DXS or DXR protein was eluted with buffer B (50 mM Tris-HCl pH 7.6, 500 mM NaCl, 500 mM imidazole and 10% glycerol). The purified protein was concentrated to approximately 1 mL by Vivaspin Turbo 15 (Sartorius Stedim Biotech, Goettingen, Germany) and was used within 12 h.

Enzyme activity assays

DXS activities were analyzed by a coupled enzyme assay using DXR (112, 113). Assay mixtures contained 100 mM Tris/HCl (pH 7.8), 10 mM $MgCl_2$, 0.3 mM thiamine pyrophosphate (TPP), 1 mM dithiothreitol (DTT), 0.3 mM nicotinamide adenine dinucleotide phosphate (NADPH), various concentrations of sodium pyruvate (0.05–5 mM) and D,L-GAP (0.2–2.0 mM), and DXR (100 or 50 μg/mL). The mixtures were incubated at 30°C for 2 min inside a temperature controlled spectrophotometer (model UV-1800, Shimadzu, Kyoto, Japan) and added to the DXS sample (final concentration of 50 or 25 μg/mL) to start the reaction. The reaction was traced by monitoring the

absorption at 340 nm at 30°C. The initial rates were measured at varying substrate concentrations, and k_{cat} and K_m values were calculated by fitting the initial rate versus substrate concentration curve to the Michaelis–Menten equation. The half values of concentrations of racemic D,L-GAP product were used as the concentrations of the D-form (DXS's substrate) for kinetic analyses. The feedback inhibitory effect of DMAPP on DXS activity was examined in assay mixtures containing 1 mM DMAPP and 25 μM TPP.

Tolerance against thermal and protease treatments

To assess the thermostability, DXS protein (about 1 mg/mL) was incubated at 30–50°C for 10 min in buffer B containing 10–50% glycerol. The incubated DXS was added (final concentration of 50 μg/mL) to assay mixtures containing 100 mM Tris/HCl (pH 7.8), 10 mM $MgCl_2$, 0.3 mM TPP, 1 mM DTT, DXR (100 μg/mL), NADPH (0.3 mM), and D,L-GAP (2.0 mM), and the residual enzyme activity was measured as in the activity assay experiment.

To examine the resistance to proteases, 0.5 mg/mL DXS was incubated at 20°C or 40°C in 50 mM Tris/HCl (pH 7.6) with 500 ng/mL trypsin (Wako Pure Chemical Industries, Osaka, Japan) or 500 ng/mL proteinase K (GE Healthcare UK Ltd, Amersham, UK) for various periods. After incubation, they were subjected to SDS-PAGE. The protein bands of DXS were detected by Coomassie brilliant blue staining and the band intensities were quantified using ImageJ software (National Institutes of Health, USA; http://imagej.nih.gov/ij/download.html).

Isoprene productions

E. coli BL21 (DE3) strains harboring a DXS expression vector or pET28a vector were transformed with pRL2831a-Ptrc-SkIspS, yielding strains co-expressing DXS and IspS or a control strain expressing only IspS, respectively. The co-expression strains were incubated in LB medium

overnight at 30°C and then inoculated to an OD_{600} of 0.25 to 500-mL Erlenmeyer flasks containing 250 mL LB medium. After incubation for 30 min at 30°C, protein expression was induced by adding IPTG at a final concentration of 0.1 mM, and the culture was divided into five sealed culture vials. The sealed culture was further incubated for 6 h or 24 h at 30°C and the headspace contents were analyzed by gas chromatography (GC14B, Shimadzu) equipped with a PEG20M 10% shinwasorb-S60-80 column (2.6 mm x 3.1 m; Shinwa Chemical Industries Ltd, Kyoto, Japan) and a flame ionization detector (FID). The amounts of isoprene production were calculated using a calibration curve prepared by using pure isoprene.

Result

Solubility and accumulation level of exogenous DXS enzymes

To assess the *in vivo* solubility of DXSes, the expression of DXS was induced in *E. coli* under the intense induction condition in which the final IPTG concentration, the incubation time, and temperature were 1 mM, 24 h, and 37°C, respectively. Generally, the protein expressed at 37°C and 1 mM IPTG concentration under the control of *T7* promoter show high tendency of protein misfolding and aggregation (114). Furthermore, in the plateau phase after the extremely long incubation (24 h), the protein degradation rate is often enhanced (115, 116). DXS proteins were also expressed to purify the recombinant DXSes under the mild induction condition in which the final IPTG concentration, the incubation time, and temperature were 0.2 mM, 5 h, and 26°C, respectively.

Lysates of the induced cells were fractionated into soluble and insoluble fractions by centrifugation and analyzed by western blotting. As shown in Fig. 4-1, in the intense induction condition, PaDXS showed the highest ratio of soluble form to insoluble form (39%), followed by EcDXS (38%), MlDXS (20%), BsDXS (19%), RsDXSB (15%), TtDXS (10%), S.6803DXS (4%), RcDXSA (2%), RcDXSB (2%), RsDXSA (1%), and HpDXS (0%). The quantitative level of the soluble form in PaDXS was also higher than that of other DXSes. In the mild induction condition, similar soluble/insoluble ratios were observed for PaDXS (33%), EcDXS (30%), MlDXS (26%), BsDXS (15%), RsDXSB (12%), TtDXS (8%), RcDXSB (1%), and HpDXS (0%) compared with those in the intense induction condition, while remarkably increased ratios were found in S.6803DXS (16%), RcDXSA (14%), and RsDXSA (13%). From these observations, we concluded that PaDXS, MlDXS, EcDXS and BsDXS exhibit a high solubility *in vivo*.

The quantitative levels of the total DXS protein (soluble and insoluble forms) were greatly different among DXSes and were not correlated with the soluble/insoluble ratio of the corresponding DXS.

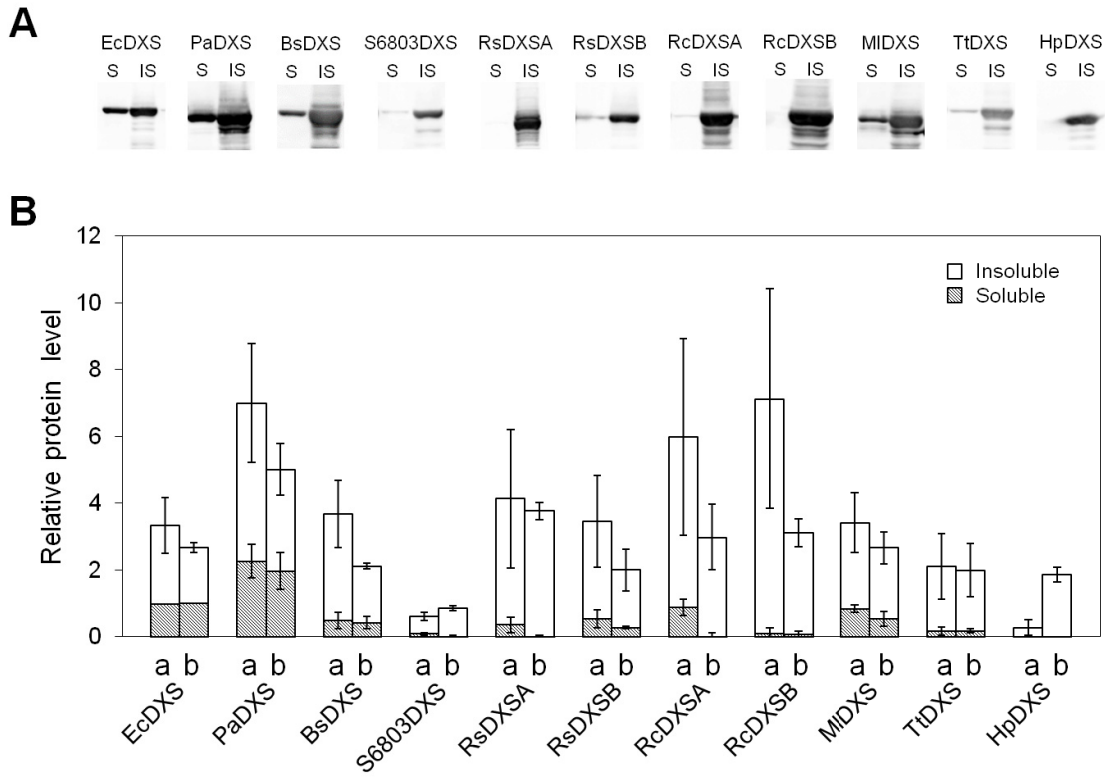

Fig. 4-1. Relative DXS protein levels.
The western blotting band images of DXSes in the intense induction condition are presented (A). S and IS mean the soluble and insoluble fraction. DXS accumulations in the soluble fraction (hatched bar) and insoluble fraction (white bar) under the mild induction condition (26°C, with 0.2 mM IPTG for 5 h) (a) and the intense induction condition (37°C, with 1 mM IPTG for 24 h) (b) were estimated from the western blotting band quantification and shown as relative levels to that in the soluble fraction of EcDXS in the intense induction condition (B). The data are presented as mean ± SD of three replicates.

Stability of mRNA

To estimate the stability of mRNA, amounts of the *dxs* mRNA were measured by qPCR. In our system, all *dxs* mRNAs were synthesized under the control of the same promoter (*T7* promoter) and then were degraded with different rates. Therefore, the difference in mRNA abundance reflects the difference in mRNA stability. The relative mRNA levels of Pa*dxs*, Bs*dxs*, Rc*dxs*A, Rs*dxs*B, and S.6803*dxs* genes are shown in Fig. 4-2. The mRNA level of S.6803*dxs* was found to be significantly lower than that of the other four *dxs* genes, indicating the lower stability of S.6803*dxs* mRNA.

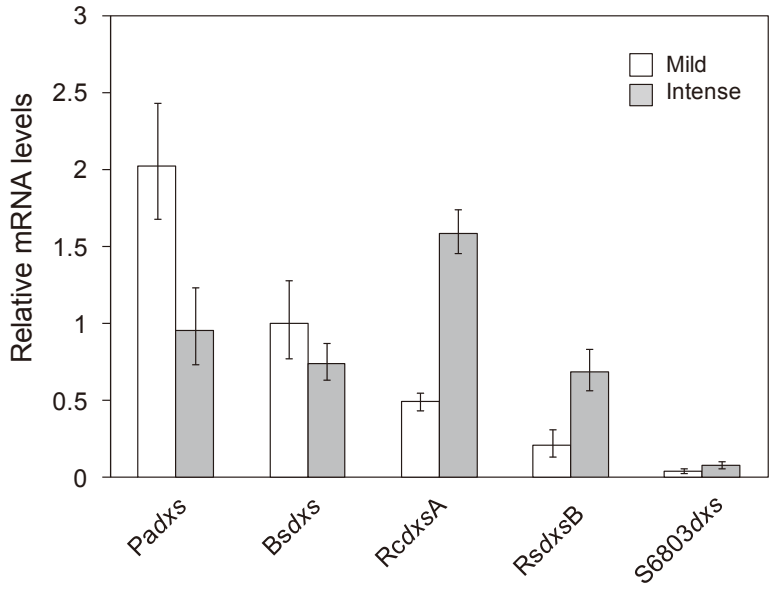

Fig. 4-2. *dxs* mRNA levels.
The mRNA levels under the mild (white bar) and intense (gray bar) induction conditions were measured by quantitative PCR using 16S rRNA as a reference gene. The *dxs* mRNA levels in strains expressing Pa*dxs*, Bs*dxs*, Rc*dxs*A, Rs*dxs*B, or S.6803*dxs* are shown as relative levels to that of Bs*dxs* in the mild induction condition. The data are presented as mean ± SD of three replicates.

Purification, activity feedback inhibition, and stability

We tried to purify N-terminal histidine-tagged DXSes, and PaDXS, BsDXS, RcDXSA, EcDXS, S.6803DXS, RsDXSA, RsDXSB, and MlDXS were successfully purified using NiNTA column, but RcDXSB, TtDXS, and HpDXS were not (Fig. 4-3).

The DXS activity was measured by coupling assay using DXR. Using the purified DXSes, we assayed their activities and found that PaDXS, BsDXS, RcDXSA, EcDXS, and RsDXSB were obviously active, but S.6803DXS, RsDXSA, and MlDXS were not. To investigate the influence of the N-terminal histidine tag in the three DXSes that failed to be purified and the three inactive DXSes, we examined the exchange of the tag position from N-terminal to C-terminal. All expression vectors except for that for C-terminal histidine-tagged HpDXS were successfully prepared, and it was revealed that the expression levels (Fig. 4-3) and activity properties were the same. The K_m and k_{cat} values for pyruvate and GAP of PaDXS, BsDXS, RcDXSA, EcDXS, and RsDXSB were compared in Fig. 4-4. RcDXSA showed the highest k_{cat} (5.5 sec^{-1}) among the five DXSes, and BsDXS has highest K_m values ($K_m^{pyruvate}$ = 310 μM, K_m^{GAP} = 2600 μM) and the second highest k_{cat} (3.2 sec^{-1}). RsDXSB exhibited the lowest K_m value to GAP (401 μM) and the lowest k_{cat} (0.4 sec^{-1}). EcDXS and PaDXS showed the moderate K_m and k_{cat} values. The parameters of EcDXS （$K_m^{pyruvate}$ = 93 μM, K_m^{GAP} = 510 μM, k_{cat} = 1.9 sec^{-1}) are similar to those reported by Brammer et al. ($K_m^{pyruvate}$ = 74.7 μM, K_m^{GAP} = 279 μM, k_{cat} = 3.48 sec^{-1}) (117). In spite of a high homology with the homolog DXS in *R. capsulatus*, RcDXSA exhibits the significantly different parameters ($K_m^{pyruvate}$ = 150 μM, K_m^{GAP} = 1100 μM, k_{cat} = 5.5 sec^{-1}) from those of the homolog reported by Hahn et al. ($K_m^{pyruvate}$ = 610 μM, K_m^{GAP} = 150 μM) (110) and Eubanks and Poulter ($K_m^{pyruvate}$ = 440 μM, K_m^{GAP} = 68 μM, k_{cat} = 1.9 sec^{-1}) (118).

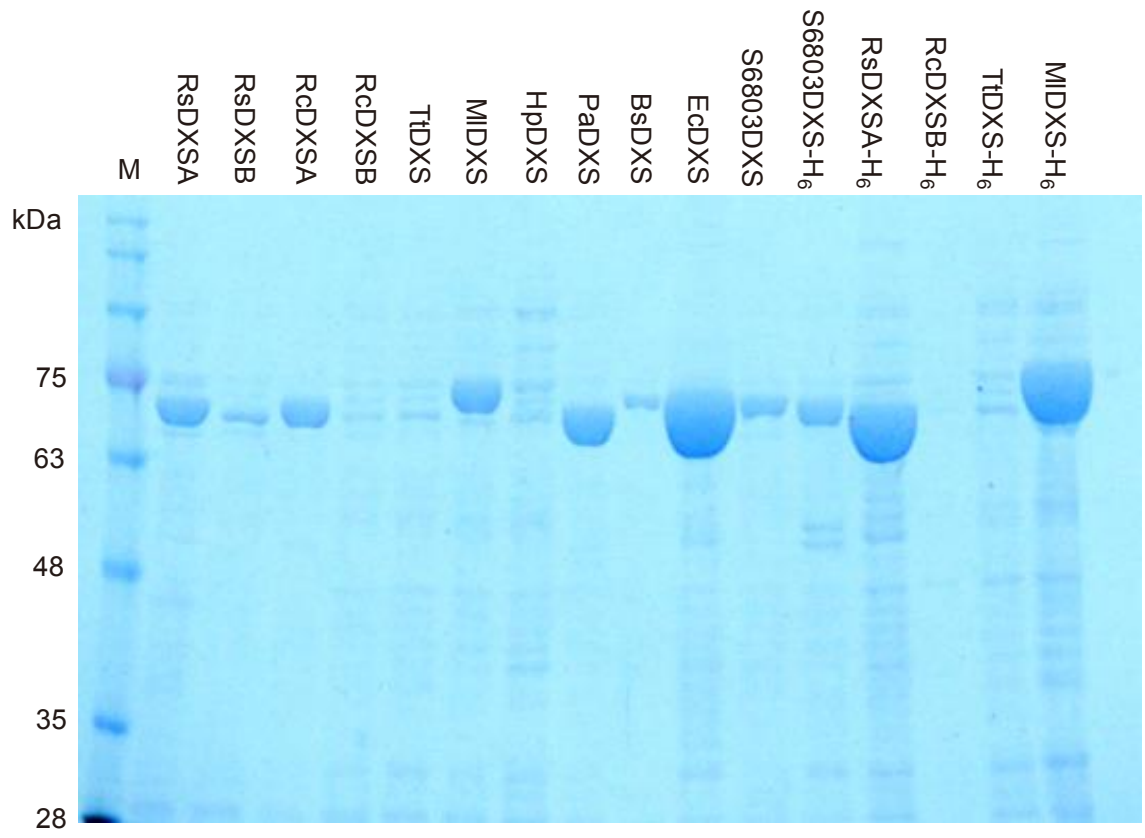

Fig. 4-3. SDS-PAGE analyses for purified DXS samples.

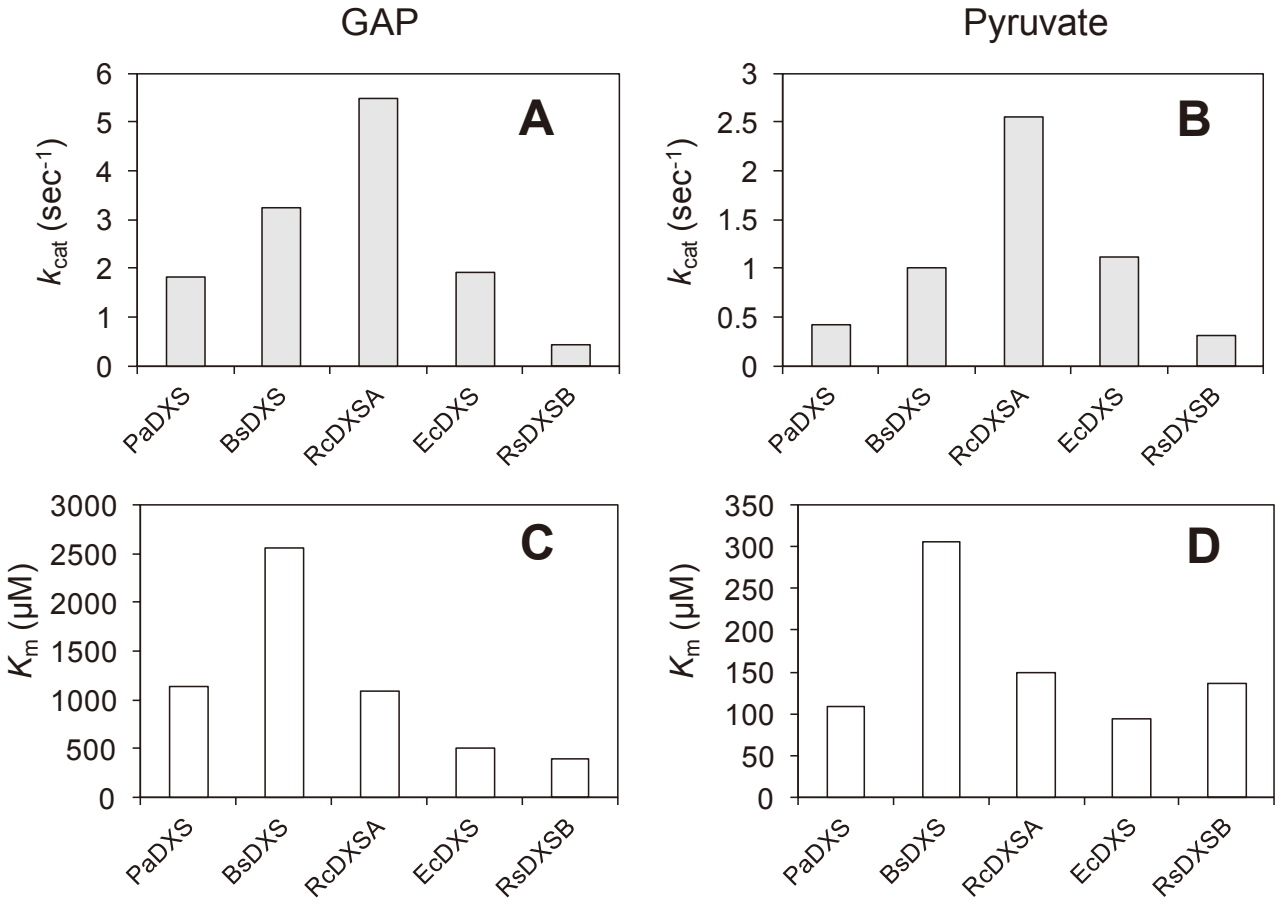

Fig. 4-4. Kinetic parameters of DXSes.
k_{cat} (panels A and B) and K_m (panels C and D) toward D-GAP (A and C) or pyruvate (B and D) of each DXS were determined by fitting the kinetic data to the Michaelis–Menten equation. The half values of concentrations of racemic D,L-GAP product were used as the concentrations of the D-form (DXS's substrate) for kinetic analyses. The reactions were conducted at 30°C in a buffer consisting of 100 mM Tris-HCl (pH 7.8), 1 mM DTT, 0.3 mM NADPH, 0.3 mM TPP, and various concentrations of sodium pyruvate (0.05–5.0 mM), D,L-GAP (0.2–2.0 mM), 10 mM $MgCl_2$, and 50 μg/mL DXR.

We found that all the purified DXSes were easily inactivated in Tris buffer without glycerol, but could be stored in the buffer containing 50% glycerol at −20°C for 48 h with no significant loss of activity, except for EcDXS (Fig. 4-5). The EcDXS activity quickly lost even in the above conditions.

To estimate the inhibitory effects of DMAPP, DXS activities were measured in the presence of 1 mM DMAPP. The inhibitory rate was only 13%, 14% and 16% in BsDXS, RsDXSB and PaDXS, respectively, but approximately 50% in RcDXSA. EcDXS showed a moderate inhibition rate (27%) (Fig. 4-6).

Among five active DXSes (PaDXS, BsDXS, RcDXSA, EcDXS and RsDXSB), EcDXS and RsDXSB were excluded from the candidates for “robust DXSes” due to the instability and the low specific activity, respectively. Therefore, BsDXS with the high feedback inhibition tolerance, PaDXS with the highest solubility and RcDXSA with the highest activity were subjected to the further comparative analyses.

To estimate the stability of PaDXS, BsDXS, and RcDXSA proteins, the residual activities were measured after heat treatments. And also, the degradation rates by proteases treatments were quantified by SDS-PAGE analyses. In the heat-resistance test, each DXS activity was determined after incubation at 30, 35, 40, and 45°C for 10 min in the presence of 10% glycerol (Fig. 4-7A), or at 50°C for 20, 40, and 60 min in the presence of 50% glycerol (Fig. 4-7B). In the presence of 10% glycerol,-the activities of PaDXS and BsDXS almost disappeared at 45°C (0% and 2%, respectively), while RcDXSA exhibited a significant activity (15%) at this temperature (Fig. 4-7A). In the presence of 50% glycerol, the residual activities of the three DXSes remained above 80% after incubation at 50°C for 20 min. After incubation at 50°C for 60 min, RcDXSA, BsDXS, and PaDXS exhibited activities of 90%, 74%, and 70%, respectively (Fig. 4-7B). In the protease-resistance test, DXSes were incubated at 20°C or 40°C with trypsin or proteinase K to estimate the structural fluctuation

(119, 120). BsDXS showed the highest protease resistance: it was not completely degraded by the protease K treatment for 28 min at 40°C, whereas other two DXSes were completely degraded in 14 min at 40°C (Fig. 4-8). PaDXS showed the lowest protease resistance in all conditions. RcDXSA showed moderate protease resistance.

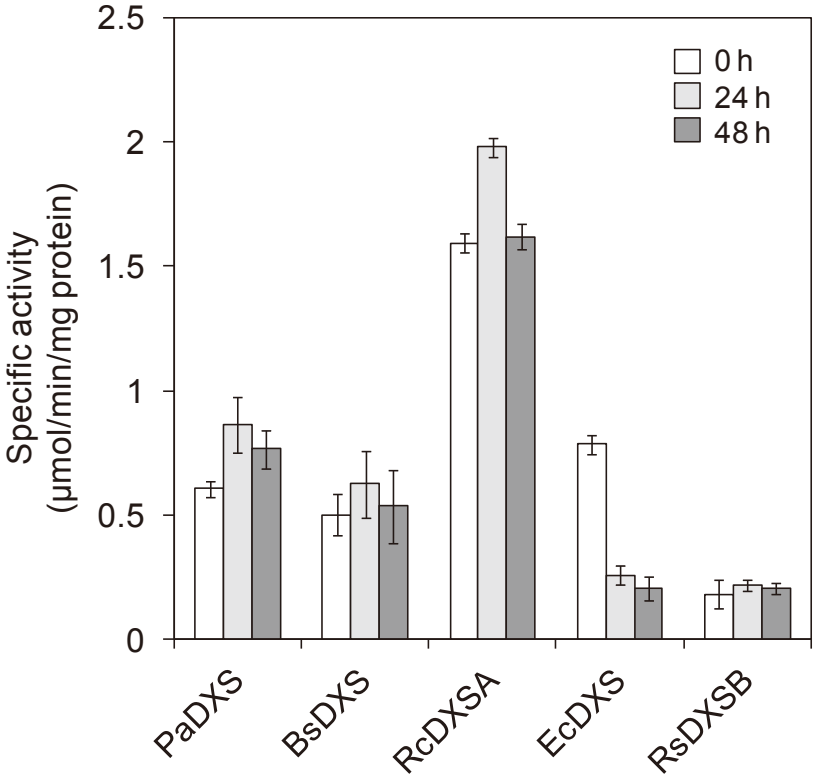

Fig. 4-5. Specific activities of DXSes stored in 50% glycerol at -20°C for 0, 24, or 48 h.
The reactions were monitored at 30°C in a buffer consisting of 100 mM Tris-HCl (pH 7.8), 1 mM DTT, 0.3 mM NADPH, 0.3 mM TPP, 500 μM sodium pyruvate, 2.0 mM D,L-GAP, 10 mM MgCl2, and 100 μg/mL DXR. The data are presented as mean ± SD of three replicates.

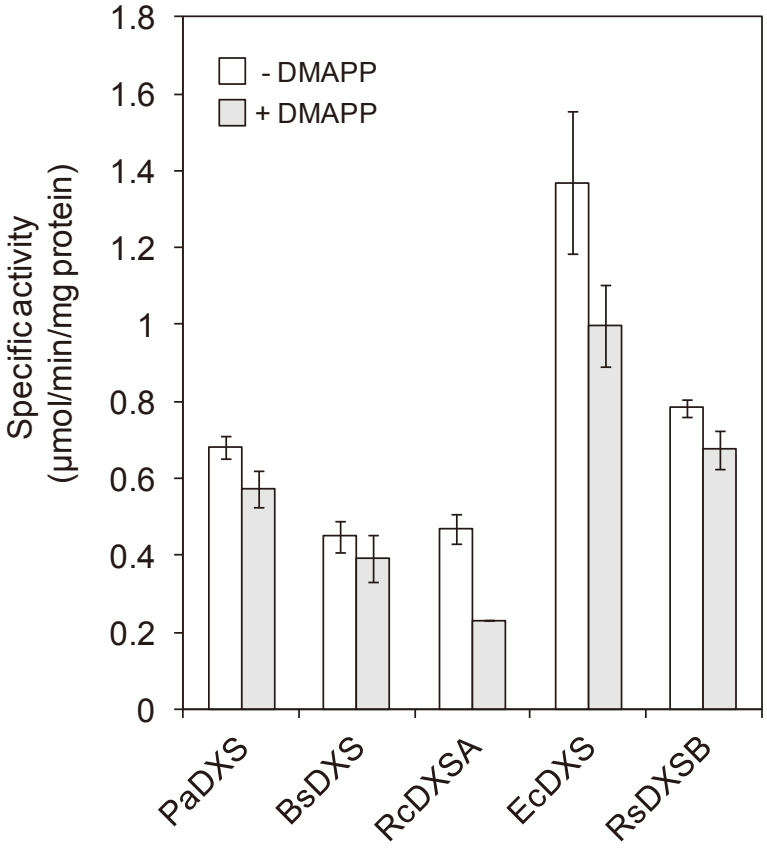

Fig. 4-6. The effects of DMAPP on the enzymatic activities.
The inhibitory effects of DMAPP on DXS activity were evaluated by measuring the specific activity in the presence or absence of DMAPP (1 mM) at 30°C under the same conditions except that TPP concentrations were 25 μM (B). The data are presented as mean ± SD of three replicates.

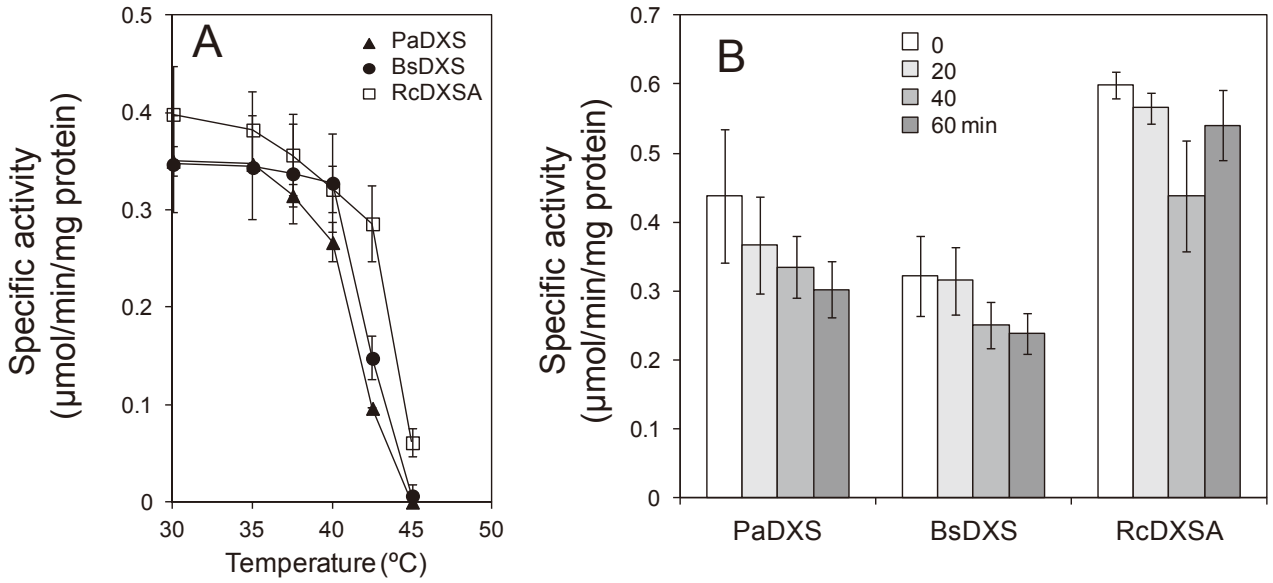

Fig. 4-7. Thermostabilities of DXSes.
The residual activities of DXSes after 10-min incubation at different temperatures (30°C, 35°C, 40°C, or 45°C) in the presence of 10% glycerol (A). The residual activities after different incubation times (0, 20, 40, and 60 min) at 50°C in the presence of 50% glycerol (B). The data are presented as mean ± SD of three replicates.

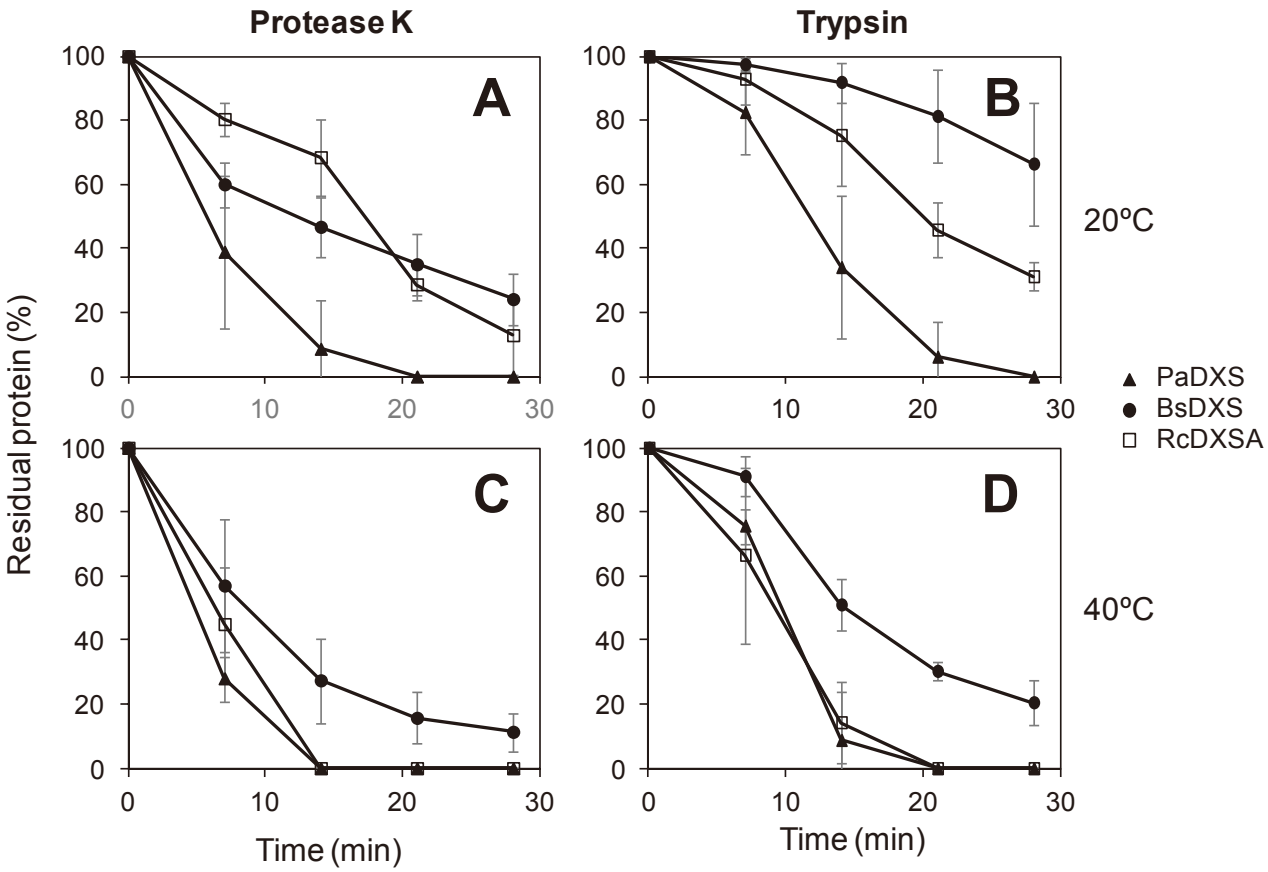

Fig. 4-8. Protease tolerances of DXSes.
DXSes were incubated at 20°C (A and B) or 40°C (C and D) for various periods with proteinase K (A and C) or trypsin (B and D). The digestion rates were determined by quantification of the SDS-PAGE bands. The data are presented as mean ± SD of three replicates.

Isoprene production

To confirm the *in vivo* activities of PaDXS, BsDXS, or RcDXSA, IspS that catalyzes the conversion of DMAPP to isoprene was co-expressed with the three DXSes in *E. coli*. Isoprene is a volatile substance and easily released into the atmosphere. Therefore, the change in the carbon flux of MEP pathway can be estimated by isoprene evolution. Cells were cultivated for 6 h or 24 h in a sealed bin after induction by IPTG, and the headspace was analyzed by gas chromatography. Although after 6 h, only the RcDXSA-overexpressing strain showed the isoprene production, after 24 h, all DXS overexpressing strains exhibited significantly higher isoprene production compared to the control strain expressing only IspS (Fig. 4-9). The BsDXS-overexpressing strain showed the highest isoprene productivity (2.1-fold increase versus control), followed by PaDXS (1.9-fold) and RcDXSA (1.6-fold). IspS protein expression levels under isoprene production conditions (30°C, sealed culture with 0.1 mM IPTG for 24 h) were estimated by western blotting (Fig. 4-10), and found to be essentially the same among three strains.

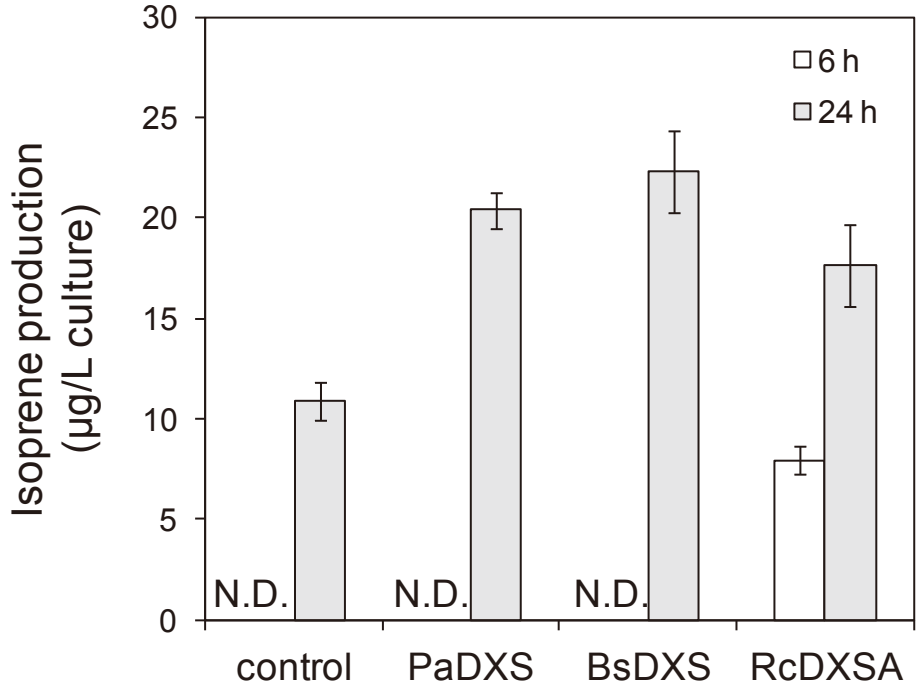

Fig. 4-9. Isoprene production.
The cultures of co-transformants of SkIspS and one of DXSes (PaDXS, BsDXS, or RcDXSA) were incubated in a sealed flask after induction by IPTG and the headspace aliquots were analyzed by gas chromatography. The control strain is the co-transformant with the IspS expression vector and pET28a with no *dxs* gene. N.D. means not detected. The data are presented as mean ± SD of three replicates.

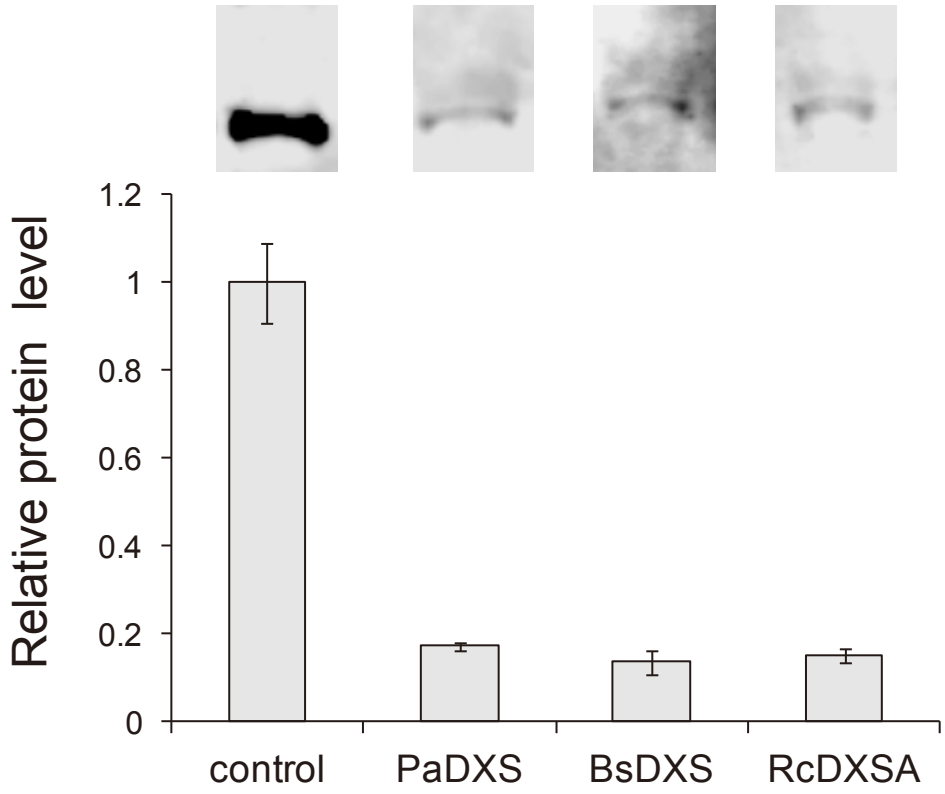

Fig. 4-10. IspS protein levels.
The IspS accumulation levels in the strains co-expressing DXS and IspS under the isoprene production condition (30°C, sealed culture with 0.1 mM IPTG for 24 h) were estimated by western blotting and shown as relative levels to that of the control strain. The control strain harbors IspS expression vector and pET28a with no *dxs* gene. The data are presented as mean ± SD of three replicates.

Discussion

Although DXS proteins were expressed under the control of the same promoter, their intracellular accumulation levels were significantly different (Fig. 4-1). PaDXS and RcDXSA showed the highest accumulation levels, which were about 10-fold higher than that of S.6803DXS. In bacteria, the accumulation level of a protein can be assumed to be determined by the mRNA stability, translation rate, and protein degradation rate (Fig. 4-11) (121-123). These determinants can be estimated roughly from qPCR, the codon adaptation index (CAI) (124), and the N-end rule (125), respectively. Because all DXSes studied here have the same N-terminal sequence (MGSSHHHHHHSSGLVPRGSH), it was assumed that degradation rates of these proteins were essentially identical. qPCR analyses for Pa*dxs*, Bs*dxs*, Rc*dxs*A, Rs*dxs*B, and S.6803*dxs* indicated that the abundance of the S.6803*dxs* mRNA was much lower than those of other *dxs* mRNAs (Fig. 4-2), providing a main cause of the low protein level of S.6803DXS and suggesting the low stability of S.6803*dxs* mRNA. The degradation of mRNA in *E. coli* is thought to be triggered by the ribonuclease RNase E (126). It has been reported that the sequence preference of RNase E is related to the GC content of the gene (127). However, in our case, no correlation between the GC content and the mRNA level was confirmed. Kaberdin proposed that the experimentally determined RNase E recognition sites were 5'-(G/A)(C/A)NG(G/U/A)-cleavage site-(A/U)(C/U)N(C/A)(C/A)-3' (128). Among the *dxs* genes, S.6803*dxs* and Rc*dxs*A possess such a site within 300 bp downstream of the start codon. Interestingly, the site in Rc*dxs*A is predicted to be protected by stem loop structure, but the site in S.6803*dxs* is not protected, implying a correlation with the observed mRNA stability. We also found that the CAI values are significantly correlated with the observed DXS accumulation levels (Fig. 4-12 and Table 4-5), demonstrating that the translation rate is another factor in determining the accumulation of DXS. With regard to CAI value, S.6803DXS exhibited significantly lower value (0.66) compared with those of RcDXSA (0.77) and PaDXS (0.73). Taking these results

together, we can assume that the low mRNA stability and low translation rate synergistically contribute to the low accumulation level in S.6803DXS.

PaDXS showed the highest ratio of the soluble to insoluble protein and the highest accumulation level of the soluble protein in cells (Fig. 4-1). In contrast, RcDXSA exhibited much lower soluble/insoluble ratio compared to PaDXS (Fig. 4-1). Interestingly, the protease resistance and thermal stability of PaDXS were significantly lower compared to those of RcDXSA (Fig. 4-7 and 4-8). In general, these two properties are considered inversely correlated with thermal fluctuations of proteins (119, 129). Therefore, PaDXS will be a protein with relatively high structural fluctuation. At first glance, this interpretation seems contradictory to the high solubility of PaDXS. The monomer of DXSes consists of three domains and form a homodimer (130); thus, several fluctuation modes are possible. We speculate that in PaDXS, the folding ability of each domain is relatively higher, decreasing the tendency of the aggregation; however, the domain-domain and/or subunit-subunit interactions are relatively lower. In contrast, in RcDXSA, the domain-domain and/or subunit-subunit interactions might be relatively stronger, but the domain folding rate might be lower, which facilitates the aggregation in cell. In fact, among purified proteins (already folded), only RcDXSA was able to freeze-thaw without precipitation (data not shown), suggesting that the folded RcDXSA has a stable quaternary structure.

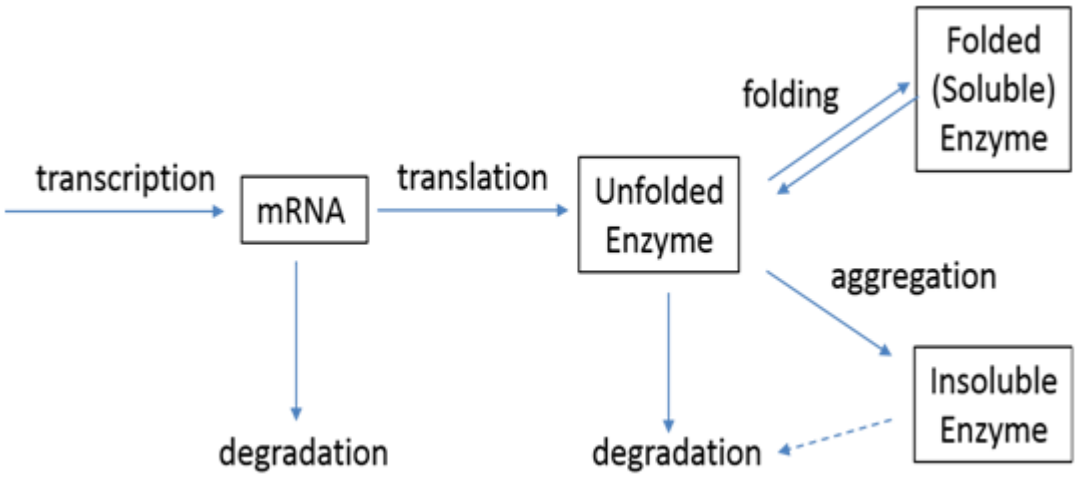

Fig. 4-11. Scheme of the protein expression and accumulation.

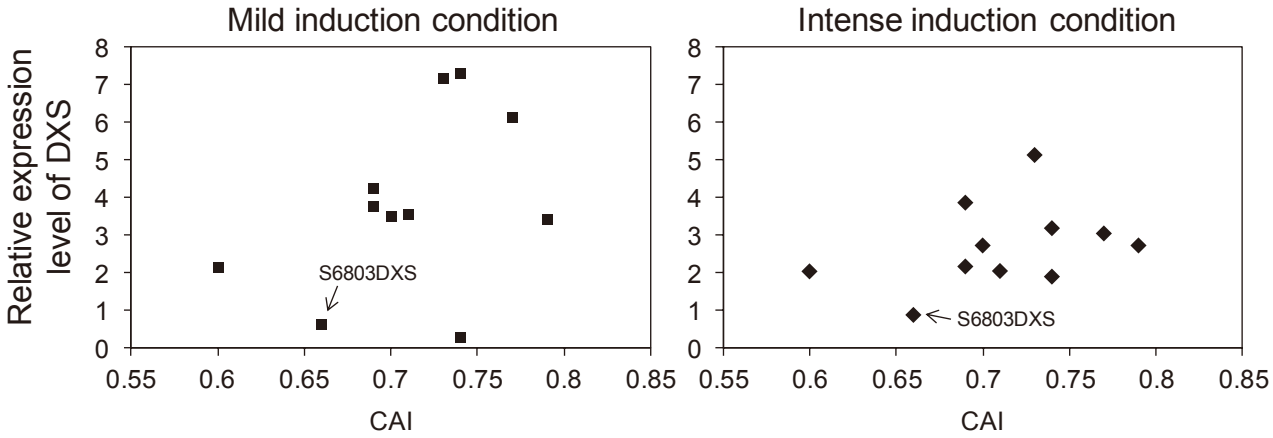

Fig. 4-12. Correlation of between the protein accumulation levels and the CAI values.

Table 4-5. Correlation between the protein accumulation levels and the rare codon rate.

	Relative total accumulation level of DXS		rare codon rate (%)*			CAI
	Mild	Intense	0-10	11-20	21-30	
EcDXS	3.43	2.74	0	0	4	0.79
RcDXSA	6.15	3.06	0	0	7	0.77
RcDXSB	7.33	3.2	0	0	8	0.74
HpDXS	0.29	1.91	0	0	10	0.74
PaDXS	7.19	5.15	0	0	7	0.73
BsDXS	3.56	2.06	0	0	8	0.71
MlDXS	3.52	2.74	0	0	9	0.7
RsDXSB	3.78	2.18	0	0	8	0.69
RsDXSA	4.26	3.88	0	0	10	0.69
S6803DXS	0.63	0.89	1	0	12	0.66
TtDXS	2.16	2.05	1	0	14	0.6

The rare codon rate and the CAI values were calculated on the website of GenScript Inc. (http://www.genscript.com/cgi-bin/tools/rare_codon_analysis).

*The value of 100 corresponds to the codon with the highest usage frequency for a given amino acid in the expression organism under study. The codons with values lower than 30 are defined as rare codons.

Regarding the activity, 11 recombinant DXSes were divided into three groups. In the first group, which includes five DXSes, PaDXS, BsDXS, RcDXSA, EcDXS, and RsDXSB, significant activity was confirmed. In the second group, which includes RcDXSB, TtDXS, and HpDXS, the yields of the purified enzymes were too low to analyze (Fig. 4-3) owing to the low expression level or the high aggregation tendency. In the third group, which includes S.6803DXS, RsDXSA, and MlDXS, although yields and solubilities were high enough for assays (Fig. 4-3), no activity was observed. In the second and third groups, the switch of the histidine-tag position from N- to C-terminus did not improve the situation. The DXSes in the third group give us an interesting insight that DXSes can adapt active and inactive states. In fact, the DXSes in the first group also lost their activities in the absence of glycerol, but they except for EcDXS could be greatly stabilized in the presence of 50% glycerol (Fig. 4-5). The transition from an active state to an inactive state is likely a general feature of bacteria DXSes. The DXSes in the third group might significantly lost their activity in the cell or during the purification process. Actually, the cell lysate of these DXSes exhibited weak activities (data not shown).

The k_{cat} of RcDXSA (5.5 sec^{-1}) was 3- and 1.7-times higher than that of PaDXS and BsDXS, respectively (Fig. 4-4). The k_{cat} of RcDXSA was higher than those previously reported for DXSes from *Populus trichocarpa* (k_{cat} = 0.64 sec^{-1}), *Streptomyces coelicolor* (k_{cat} = 1.1 sec^{-1}) and *E. coli* (k_{cat} = 0.8 sec^{-1}) (109, 131). Considering the kinetic parameters and concentrations of pyruvate (5.2 mM) and GAP (1.8 mM) in *E. coli* (132), the ratio of the *in vivo* specific activities of PaDXS, BsDXS, and RcDXSA was predicted to be 1:1:3. The soluble protein level of RcDXSA was 2.6 times lower than that of PaDXS and 2 times higher than that of BsDXS in the mild induction condition. Taken together, RcDXSA was estimated to have the highest total DXS activity in *E. coli*, followed by PaDXS and BsDXS (RcDXSA:PaDXS:BsDXS = 6:5:1). Interestingly, these estimated total activities have no significant correlation with isoprene productivities of three strains co-expressing one of the

candidate DXSes and IspS (Fig. 4-9). A possible explanation is that other steps might restrict the isoprene production. Many researches showed that IspG is another rate-limiting enzyme in the MEP pathway (133, 134). Recently, Gao et al. (97) and Chaves et al. (42) were clearly demonstrated using cyanobacteria that the ratio of IPP to DMAPP influences the isoprene productivity seriously due to the inhibitory effect of IPP on the IspS activity. In addition, the IspS expression levels of the three co-expressing strains were significantly lower than that of the control strain expressing only IspS (PaDXS: 17%, BsDXS: 14% and RcDXSA: 15%) (Fig. 4-10). Therefore, the increase of the carbon flux into MEP pathway might not be reflected to the changes in the isoprene productivity strongly. Another possibility is that the different sensitivities of individual DXSes to feedback inhibition, which has opposite trend to that in total activities, might offset the different total activities.

The feedback mechanism of DXS was proposed by Banerjee et al (109).: IPP or DMAPP bind to the TPP binding pocket in the competitive manner. They demonstrated that the activity of PtDXS was inhibited to 75% by the addition of 1 mM DMAPP to the reaction solution containing 25 μM TPP. In the same condition, we estimated the inhibitory effects of BsDXS (13%), RsDXSB (14%), PaDXS (16%), EcDXS (23%), and RcDXSA (50%) (Fig. 4-6). To analyze the factors determining their sensitivity to feedback inhibition, the amino acid residues that contact with TPP molecule were predicted based on the crystal structures of DXS from *Deinococcus radiodurans* (DrDXS) (130) and the amino acid sequence alignment, and compared between relatively low sensitive DXSes (BsDXS, RsDXS and PaDXS) and relatively high sensitive ones (RcDXA and PtDXS) (Fig. 4-13). Interestingly, almost of all the contact residues are conserved among them, and no significant relationship between the sequence and the sensitivity could be found. By carefully observing the outer region, a significant amino acid sequence variation was found in the regions corresponding to the flexible loop from Met198 to Ser244 in DrDXS and the hydrophobic core around Trp303 in DrDXS, which might regulate the cofactor selectivity.

PaDXS, BsDXS and RcDXA were characterized in detail as candidates for a member of a robust isoprenoid biosynthesis system, and found to exhibit promising properties but interesting individuality. We are now examining the heterologous expression of these DXSes in cyanobacteria, and estimating the in *vivo* soluble protein levels and the effect on the carbon flux in MEP pathway.

Fig. 4-13. Amino acid sequence alignment of 7 DXSes.
Red and bold characters represent the amino acid residues that are predicted to contact with TPP molecule. The stars show the site where the amino acid residues are conserved among 7 DXSes.

```
BsDXS       312:KAAAPSWSGLVSGTVQRMAREDGRIVAITPAMPVGSKLEGFAKEFPDRMFDVGIAEQHAA 371
RsDXSB      316:VSNAPSYTKVFAQSLIKEAEVDERICAVTAAMPDGTGLNLFGERFPKRTFDVGIAEQHAV 375
PaDXS       321:KSNAPSYTSVFARALVDQASRDDKIAAVTAAMPDGTGLNLFAERFPRRCFDVGIAEQHAV 380
EcDXS       315:SGGLPSYSKIFGDWLCETAAKDNKLMAITPAMREGSGMVEFSRKFPDRYFDVAIAEQHAV 374
RcDXSA      317:IPNAPNYTAVFGERLTEEAARDQAIVAVTAAMPTGTGLDIMQKRFPRRVFDVGIAEQHAV 376
PtDXS       359:SPSTQSYTTYFAEALTAEAEVDKDIVAIHAAMGGGTGLNLFLRRFPTRCFDVGIAEQHAV 418
DrDXS       320:SAYSWSAAFGEAVTEWAK--TDPRTFVVTPAMREGSGLVEFSRVHPHRYLDVGIAEEVAV 377
                                      **                  ******  **

BsDXS       372:TMAAAMAMQGMKPFLAIYSTFLQRAYDQVVHDICRQNANVFIGIDRAGLVGADGETHQGV 431
RsDXSB      365:TFSAALAAGGMRPFCAIYSTFLQRGYDQIVHDVAIQRLPVRFAIDRAGLVGADGATHAGS 435
PaDXS       381:TFAAGLAAGGMKPFCALYSTFLQRGYDQIVHDVAIQRLPVRFAIDRAGLVGADGATHAGA 440
EcDXS       375:TFAAGLAIGGYKPIVAIYSTFLQRAYDQVLHDVAIQKLPVLFAIDRAGIVGADGQTHQGA 434
RcDXSA      377:TFAAGMAAAGLKPFLALYSSFVQRGYDQLVHDVALQNLPVRLMIDRAGLVGQDGATHAGA 436
PtDXS       419:TFAAGLACEGLKPFCAIYSSFLQRAYDQVVHDVDLQKLPVRFAMDRAGLVGADGPTHCGA 478
DrDXS       378:TTAAGMALQGMRPVVAIYSTFLQRAYDQVLHDVAIEHLNVTFCIDRAGIVGADGATHNGV 437
                 *  *       *  * *  * ** ***  **            **** ** ** ** *

BsDXS       432:FDIAFMRHIPNMVLMMPKDENEGQHMVHTALSYDEGPIAMRFPRGNGLGVKMDEQLKTIP 491
RsDXSB      425:FDVAFLSNLPGIVVMAAADEAELVHMVATAAAHDEGPIAFRYPRGDGVGVEMPVKGVPLQ 495
PaDXS       441:YDIAFLSNLPGMVVMAAADEADLVHMVATAAAHDEGPIAFRYPRGEGTGVEMPERGIPLE 500
EcDXS       435:FDLSYLRCIPEMVIMTPSDENECRQMLYTGYHYNDGPSAVRYPRGNAVGVELTPLEKLP- 493
RcDXSA      437:FDVSMLANLPNFTVMAAADEAELCHMVVTAAAHDSGPIALRYPRGEGRGVEMPERGEVLE 496
PtDXS       479:FDVTFMACLPNMVVMAPSDEAELFHMVATATAIDDRPSCFRYPRGNGVGVQLPPGNKGVP 538
DrDXS       438:FDLSFLRSIPGVRIGLPKDAAELRGMLKYAQTHD-GPFAIRYPRGNTAQVPAGTWPDLK- 495
                 **       *         *      *          *    *****

BsDXS       492:IGTWEVLRPGNDAVILTFGTTIEMA--IEAAEELQKEGLSVRVVNARFIKPIDEKMMKSI 549
RsDXSB      496:IGRGRVVSEGTRIALLSFGTRLAEV--QVAAEALAARGISPTVADARFAKPLDRDLILQL 553
PaDXS       501:IGKGRMISEGRRVAILSFGTRLSEV--LVAREALAARGIEPTIADARFAKPLDRELILRL 558
EcDXS       494:IGKGIVKCRGEKLAILNFGTLMPEA--AKVAESLNATLVDMRFVKPLDEALILEMAASHE 551
RcDXSA      497:IGKGRVMTEGTEVAILSFGAHLAQA--LKAAEMLEAEGVSTTVADARFCRPLDTDLIDRL 554
PtDXS       539:LEVGKGRMLIEGERVALLGYGTAVQSCLAAASLLERHGIRLTVADARFCKPLDHALIRSL 598
DrDXS       496:WGEWERLKGGDDVVILAGGKALDYA-LKAAEDLPGVG-----VVNARFVKPLDEEMLREV 550
                                 *         *

BsDXS       550:-LKEGLPILTIEEAVLEGGFGSSILEFAHDQGEYHT--PIDRMGIPDRFIEHGSVTALLE 606
RsDXSB      554:-AAHHEALITIEEGAI-GGFGSHVAQLLAEAGVFDRGFRYRSMVLPDTFIDHNSAEVMYA 611
PaDXS       559:-AREHEALITIEEGAL-GGFGSHVAQLLLEEGALDGGLKFRQMVLPDTFIDHADAKAMYR 616
EcDXS       552:-ALVTVEENAIMGGAG-SGVNEVLMAHRKPV-------PVLNIGLPDFFIPQGTQEEMRA 602
RcDXSA      555:-IEGHAALITLEQGAM-GGFGAMVLHYLARTGQLEKGRAIRTMTLPDCYIDHGSPEEMYA 612
PtDXS       599:-AKSHEILITVEEGSI-GGFGSHVVQFLALDGLLDGKLKWRPVVLPDRYIDHGSPADQLV 656
DrDXS       551:GGRA-RALITVEDNTVVGGFGGAVLEALNSMNLH---PTVRVLGIPDEFQEHATAESVHA 605
                                 *                          **

BsDXS       607:EIGLTKQQVANRIRLLMPPKTHKGIGS 633
RsDXSB      612:TAGLNAADIERKALETLGVEVL-ARRA 637
PaDXS       617:DAGMNAADIERKVLEVMGVAQIGERRA 643
EcDXS       603:ELGLDATGMEAKIKAWLA 620
RcDXSA      613:WAGLTANDIRDTALAAARPSKSVRIVHSA 641
PtDXS       657:EAGLTPSHIAATVFSILGQRREALEIMSS 685
DrDXS       606:RAGIDAPAIRTVLAEL-GVDVPIEV 629
```

Fig. 4-13. Amino acid sequence alignment of 7 DXSes. (continued)

CHAPTER 5

General Conclusion and Future Research

General Conclusion

In this dissertation, I aimed to enhance the isoprenoid biosynthesis in the photosynthetic cyanobacterium Synechocystis PCC 6803 in the view of the MEP pathway, which is the primary pathway by which isoprenoids are synthesized.

As shown in Chapter 2, I demonstrated for the first time that the overexpression of DXS is effective to increase of isoprenoid biosynthesis in cyanobacterium. However, the protein expression level of DXS is only 1.5-fold, which is significantly smaller than that expected from the transcriptional level, indicating that the control of the DXS protein level is the most critical issue to be addressed. Furthermore, I clearly revealed that the cell membrane and phycobiliproteins are huge carbon sinks and the carbon flows into them are strong competing pathways with the MEP pathway.

As described in Chapter 3, I successfully showed that the over-expression of the *dxs* gene leads to the serious perturbation in the post-transcriptional regulation of cyanobacteria, resulting in the significant promotion of insolubilization of the DXS protein. Collectively, I can conclude that the introduction of the exogenous DXS with the high refolding property in cyanobacteria, or the enhancement of the post-transcriptional regulation by the overexpression of the chaperone systems, such as the heat-shock proteins should be needed to dramatically boost the MEP pathway of cyanobacteria.

In Chapter 4, I discussed the exogenous DXSes to be introduced in cyanobacteria. To explore the exogenous DXSes with the high activity and high stability, 11 *dxs* genes from 9 organisms were introduced to *Escherichia coli*, expressed heterologously, purified homogenously and compered their activities and stabilities. As already shown, I successfully found that the DXSes

from *Rhodobacter capsulatus* (RcDXSA), *Paracoccus aminophilus* DXS (PaDXS) and *Bacillus subtilis* DXS (BsDXS) show the highest activity, the highest solubility, and the highest protease tolerance among the DXSes we tested, respectively. Importantly, I evaluated their feedback inhibitory properties against DMAPP, which is a product of the MEP pathway, and revealed for the first time that PaDXS and BsDXS have a significantly high feedback inhibition tolerance. I believe that these DXSes will express in cyanobacteria greatly, can fold into their active form without the excessive help from the post-transcriptional regulation systems, and effectively increase the carbon flux to the MEP pathway. In addition, these molecular level information on the various DXSes should be useful not only for the design of the highly isoprenoid-productive cyanobacteria, but also for the enhancement of production yield of plants and crops.

In many previous studies, the overexpression of proteins was performed to improve the desirable metabolites in cyanobacteria (Table 5-1). But, in spite of the overexpression, the improvement of metabolites was often unsuccessful. The causes were considered that the enzyme is not a rate-limiting enzyme or that the overexpression is non-effective with the flux increment to the metabolite due to the leakage to the other pathway or the inhibitory effect of the production. In the studies, the overexpression was generally evaluated by the transcriptional levels and the metabolite productivities or only the metabolite productivities. In some studies, the overexpression was also estimated by protein level. However, they were limited to the exogenous proteins and the soluble fraction at the specific culture time. In this study, to improve the isoprenoid productivity, the overexpression of DXS was examined and the *dxs* transcriptional level, the soluble DXS protein level, and the isoprenoid productivity were comprehensively analyzed throughout the culture. As a result, the isoprenoid productivity in the DXS overexpressing strain was increased only 1.5-fold compared to that in the WT strain. Interestingly, the DXS overexpressing strain showed the lower

increment of the soluble DXS expression level (1.5-fold) compared with that expected from the *dxs* transcriptional level (4-fold). This result indicates that the estimation by the transcriptional level is not enough to confirm the overexpression of the targeted protein in cyanobacteria. Furthermore, to confirm the cause of the low protein level, the insoluble fraction protein should be analyzed in cyanobacteria. In the DXS overexpressing strains, the DXS protein strangely was turned to be the low solubility. This interesting but important phenomenon suggests that the protein expression is strictly regulated in cyanobacteria and is difficult to control artificially. Therefore, I need to reconsider all previous overexpression studies. Although the overexpression was successful at the transcriptional level, it may not be successful at the protein level. The enzymes, which the overexpression is defined to be non-effective to metabolites in past, may be actually effective. In addition, it should be also consider that the DXS overexpression at protein level in overexpression strain was able to be confirmed at some specific culture times. Therefore, the protein overexpression observed at the specific culture time is necessarily not applicable to throughout the culture. For example, in Gao et al (97)., they confirmed DXS overexpression by the increased DXS activity (1.9-fold) in cultures at OD730 of 1.5-2.0. However, the overexpression of DXS led to only about 20% increase in isoprenoid productivity. In the study, the isoprenoid productivity is defined by a total accumulation of isoprenoid in the long culture for 72 h. There is no guarantee that the DXS overexpression is successful throughout the culture. Therefore, the effect of DXS overexpression may be limited to the only short term in the culture.

In this way, my study indicates that the protein overexpression in cyanobacteria is not simple. We need to more carefully confirm whether the protein overexpression is really successful in cyanobacteria and then the effect of the overexpression to the metabolism should be analyzed and discussed.

Table 5-1. The protein overexpression and the estimation in previous study.

Chemical target	Cyanobacterial strain	Gene(s) expressed	Endogenous or exogenous	Estimation of overexpression	Ref.
Isoprene	PCC 6803	*isps*	exogenous	productivity	136
Isoprene	PCC 6803	*isps*	exogenous	transcriptional level, soluble protein level, productivity	96
		dxs	endogenous	productivity	
limonene	PCC6803	*lims*	exogenous	transcriptional level, soluble protein level, productivity	99
		dxs, crtE, ipi	endogenous	productivity	
limonene	PCC7120	*lims*	exogenous	whole-cell protein level, productivity	137
		dxs, ipphp, gpps	exogenous	productivity	
PHB	PCC 6803	*phaA, phaB, phaC*	endogenous	transcriptional level, productivity	138
carotenoids	PCC 6803	*ipi, crtR, crtP , crtB*	endogenous	transcriptional level, productivity	47
sucrose	PCC 6803	*sps, spp, ugp*	endogenous	transcriptional level, productivity	33
acetone	PCC 6803	*cftAB, adc*	endogenous	transcriptional level, productivity	139
fatty acid	PCC 7942	*tesA*	endogenous	productivity	140
ethylene	PCC 6803	*efe*	endogenous	productivity	141

Future Research

In this dissertation, I especially focused on DXS among the MEP pathway enzymes. In recent study (97), however, it was reported that the IspG, IDI, and potentially IspD are the other rate limiting step enzymes in the MEP pathway. To produce isoprene directly from CO_2, they engineered the MEP pathway in the cyanobacterium Synechococcus elongates. They chose plant-derived isoprene synthases (IspS) with high activities, and introduced them, followed by the improvement in isoprene production activity by introducing an exogenous IDI and IspG. The engineered strain directed about 40% of photosynthetically fixed carbon toward the isoprene biosynthetic pathway. In consideration of the post-transcriptional regulation, including the chaperone and clearance systems, and the feedback inhibition regulation, it is strongly desirable that not only DXS but these enzymes (IspG, IDI, and IspD) also should be replaced with the corresponding exogenous enzymes.

In the series of my studies, I used constitutive promoters, *trc* and *psbA*II promoters, for the expression of the IspS and DXS genes. I think that ideally the isoprenoid production should be induced vigorously in the stationary phase to avoid the competition with the cell growth (especially cell membrane and phycobiliproteins syntheses). Therefore, the promoter specifically induced at the stationary phase without artificial inducers is essential. However, such promoter has not been reported in cyanobacteria, excepted for an article by Berla et al. (135). They analyzed DNA microarrays to identify highly expressed genes during stationary-phase growth of *Synechocystis* sp. PCC 6803. They found that many stationary-phase specific genes are on endogenous plasmids, and proposed that the corresponding promoters upstream of genes will be useful for synthetic biology applications with this phototrophic host. To explore the stationary phase-specific promoters for cyanobacteria, we performed the next generation transcriptome analysis and successfully identified several highly induced genes during stationary-phase. The corresponding promoters upstream of

genes were already introduced into the *Synechocystis* sp. PCC 6803 together with the reporter proteins (inactive DXS and GFP), and the expression profiles are being evaluating. I am also planning to examine the highly effective isoprenoid production in cyanobacteria by combining the stationary-phase specific promoter and the exogenous the MEP pathway enzymes.

Finally, cyanobacteria are promising for sustainable production of isoprenoids and other chemicals. For that reason a large number of researches are in progress worldwide. Although it is promising there are still a large number of bottlenecks that need to be solved before cyanobacteria can be commercially used as industrial microorganisms. In especially, the low productivity leads the high-cost production and prevents the industrial utilization of cyanobacteria. Therefore, the further work needs to be done to increase yields and productivities by the metabolic engineering. This work provides a new knowledge for the metabolic engineering of cyanobacteria. This knowledge is helpful to the effective metabolic engineering of cyanobacteria and will be promote the realization of the industrial production by cyanobacteria.

Acknowledgements

It is my pleasure to write this message and express my gratitude to all those who have directly or indirectly contributed to the creation of this thesis.

I would like to express my deepest gratitude to my supervisor, Assistant Prof. Masaki Ihara, for his valuable guidance, support, and encouragement in my academic research work.

I also want to thank members of the laboratory, past and present (Yusuke Kawano, Ayaka Sato, Thiharu Hori, Yusuke Fujiwara, Shingo Hotta, Tesuya Kudoh, Midori Sekine, Manami Mizuguchi, Yusuke Mochizuki, Genma Kubota, Arisu Uchida, Mayu Kameyama, Rintaro Fujii, Noriko Kozai, Yukiko Higasi, Kayoko Kawauchi, Sota Aihara, Miho Urano, Ayako Okabe; Izumi Matsuno) for their help and discussion on this research.

Finally, I am grateful to my family for their understanding, encouragement and support.

References

1. **Hoffert, M. I., Caldeira, K., Benford, G., Criswell, D. R., Green, C., Herzog, H., Jain, A. K., Kheshgi, H. S., Lackner, K. S., Lewis, J. S., and other authors:** Advanced technology paths to global climate stability: Energy for a greenhouse planet, Science, **298**, 981-987 (2002).
2. **Lewis, N. S. and Nocera, D. G.:** Powering the planet: Chemical challenges in solar energy utilization, Proceedings of the National Academy of Sciences of the United States of America, **103**, 15729-15735 (2006).
3. **Barber, J.:** Photosynthetic energy conversion: natural and artificial, Chemical Society Reviews, **38**, 185-196 (2009).
4. **Ikeyama, S., Abe, R., Shiotani, S., and Amao, Y.:** Novel artificial coenzyme based on reduced form of diquat for formate dehydrogenase in the catalytic conversion of CO2 to formic acid, Chemistry Letters, **45**, 907-909 (2016).
5. **Liu, Y. Y., Huang, B. B., Dai, Y., Zhang, X. Y., Qin, X. Y., Jiang, M. H., and Whangbo, M. H.:** Selective ethanol formation from photocatalytic reduction of carbon dioxide in water with BiVO4 photocatalyst, Catalysis Communications, **11**, 210-213 (2009).
6. **Ajikumar, P. K., Tyo, K., Carlsen, S., Mucha, O., Phon, T. H., and Stephanopoulos, G.:** Terpenoids: Opportunities for biosynthesis of natural product drugs using engineered microorganisms, Molecular Pharmaceutics, **5**, 167-190 (2008).
7. **Ajikumar, P. K., Xiao, W. H., Tyo, K. E. J., Wang, Y., Simeon, F., Leonard, E., Mucha, O., Phon, T. H., Pfeifer, B., and Stephanopoulos, G.:** Isoprenoid pathway optimization for taxol precursor overproduction in *Escherichia coli*, Science, **330**, 70-74 (2010).
8. **Das, A., Yoon, S. H., Lee, S. H., Kim, J. Y., Oh, D. K., and Kim, S. W.:** An update on microbial carotenoid production: application of recent metabolic engineering tools, Applied

Microbiology and Biotechnology, **77**, 505-512 (2007).

9. **Cordoba, E., Porta, H., Arroyo, A., Roman, C. S., Medina, L., Rodriguez-Concepcion, M., and Leon, P.:** Functional characterization of the three genes encoding 1-deoxy-D-xylulose 5-phosphate synthase in maize, Journal of Experimental Botany, **62**, 2023-2038 (2011).
10. **Estevez, J. M., Cantero, A., Reindl, A., Reichler, S., and Leon, P.:** 1-deoxy-D-xylulose-5-phosphate synthase, a limiting enzyme for plastidic isoprenoid biosynthesis in plants, Journal of Biological Chemistry, **276**, 22901-22909 (2001).
11. **Xue, D., Abdallah, II, de Haan, I. E. M., Sibbald, M., and Quax, W. J.:** Enhanced C-30 carotenoid production in Bacillus subtilis by systematic overexpression of MEP pathway genes, Applied Microbiology and Biotechnology, **99**, 5907-5915 (2015).
12. **Goldstein, J. L. and Brown, M. S.:** Regulation of the mevalonate pathway, Nature, **343**, 425-430 (1990).
13. **Brenner, M. P.:** Engineering microorganisms for energy production. Report JSR-05-300, U. S. Department of Energy, (Washinton, DC) (2006).
14. **Dismukes, G. C., Carrieri, D., Bennette, N., Ananyev, G. M., and Posewitz, M. C.:** Aquatic phototrophs: efficient alternatives to land-based crops for biofuels, Current Opinion in Biotechnology, **19**, 235-240 (2008).
15. **Deng, M. D. and Coleman, J. R.:** Ethanol synthesis by genetic engineering in cyanobacteria, Applied and Environmental Microbiology, **65**, 523-528 (1999).
16. **Dexter, J. and Fu, P. C.:** Metabolic engineering of cyanobacteria for ethanol production, Energy & Environmental Science, **2**, 857-864 (2009).
17. **Lan, E. I. and Liao, J. C.:** Metabolic engineering of cyanobacteria for 1-butanol production from carbon dioxide, Metabolic Engineering, **13**, 353-363 (2011).

18. **Gao, Z. X., Zhao, H., Li, Z. M., Tan, X. M., and Lu, X. F.:** Photosynthetic production of ethanol from carbon dioxide in genetically engineered cyanobacteria, Energy & Environmental Science, **5**, 9857-9865 (2012).

19. **Lan, E. I. and Liao, J. C.:** ATP drives direct photosynthetic production of 1-butanol in cyanobacteria, Proceedings of the National Academy of Sciences of the United States of America, **109**, 6018-6023 (2012).

20. **Atsumi, S., Higashide, W., and Liao, J. C.:** Direct photosynthetic recycling of carbon dioxide to isobutyraldehyde, Nature Biotechnology, **27**, 1177-U1142 (2009).

21. **Schirmer, A., Rude, M. A., Li, X., Popova, E., and del Cardayre, S. B.:** Microbial Biosynthesis of Alkanes, Science, **329**, 559-562 (2010).

22. **Liu, X. Y., Sheng, J., and Curtiss, R.:** Fatty acid production in genetically modified cyanobacteria, Proceedings of the National Academy of Sciences of the United States of America, **108**, 6899-6904 (2011).

23. **Tan, X. M., Yao, L., Gao, Q. Q., Wang, W. H., Qi, F. X., and Lu, X. F.:** Photosynthesis driven conversion of carbon dioxide to fatty alcohols and hydrocarbons in cyanobacteria, Metabolic Engineering, **13**, 169-176 (2011).

24. **Kaiser, B. K., Carleton, M., Hickman, J. W., Miller, C., Lawson, D., Budde, M., Warrener, P., Paredes, A., Mullapudi, S., Navarro, P., Cross, F., and Roberts, J. M.:** Fatty Aldehydes in Cyanobacteria Are a Metabolically Flexible Precursor for a Diversity of Biofuel Products, Plos One, **8** (2013).

25. **Wang, W., Liu, X., and Lu, X.:** Engineering cyanobacteria to improve photosynthetic production of alka(e)nes, Biotechnology for Biofuels, **6** (2013).

26. **Masukawa, H., Inoue, K., and Sakurai, H.:** Effects of disruption of homocitrate synthase genes on *Nostoc* sp strain PCC 7120 photobiological hydrogen production and nitrogenasev,

Applied and Environmental Microbiology, **73**, 7562-7570 (2007).

27. **Sakurai, H., Masukawa, H., Zhang, X., and Ikeda, H.:** Improvement of nitrogenase-based photobiological hydrogen production by cyanobacteria by gene engineering - hydrogenases and homocitrate synthase, Photosynthesis Research, **91**, 282-282 (2007).

28. **Masukawa, H., Inoue, K., Sakurai, H., Wolk, C. P., and Hausinger, R. P.:** Site-directed mutagenesis of the *anabaena* sp. strain PCC 7120 nitrogenase active site to increase photobiological hydrogen production, Applied and Environmental Microbiology, **76**, 6741-6750 (2010).

29. **Ducat, D. C., Sachdeva, G., and Silver, P. A.:** Rewiring hydrogenase-dependent redox circuits in cyanobacteria, Proceedings of the National Academy of Sciences of the United States of America, **108**, 3941-3946 (2011).

30. **Gutthann, F., Egert, M., Marques, A., and Appel, J.:** Inhibition of respiration and nitrate assimilation enhances photohydrogen evolution under low oxygen concentrations in *Syneehocystis* sp PCC 6803, Biochimica Et Biophysica Acta-Bioenergetics, **1767**, 161-169 (2007).

31. **Ihara, M., Kawano, Y., Urano, M., and Okabe, A.:** Light driven co2 fixation by using cyanobacterial photosystem i and nadph-dependent formate dehydrogenase, PloS one, **8**, e71581-e71581 (2013).

32. **Niederholtmeyer, H., Wolfstaedter, B. T., Savage, D. F., Silver, P. A., and Way, J. C.:** Engineering cyanobacteria to synthesize and export hydrophilic products, Applied and Environmental Microbiology, **76**, 3462-3466 (2010).

33. **Du , W., Liang, F., Duan, Y., Tan, X., and Lu, X.:** Exploring the photosynthetic production capacity of sucrose by cyanobacteria, Metabolic Engineering, **19**, 17-25 (2013).

34. **Ducat, D. C., Avelar-Rivas, J. A., Way, J. C., and Silver, P. A.:** Rerouting Carbon Flux To

Enhance Photosynthetic Productivity, Applied and Environmental Microbiology, **78**, 2660-2668 (2012).

35. **Miyake, M., Kataoka, K., Shirai, M., and Asada, Y.:** Control of poly-beta-hydroxybutyrate synthase mediated by acetyl phosphate in cyanobacteria, Journal of Bacteriology, **179**, 5009-5013 (1997).

36. **Takahashi, H., Miyake, M., Tokiwa, Y., and Asada, Y.:** Improved accumulation of poly-3-hydroxybutyrate by a recombinant cyanobacterium, Biotechnology Letters, **20**, 183-186 (1998).

37. **Miyake, M., Takase, K., Narato, M., Khatipov, E., Schnackenberg, J., Shirai, M., Kurane, R., and Asada, Y.:** Polyhydroxybutyrate production from carbon dioxide by cyanobacteria, Applied Biochemistry and Biotechnology, **84-6**, 991-1002 (2000).

38. **Wu, G. F., Wu, Q. Y., and Shen, Z. Y.:** Accumulation of poly-beta-hydroxybutyrate in cyanobacterium *Synechocystis* sp PCC6803, Bioresource Technology, **76**, 85-90 (2001).

39. **Panda, B., Jain, P., Sharma, L., and Mallick, N.:** Optimization of cultural and nutritional conditions for accumulation of poly-beta-hydroxybutyrate in *Synechocystis* sp PCC 6803, Bioresource Technology, **97**, 1296-1301 (2006).

40. **Tyo, K. E., Zhou, H., and Stephanopoulos, G. N.:** High-throughput screen for poly-3-hydroxybutyrate in Escherichia coli and *Synechocystis* sp strain PCC6803, Applied and Environmental Microbiology, **72**, 3412-3417 (2006).

41. **Mallick, N., Gupta, S., Panda, B., and Sen, R.:** Process optimization for poly(3-hydroxybutyrate-co-3-hydroxyvalerate) co-polymer production by Nostoc muscorum, Biochemical Engineering Journal, **37**, 125-130 (2007).

42. **Sharma, L., Singh, A. K., Panda, B., and Mallick, N.:** Process optimization for poly-beta-hydroxybutyrate production in a nitrogen fixing cyanobacterium, Nostoc

muscorum using response surface methodology, Bioresource Technology, **98**, 987-993 (2007).

43. **Tyo, K. E. J., Espinoza, F. A., Stephanopoulos, G., and Jin, Y.-S.:** Identification of Gene Disruptions for Increased Poly-3-hydroxybutyrate Accumulation in *Synechocystis* PCC 6803, Biotechnology Progress, **25**, 1236-1243 (2009).

44. **Wang, B., Pugh, S., Nielsen, D. R., Zhang, W. W., and Meldrum, D. R.:** Engineering cyanobacteria for photosynthetic production of 3-hydroxybutyrate directly from CO2, Metabolic Engineering, **16**, 68-77 (2013).

45. **Lindberg, P., Park, S., and Melis, A.:** Engineering a platform for photosynthetic isoprene production in cyanobacteria, using *Synechocystis* as the model organism, Metabolic Engineering, **12**, 70-79 (2010).

46. **Bentley, F. K., Garcia-Cerdan, J. G., Chen, H.-C., and Melis, A.:** Paradigm of Monoterpene (beta-phellandrene) Hydrocarbons Production via Photosynthesis in Cyanobacteria, Bioenergy Research, **6**, 917-929 (2013).

47. **Lagarde, D., Beuf, L., and Vermaas, M.:** Increased production of zeaxanthin and other pigments by application of genetic engineering techniques to *Synechocystis* sp strain PCC 6803, Applied and Environmental Microbiology, **66**, 64-72 (2000).

48. **Ajikumar, P. K., Xiao, W.-H., Tyo, K. E. J., Wang, Y., Simeon, F., Leonard, E., Mucha, O., Phon, T. H., Pfeifer, B., and Stephanopoulos, G.:** Isoprenoid pathway optimization for taxol precursor overproduction in *Escherichia coli*, Science, **330**, 70-74 (2010).

49. **Zhao, Y., Yang, J., Qin, B., Li, Y., Sun, Y., Su, S., and Xian, M.:** Biosynthesis of isoprene in *Escherichia coli* via methylerythritol phosphate (MEP) pathway, Applied Microbiology and Biotechnology, **90**, 1915-1922 (2011).

50. **Nogales, J., Gudmundsson, S., Knight, E. M., Palsson, B. O., and Thiele, I.:** Detailing the

optimality of photosynthesis in cyanobacteria through systems biology analysis, Proceedings of the National Academy of Sciences of the United States of America, **109**, 2678-2683 (2012).

51. **Ninomiya, N., Ashida, H., and Yokota, A.:** Improvement of cyanobacterial RuBisCO by introducing the latch structure involved in high affinity for CO2 in red algal RuBisCO, Photosynthesis Research, **91**, 232-232 (2007).

52. **Ninomiya, N., Ashida, H., and Yokota, A.:** Improvement of cyanobacterial RuBisCO by introducing the latch structure of red algal RuBisCO with high specificity for CO2 fixation, Plant and Cell Physiology, **48**, S71-S71 (2007).

53. **Angermayr, S. A., Paszota, M., and Hellingwerf, K. J.:** Engineering a Cyanobacterial Cell Factory for Production of Lactic Acid, Applied and Environmental Microbiology, **78**, 7098-7106 (2012).

54. **Ducat, D. C., Way, J. C., and Silver, P. A.:** Engineering cyanobacteria to generate high-value products, Trends in Biotechnology, **29**, 95-103 (2011).

55. **Wanke, M., Skorupinska-Tudek, K., and Swiezewska, E.:** Isoprenoid biosynthesis via 1-deoxy-D-xylulose 5-phosphate/2-C-methyl-D-erythritol 4-phosphate (DOXP/MEP) pathway, Acta Biochimica Polonica, **48**, 663-672 (2001).

56. **Lichtenthaler, H. K.:** Non-mevalonate isoprenoid biosynthesis: enzymes, genes and inhibitors, Biochemical Society Transactions, **28**, 785-789 (2000).

57. **Ershov, Y. V., Gantt, R. R., Cunningham, F. X., and Gantt, E.:** Isoprenoid biosynthesis in *Synechocystis* sp strain PCC6803 is stimulated by compounds of the pentose phosphate cycle but not by pyruvate or deoxyxylulose-5-phosphate, Journal of Bacteriology, **184**, 5045-5051 (2002).

58. **Gabrielsen, M., Bond, C. S., Hallyburton, I., Hecht, S., Bacher, A., Eisenreich, W.,**

Rohdich, F., and Hunter, W. N.: Hexameric assembly of the bifunctional methylerythritol 2,4-cyclodiphosphate synthase and protein-protein associations in the deoxy-xylulose-dependent pathway of isoprenoid precursor biosynthesis, Journal of Biological Chemistry, **279**, 52753-52761 (2004).

59. **Ildiko, D., Mihaly, K., Zoltan, G., and Bettina, U.:** Carotenoids, versatle components of oxygenic photosynthesis, Progress in Lipid Research, **52**, 539-561 (2013).

60. **Lee, P. C. and Schmidt-Dannert, C.:** Metabolic engineering towards biotechnological production of carotenoids in microorganisms, Applied Microbiology and Biotechnology, **60**, 1-11 (2002).

61. **Yoon, S. H., Park, H. M., Kim, J. E., Lee, S. H., Choi, M. S., Kim, J. Y., Oh, D. K., Keasling, J. D., and Kim, S. W.:** Increased beta-carotene production in recombinant *Escherichia coli* harboring an engineered isoprenoid precursor pathway with mevalonate addition, Biotechnology Progress, **23**, 599-605 (2007).

62. **Zhao, J., Li, Q., Sun, T., Zhu, X., Xu, H., Tang, J., Zhang, X., and Ma, Y.:** Engineering central metabolic modules of *Escherichia coli* for improving beta-carotene production, Metabolic Engineering, **17**, 42-50 (2013).

63. **Wilson, A., Ajlani, G., Verbavatz, J. M., Vass, I., Kerfeld, C. A., and Kirilovsky, D.:** A soluble carotenoid protein involved in phycobilisome-related energy dissipation in cyanobacteria, Plant Cell, **18**, 992-1007 (2006).

64. **Mohamed, H. E., van de Meene, A. M. L., Roberson, R. W., and Vermaas, W. F. J.:** Myxoxanthophyll is required for normal cell wall structure and thylakoid organization in the cyanobacterium, *Synechocystis* sp strain PCC 6803, Journal of Bacteriology, **187**, 6883-6892 (2005).

65. **Kerfeld, C. A.:** Water-soluble carotenoid proteins of cyanobacteria, Archives of

Biochemistry and Biophysics, **430**, 2-9 (2004).

66. **Stanier, R., Kunisawa, R., Mandel, M., and Cohen-Bazire, G.:** Purification and properties of unicellular blue-green algae (order *Chroococcales*). pp. 171–205, in, vol. 35, Bacterological reviews (1971).

67. **Sozer, O., Komenda, J., Ughy, B., Domonkos, I., Laczko-Dobos, H., Malec, P., Gombos, Z., and Kis, M.:** Involvement of Carotenoids in the Synthesis and Assembly of Protein Subunits of Photosynthetic Reaction Centers of *Synechocystis* sp PCC 6803, Plant and Cell Physiology, **51**, 823-835 (2010).

68. **Mantoura, R. F. C. and Llewellyn, C. A.:** The rapid determination of algal chlorophyll and carotenoid pigments and their breakdown products in natural waters by reverse-phase high-performance liquid chromatography, pp. 297-314, in, vol. 151, Analytica Chimica Acta (1983).

69. **Folch, J., Lees, M., and Sloane Stanley, G.:** A simple method for the isolation and purification of total lipides from animal tissues., pp. 497-509, in, vol. 226, Journal of Biological Chemistry (1957).

70. **Hodge, J. E. and Hofreiter, B. T.:** Determination of reducing sugars and carbohydrates, pp. 380-394, in: Whistler, R. L., Wolfrom, M. L., Be-Miller, J. N., and Shafizadeh, F. (Ed.). Academic Press, Methods in carbo-hydrate chemistry (1962).

71. **Sheng, J., Vannela, R., and Rittrnann, B. E.:** Evaluation of methods to extract and quantify lipids from *Synechocystis* PCC 6803, Bioresource Technology, **102**, 1697-1703 (2011).

72. **Lupas, A., Engelhardt, H., Peters, J., Santarius, U., Volker, S., and Baumeister, W.:** Domain-structure of the acetogenium-kivui surface-layer revealed by electron crystallography and sequence-analysis, Journal of Bacteriology, **176**, 1224-1233 (1994).

73. **Peters, J., Rudolf, S., Oschkinat, H., Mengele, R., Sumper, M., Kellermann, J.,**

Lottspeich, F., and Baumeister, W.: Evidence for tyrosine-linked glycosaminoglycan in a bacterial surface protein, Biological Chemistry Hoppe-Seyler, **373**, 171-176 (1992).

74. **Kulkarni, R. D., Schaefer, M. R., and Golden, S. S.:** Transcriptional and posttranscriptional components of psba response to high light-intensity in synechococcus-sp strain-PCC-7942, Journal of Bacteriology, **174**, 3775-3781 (1992).

75. **Mulo, P., Laakso, S., Maenpaa, P., and Aro, E. M.:** Stepwise photoinhibition of photosystem II - Studies with *Synechocystis* species PCC 6803 mutants with a modified D-E loop of the reaction center polypeptide D1, Plant Physiology, **117**, 483-490 (1998).

76. **Maier, T., Guell, M., and Serrano, L.:** Correlation of mRNA and protein in complex biological samples, Febs Letters, **583**, 3966-3973 (2009).

77. **Vogel, C. and Marcotte, E. M.:** Insights into the regulation of protein abundance from proteomic and transcriptomic analyses, Nature Reviews Genetics, **13**, 227-232 (2012).

78. **Gottesman, S., Wickner, S., and Maurizi, M. R.:** Protein quality control: Triage by chaperones and proteases, Genes & Development, **11**, 815-823 (1997).

79. **Gygi, S. P., Rochon, Y., Franza, B. R., and Aebersold, R.:** Correlation between protein and mRNA abundance in yeast, Molecular and Cellular Biology, **19**, 1720-1730 (1999).

80. **Tartaglia, G. G., Pechmann, S., Dobson, C. M., and Vendruscolo, M.:** Life on the edge: a link between gene expression levels and aggregation rates of human proteins, Trends in Biochemical Sciences, **32**, 204-206 (2007).

81. **Steiger, S., Schafer, L., and Sandmann, G.:** High-light-dependent upregulation of carotenoids and their antioxidative properties in the cyanobacterium Synechocystis PCC 6803, Journal of Photochemistry and Photobiology B-Biology, **52**, 14-18 (1999).

82. **Mizusawa, N. and Wada, H.:** The role of lipids in photosystem II, Biochimica Et Biophysica Acta-Bioenergetics, **1817**, 194-208 (2012).

83. **Rohmer, M., Seemann, M., Horbach, S., BringerMeyer, S., and Sahm, H.:** Glyceraldehyde 3-phosphate and pyruvate as precursors of isoprenic units in an alternative non-mevalonate pathway for terpenoid biosynthesis, Journal of the American Chemical Society, **118**, 2564-2566 (1996).

84. **Harker, M. and Bramley, P.:** Expression of prokaryotic 1-deoxy-D-xylulose-5-phosphatases in Escherichia coli increases carotenoid and ubiquinone biosynthesis., FEBS Letters, **448**, 115-119 (1999).

85. **Eisenreich, W., Bacher, A., Arigoni, D., and Rohdich, F.:** Biosynthesis of isoprenoids via the non-mevalonate pathway, Cellular and Molecular Life Sciences, **61**, 1401-1426 (2004).

86. **Kesselmeier, J. and Staudt, M.:** Biogenic volatile organic compounds (VOC): An overview on emission, physiology and ecology, Journal of Atmospheric Chemistry, **33**, 23-88 (1999).

87. **Stephanopoulos, G.:** Challenges in engineering microbes for biofuels production, Science, **315**, 801-804 (2007).

88. **Rodriguez-Concepcion, M. and Boronat, A.:** Elucidation of the methylerythritol phosphate pathway for isoprenoid biosynthesis in bacteria and plastids. A metabolic milestone achieved through genomics, Plant Physiology, **130**, 1079-1089 (2002).

89. **Bloch, K.:** Sterol molecule - structure, biosynthesis, and function, Steroids, **57**, 378-383 (1992).

90. **Rohmer, M.:** The discovery of a mevalonate-independent pathway for isoprenoid biosynthesis in bacteria, algae and higher plants, Natural Product Reports, **16**, 565-574 (1999).

91. **Hunter, W. N.:** The non-mevalonate pathway of isoprenoid precursor biosynthesis, Journal of Biological Chemistry, **282**, 21573-21577 (2007).

92. **Takagi, M., Kuzuyama, T., Takahashi, S., and Seto, H.:** A gene cluster for the mevalonate

pathway from *Streptomyces* sp strain CL190, Journal of Bacteriology, **182**, 4153-4157 (2000).

93. **Kuzuyama, T., Takagi, M., Takahashi, S., and Seto, H.:** Cloning and characterization of 1-deoxy-D-xylulose 5-phosphate synthase from *Streptomyces* sp strain CL190, which uses both the mevalonate and nonmevalonate pathways for isopentenyl diphosphate biosynthesis, Journal of Bacteriology, **182**, 891-897 (2000).

94. **Steinbuchel, A.:** Production of rubber-like polymers by microorganisms, Current Opinion in Microbiology, **6**, 261-270 (2003).

95. **Bentley, F. K., Zurbriggen, A., and Melis, A.:** Heterologous Expression of the Mevalonic Acid Pathway in Cyanobacteria Enhances Endogenous Carbon Partitioning to Isoprene, Molecular Plant, **7**, 71-86 (2014).

96. **Pade, N., Erdmann, S., Enke, H., Dethloff, F., Duhring, U., Georg, J., Wambutt, J., Kopka, J., Hess, W. R., Zimmermann, R., Kramer, D., and Hagemann, M.:** Insights into isoprene production using the cyanobacterium *Synechocystis* sp PCC 6803, Biotechnology for Biofuels, **9** (2016).

97. **Gao, X., Gao, F., Liu, D., Zhang, H., Nie, X. Q., and Yang, C.:** Engineering the methylerythritol phosphate pathway in cyanobacteria for photosynthetic isoprene production from CO2, Energy & Environmental Science, **9**, 1400-1411 (2016).

98. **Chaves, J. E., Romero, P. R., Kirst, H., and Melis, A.:** Role of isopentenyl-diphosphate isomerase in heterologous cyanobacterial (*Synechocystis*) isoprene production., Photosynthesis Research, **130**, 517-527 (2016).

99. **Kiyota, H., Okudac, Y., Ito, M., Hirai, M. Y., and Ikeuchi, M.:** Engineering of cyanobacteria for the photosynthetic production of limonene from CO2, Journal of Biotechnology, **185**, 1-7 (2014).

100. **Kudoh, K., Kawano, Y., Hotta, S., Sekine, M., Watanabe, T., and Ihara, M.:** Prerequisite for highly efficient isoprenoid production by cyanobacteria discovered through the over-expression of 1-deoxy-D-xylulose 5-phosphate synthase and carbon allocation analysis, Journal of Bioscience and Bioengineering, **118**, 20-28 (2014).

101. **Pulido, P., Toledo-Ortiz, G., Phillips, M. A., Wright, L. P., and Rodriguez-Concepcion, M.:** Arabidopsis J-Protein J20 Delivers the First Enzyme of the Plastidial Isoprenoid Pathway to Protein Quality Control, Plant Cell, **25**, 4183-4194 (2013).

102. **Ishizuka, T., Shimada, T., Okajima, K., Yoshihara, S., Ochiai, Y., Katayama, M., and Ikeuchi, M.:** Characterization of cyanobacteriochrome TePixJ from a thermophilic cyanobacterium *Thermosynechococcus elongatus* strain BP-1, Plant and Cell Physiology, **47**, 1251-1261 (2006).

103. **Elhai, J. and Wolk, C. P.:** Conjugal transfer of DNA to cyanobacteria, Methods in Enzymology, **167**, 747–754 (1988).

104. **Chomczynski, P. and Sacchi, N.:** The single-step method of RNA isolation by acid guanidinium thiocyanate-phenol-chloroform extraction: twenty-something years on, Nature Protocols, **1**, 581-585 (2006).

105. **Pulido, P., Llamas, E., Llorente, B., Ventura, S., Wright, L. P., and Rodriguez-Concepcion, M.:** Specific Hsp100 chaperones determine the fate of the first enzyme of the plastidial isoprenoid pathway for either refolding or degradation by the stromal clp protease in arabidopsis, Plos Genetics, **12** (2016).

106. **Duppre, E., Rupprecht, E., and Schneider, D.:** Specific and promiscuous functions of multiple DnaJ proteins in *Synechocystis* sp PCC 6803, Microbiology-Sgm, **157**, 1269-1278 (2011).

107. **Zhou, K., Zou, R. Y., Stephanopoulos, G., and Too, H. P.:** Enhancing solubility of

deoxyxylulose phosphate pathway enzymes for microbial isoprenoid production, Microbial Cell Factories, **11** (2012).

108. **Asayama, M.:** Overproduction and easy recovery of target gene products from cyanobacteria, photosynthesizing microorganisms, Applied Microbiology and Biotechnology, **95**, 683-695 (2012).

109. **Banerjee, A., Wu, Y., Banerjee, R., Li, Y., Yan, H. G., and Sharkey, T. D.:** Feedback inhibition of deoxy-D-xylulose-5-phosphate synthase regulates the methylerythritol 4-phosphate pathway, Journal of Biological Chemistry, **288**, 16926-16936 (2013).

110. **Hahn, F. M., Eubanks, L. M., Testa, C. A., Blagg, B. S. J., Baker, J. A., and Poulter, C. D.:** 1-deoxy-D-xylulose 5-phosphate synthase, the gene product of open reading frame (ORF) 2816 and ORF 2895 in *Rhodobacter capsulatus*, Journal of Bacteriology, **183**, 1-11 (2001).

111. **Huang, G., Qing, F., Lechno-Yossef, S., Wojciuch, E., Wolk, C. P., Kaneko, T., and Tabata, S.:** Clustered genes required for the synthesis of heterocyst envelope polysaccharide in *Anabaena* sp strain PCC 7120, Journal of Bacteriology, **187**, 1114-1123 (2005).

112. **Matsushima, D., Jenke-Kodama, H., Sato, Y., Fukunaga, Y., Sumimoto, K., Kuzuyama, T., Matsunaga, S., and Okada, S.:** The single cellular green microalga *Botryococcus braunii*, race B possesses three distinct 1-deoxy-D-xylulose 5-phosphate synthases, Plant Science, **185**, 309-320 (2012).

113. **Altincicek, B., Hintz, M., Sanderbrand, S., Wiesner, J., Beck, E., and Jomaa, H.:** Tools for discovery of inhibitors of the 1-deoxy-D-xylulose 5-phosphate (DXP) synthase and DXP reductoisomerase: an approach with enzymes from the pathogenic bacterium Pseudomonas aeruginosa, Fems Microbiology Letters, **190**, 329-333 (2000).

114. **Rabhi-Essafi, I., Sadok, A., Khalaf, N., and Fathallah, D. M.:** A strategy for high-level expression of soluble and functional human interferon alpha as a GST-fusion protein in E.coli,

Protein Engineering Design & Selection, **20**, 201-209 (2007).

115. **Sivashanmugam, A., Murray, V., Cui, C. X., Zhang, Y. H., Wang, J. J., and Li, Q. Q.:** Practical protocols for production of very high yields of recombinant proteins using *Escherichia coli*, Protein Science, **18**, 936-948 (2009).

116. **Yu, Y., Pandeya, D. R., Liu, M. L., Liu, M. J., and Hong, S. T.:** Expression and purification of a functional human hepatitis B virus polymerase, World Journal of Gastroenterology, **16**, 5752-5758 (2010).

117. **Brammer, L. A., Smith, J. M., Wade, H., and Meyers, C. F.:** 1-deoxy-D-xylulose 5-phosphate synthase catalyzes a novel random sequential mechanism, Journal of Biological Chemistry, **286**, 36522-36531 (2011).

118. **Eubanks, L. M. and Poulter, C. D.:** *Rhodobacter capsulatus* 1-deoxy-D-xylulose 5-phosphate synthase: Steady-state kinetics and substrate binding, Biochemistry, **42**, 1140-1149 (2003).

119. **Ahmad, S., Kumar, V., Ramanand, K. B., and Rao, N. M.:** Probing protein stability and proteolytic resistance by loop scanning: A comprehensive mutational analysis, Protein Science, **21**, 433-446 (2012).

120. **DePristo, M. A., Weinreich, D. M., and Hartl, D. L.:** Missense meanderings in sequence space: A biophysical view of protein evolution, Nature Reviews Genetics, **6**, 678-687 (2005).

121. **Regnier, P. and Arraiano, C. M.:** Degradation of mRNA in bacteria: emergence of ubiquitous features, Bioessays, **22**, 235-244 (2000).

122. **Lithwick, G. and Margalit, H.:** Hierarchy of sequence-dependent features associated with prokaryotic translation, Genome Research, **13**, 2665-2673 (2003).

123. **Farrell, C. M., Grossman, A. D., and Sauer, R. T.:** Cytoplasmic degradation of ssrA-tagged proteins, Molecular Microbiology, **57**, 1750-1761 (2005).

124. **Sharp, P. M. and Li, W. H.:** The codon Adaptation Index--a measure of directional synonymous codon usage bias, and its potential applications, Nucleic acids research, **15**, 1281-1295 (1987).

125. **Bachmair, A., Finley, D., and Varshavsky, A.:** In vivo half-life of a protein is a function of its amino-terminal residue, Science (New York, N.Y.), **234**, 179-186 (1986).

126. **Laalami, S., Zig, L., and Putzer, H.:** Initiation of mRNA decay in bacteria, Cellular and Molecular Life Sciences, **71**, 1799-1828 (2014).

127. **Lenz, G., Doron-Faigenboim, A., Ron, E. Z., Tuller, T., and Gophna, U.:** Sequence features of e. coli mrnas affect their degradation, Plos One, **6** (2011).

128. **Kaberdin, V. R.:** Probing the substrate specificity of *Escherichia coli* RNase E using a novel oligonucleotide-based assay, Nucleic Acids Research, **31**, 4710-4716 (2003).

129. **Joo, J. C., Pack, S. P., Kim, Y. H., and Yoo, Y. J.:** Thermostabilization of *Bacillus circulans* xylanase: Computational optimization of unstable residues based on thermal fluctuation analysis, Journal of Biotechnology, **151**, 56-65 (2011).

130. **Xiang, S., Usunow, G., Lange, G., Busch, M., and Tong, L.:** Crystal structure of 1-deoxy-d-xylulose 5-phosphate synthase, a crucial enzyme for isoprenoids biosynthesis, Journal of Biological Chemistry, **282**, 2676-2682 (2007).

131. **Cane, D. E., Chow, C., Lillo, A., and Kang, I.:** Molecular cloning, expression and characterization of the first three genes in the mevalonate-independent isoprenoid pathway in Streptomyces coelicolor, Bioorganic & Medicinal Chemistry, **9**, 1467-1477 (2001).

132. **Schaub, J., Schiesling, C., Reuss, M., and Dauner, M.:** Integrated sampling procedure for metabolome analysis, Biotechnology Progress, **22**, 1434-1442 (2006).

133. **Zhou, K., Zou, R. Y., Stephanopoulos, G., and Too, H. P.:** Metabolite Profiling Identified Methylerythritol Cyclodiphosphate Efflux as a Limiting Step in Microbial Isoprenoid

Production, Plos One, **7** (2012).

134. **Liu, H. W., Wang, Y., Tang, Q., Kong, W. T., Chung, W. J., and Lu, T.:** MEP pathway-mediated isopentenol production in metabolically engineered Escherichia coli, Microbial Cell Factories, **13** (2014).

135. **Berla, B. M. and Pakrasi, H. B.:** Upregulation of Plasmid Genes during Stationary Phase in *Synechocystis* sp Strain PCC 6803, a Cyanobacterium, Applied and Environmental Microbiology, **78**, 5448-5451 (2012).

136. **Bentley, F. K. and Melis, A.:** Diffusion-based process for carbon dioxide uptake and isoprene emission in gaseous/aqueous two-phase photobioreactors by photosynthetic microorganisms, Biotechnology and Bioengineering, **109**, 100-109 (2012).

137. **Halfmann, C., Gu, L. P., and Zhou, R. B.:** Engineering cyanobacteria for the production of a cyclic hydrocarbon fuel from CO2 and H2O, Green Chemistry, **16**, 3175-3185 (2014).

138. **Khetkorn, W., Incharoensakdi, A., Lindblad, P., and Jantaro, S.:** Enhancement of poly-3-hydroxybutyrate production in *Synechocystis* sp PCC 6803 by overexpression of its native biosynthetic genes, Bioresource Technology, **214**, 761-768 (2016).

139. **Zhou, J., Zhang, H. F., Zhang, Y. P., Li, Y., and Ma, Y. H.:** Designing and creating a modularized synthetic pathway in cyanobacterium *Synechocystis* enables production of acetone from carbon dioxide, Metabolic Engineering, **14**, 394-400 (2012).

140. **Ruffing, A. M. and Jones, H. D. T.:** Physiological effects of free fatty acid production in genetically engineered *Synechococcus elongatus* PCC 7942, Biotechnology and Bioengineering, **109**, 2190-2199 (2012).

141. **Guerrero, F., Carbonell, V., Cossu, M., Correddu, D., and Jones, P. R.:** Ethylene Synthesis and Regulated Expression of Recombinant Protein in *Synechocystis* sp PCC 6803, Plos One, **7** (2012).